**The Thesis Committee for Xiwei Guo**
**Certifies that this is the approved version of the following thesis:**

# Morphodynamics of large anabranching rivers: the case of the Madeira River, Brazil

**APPROVED BY**
**SUPERVISING COMMITTEE:**

**Supervisor:**

Edgardo M. Latrubesse

Timothy P. Beach

Carlos E. Ramos-Scharrón

# Morphodynamics of large anabranching rivers: the case of the Madeira River, Brazil

**by**

**Xiwei Guo**

**Thesis**

Presented to the Faculty of the Graduate School of

The University of Texas at Austin

in Partial Fulfillment

of the Requirements

for the Degree of

**Master of Arts**

**The University of Texas at Austin**

**August 2017**

## Acknowledgements

I would like to appreciate all members of the Department of Geography and the Environment of The University of Texas at Austin for providing me a great platform to work and study during the two years. I am particularly grateful to members of my supervising committee, Dr. Edgardo Latrubesse, Dr. Timothy Beach, and Dr. Carlos Ramos-Scharrón for their mentoring throughout the progress of the thesis.

# Abstract

## Morphodynamics of large anabranching rivers: the case of the Madeira River, Brazil

Xiwei Guo, M.A.

The University of Texas at Austin, 2017

Supervisor: Edgardo M. Latrubesse

Anabranching channels are the dominant channel pattern of large rivers worldwide. The top nine largest rivers of the world by water discharge, in particular, all develop anabranching channels. Given the limited understanding on large river morphodynamics and the mechanisms of formation and process of anabranching channels, this thesis focuses on elucidating the morphodynamic conditions of a 150-km channel segment of the Madeira River, the largest tributary of the Amazon River and the fourth or fifth largest river in the world with anabranching channels, by extensively using field measurement and remote sensing data. The studied river channels are divided into three reaches: 1) Box-shaped channels with upstream and downstream anabranching structures; 2) A pseudo-meander with a downstream anabranching structure; 3) A single-threaded straight channel with a downstream anabranching structure. The analysis of the spatial-temporal channel changes of the three reaches since 1985 demonstrates the slow process of channel lateral migration and the stability of large anabranching rivers. Besides three sites with special geomorphological settings, more than 87% of the channel analyzed did not have traceable

lateral migration. The area being eroded and deposited stayed relatively equivalent until after 2010, in which channel incision (erosion) significantly exceeded the amount of deposition, possibly due to the closure of two large dams on the Madeira mainstem upstream. Channel morphology and flow scheme vary largely among different channel structures, while geologic controls play an important role in a number of places that result in channel deepening and suspension of channel migration. The three reaches are dominated by nearly upright banks, which makes the channel width stay constant with increasing discharge and impedes channel-floodplain interactions. Bed shear stress, stream power, and sediment transport are further analyzed and discussed. The hydro-geomorphological features of two anabranching structures, one in reach 2 and one in reach 3, each demonstrates floodplain avulsion (erosion-triggered) and in-channel accretion (deposition-triggered), which are the two mechanisms of anabranching channel formation.

*Key words: large rivers, anabranching channels, channel patterns, morphodynamics, Amazon*

# Table of Contents

# Chapter 1: Introduction

Rivers play important roles in the natural environment and human society. They are one of the most fundamental natural components of the world, which significantly support the functioning of the Earth system. Given that most human populations around the world live close to rivers, they provide critical water resource to support economic growth and social development. As we increasingly promote sustainable development today, it is ever more crucial to better understand rivers in order to better manage them.

The form and process of channel patterns, particularly of alluvial rivers, has been a fundamental issue in fluvial geomorphology (Leopold and Wolman, 1957; Chitale, 1973; Schumm, 1985), yet it has not been fully understood (Latrubesse, 2008; Kleinhens, 2010; Lewin and Ashworth, 2014). An alluvial river system contains channels, floodplains, hillslopes, and other landforms. Flow and sediment regimes generated within the system control the process of a river (Schumm, 1977; Charlton, 2007). In alluvial channels, the banks and beds are composed of alluvium, which is the material transported by the streamflow from upstream. Alluvial rivers continuously change the channel shape through the processes of erosion and deposition (Schumm, 1985; Latrubesse and Park, 2017). Alternations of channel patterns in a river and differences of channel patterns among various rivers indicate differences of hydrologic and geomorphologic settings of fluvial systems. Those natural settings include, but are not limited to, streamflow and sediment regime, grain size, channel morphology, slope, vegetation, and bank cohesiveness (Leopold and Wolman, 1957; Parker, 1976; Bridge, 1993; Knighton and

Nanson, 1993; Rosgen, 1994; van den Berg, 1995; Millar, 2000). Morphodynamics is the study of morphological changes of river channels and floodplains by focusing on understanding the physical nature of the erosional and depositional processes (e.g. Formann and Habersack, 2007; Tal and Paola, 2010; Church and Ferguson, 2015). The balance between erosion (degradation) and deposition (aggradation) is determined by a variety of factors, including water and sediment discharge, bed grain size, slope, riparian vegetation, cohesiveness of banks, and others (Lane, 1955; Leopold and Wolman, 1957). The understanding of river morphodynamics is essential to the study of fluvial geomorphology, thus it has profound significance to better understand our planet and support human development.

Traditionally, patterns of river channels are classified as straight, braided, and meandering, based on the plan-view patterns of rivers (Leopold and Wolman, 1957). Each channel pattern has unique combinations of elements of the natural settings. Quantitative and qualitative approaches have been extensively proposed, aiming to elucidate the ultimate causes of channel pattern differences. Common methods in those studies include field work, laboratory experiments, and model simulations, which encompasses empirical and theoretical approaches (e.g. Ashmore, 1982; Bledsoe and Watson, 2001). In discriminating channel patterns, a number of quantitative and qualitative approaches have helped sort out some of the complexities, although big controversies still exist. In quantitative approaches, Leopold and Wolman (1957) discriminated meandering and braided channels by comparing bankfull discharge with

channel gradient (slope) and proposed a line dividing the zone of meandering and the zone of braided. The line is represented as

$$s = 0.013{Q_{bf}}^{-0.44}$$

where *s* denotes channel gradient and $Q_{bf}$ denotes bankfull discharge. They pointed out that the positions of channels in this discharge-slope comparison above the line is likely braided, and those below the line is likely meandering. Using the similar approach, van den Berg (1995) proposed that alluvial channel patterns could be discriminated by bed median grain size and unit stream power, and threshold-condition line dividing zones of braided channels and single-thread channels, which include meandering, is represented as:

$$\omega = 900{D_{50}}^{0.42}$$

where $\omega$ denotes specific stream power at the transition between multi-thread and single-thread channels, and $D_{50}$ denotes median bed grain size. Other approaches, such as the bedload and *w/d* (the ratio of channel width to depth) approach (Schumm, 1985), channel stability approach (Parker, 1976), bifurcation approach (Richardson and Thorne, 2001), flow stochasticity approach (Langbein and Leopold, 1970), and inter-channel-pattern threshold approach (Eaton et al., 2010) have been proposed in order to sort out the main causes behind in forming different types of channel patterns on Earth's surface.

Large rivers and their basins are dominant geomorphological features and important components in the geologic history (Potter, 1978; Latrubesse 2008; Latrubesse 2015). They present diverse hydrodynamic and morphodynamic conditions, which differ from those of smaller rivers (Latrubesse, 2008; Nicholas, 2013; Lewin and Ashworth,


Figure 1.1
Channel of the Amazon River, the largest river of the world by water discharge, near the confluence of it and the Purus River. The unique anabranching channel, separated by vegetated stable islands, is the dominant channel pattern in many large rivers worldwide.

2014). There has been a long debate on how to determine the size of rivers, and how large is considered "large" (Miall, 2006). Latrubesse (2008) defined large rivers to have the annual mean discharge greater than 1,000 $m^3/s$. Among them, large rivers with annual mean discharge greater than 17,000 $m^3/s$ are defined "mega rivers", which is consisted of the top ten largest rivers of the world. Latrubesse (2008) pointed out that large rivers are unique also in terms of their channel patterns, as the top nine largest rivers: Amazon, Congo, Orinoco, Yangtze, Madeira, Negro, Brahmaputra, Japura, and Parana all develop anabranching channels. Latrubesse (2008) further proposed that none of the approaches discriminating channel patterns is sufficient for discrimination of large river channel patterns because of the insufficiency of large river discoveries and the lack of data of large rivers in previous studies. Compared to smaller rivers, large rivers are less studied, thus still lack a comprehensive understanding of their form and process. As the dominant

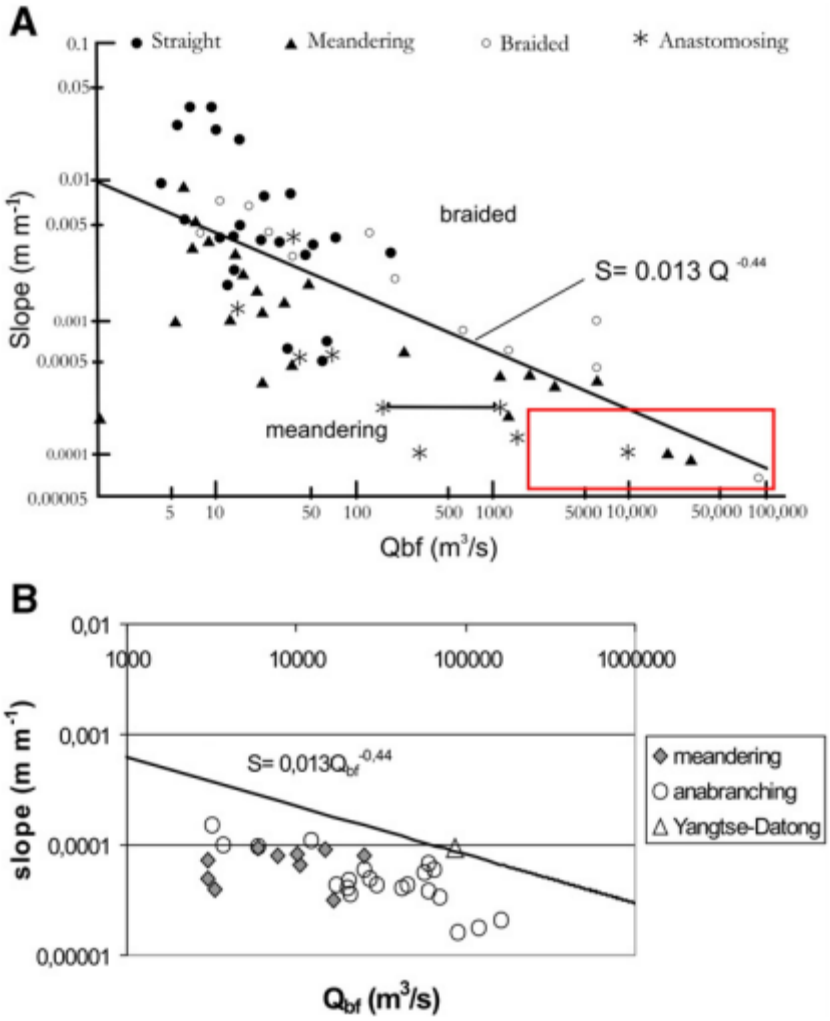


Figure 1.2
Leopold and Wolman (1957)'s equation that discriminates braided and meandering channels for small and mid-sized rivers is not sufficient to discriminate large river channel patterns as meandering and anabranching channels are clustered for rivers with discharge higher than 1,000 m³/s. The figure is from Latrubesse (2008).

channel pattern of large rivers, mechanism of anabranching channels is poorly understood.

The category of anabranching channels in the classification of channel patterns was a highly debated issue over the past two-to-three decades as fluvial geomorphologists

progressively gain more understanding on it. Geomorphologists have often used the terms "braided", "anabranch", and "anastomose" to describe multi-channel channel systems, but their actual meanings differ in terms of a variety of aspects, including planform characteristics, formation mechanism, and channel stability (Makaske, 2001; Carling et al., 2014). While "braided" describes mobile non-equilibrium channels that are mostly separated by fluvial bars, "anabranching" and "anastomosing" are used to describe multi-channel systems that are in equilibrium state (Rosgen, 1994; Nanson and Knighton, 1996). Aside from the other three patterns, anabranching channels develop a distinctive pattern of multiple interconnected channels with the flow divided by stable alluvial islands up to bankfull discharge (Nanson and Knighton, 1996; Knighton, 1998; Nanson, 2013). Bifurcation, anabranch, and confluence are the essential units composing anabranching channels. The term "anastomosing" is widely used as a subset of "anabranching" to describe those anabranching systems associated with low energy, fine grain, and highly-limited channel mobility (Nanson and Knighton, 1996; Makaske et al., 2002). Nowadays, anabranching is considered one of the major channel patterns in nature, as with braided, meandering, and straight (Latrubesse, 2008; Eaton et al., 2010).

Discussions on the formation mechanism of anabranching channels have been thoroughly made in the past two more decades, but they are largely on a case-by-case basis, and the general mechanism still remains controversial. Early studies treated anabranching channels as collections of either braided, meandering, or straight channels by looking at each anabranch (branches within an anabranching channel system) separately (e.g. Schumm, 1985; van den Burg, 1995), therefore didn't have in-depth

analysis of the form and process of anabranching channels as a whole. Different approaches have been widely used in the analysis of anabranching channels in the context of hydrodynamics (fluid dynamics, sediment transport), morphodynamics (channel evolution, channel-floodplain interactions, geologic settings), and other related aspects (e.g. riparian vegetation, human impact). Initially, anabranching channels are the product of either in-channel vertical accretion (deposition-triggered) or floodplain avulsion (erosion-triggered) (Miller, 1991; Nanson and Knighton, 1996; Carling et al., 2014). The former mode splits a pre-single-threaded channel into two or more anabranch channels (anabranches), and the later model forms one or more new channels in the floodplain that are interconnected with the old channel. Nanson and Knighton (1996) classified anabranching channels into six categories: cohesive sediment (anastomosing), sand-dominated with island forming, mixed-load and laterally active, sand-dominated with ridge forming, gravel-dominated and laterally active, and gravel-dominated and stable. Although this classification explicitly describes anabranching channels by a variety of channel characteristics, including stream power, types of sediment load, bank texture, and so forth, the diverse patterns of large anabranching rivers in thousands of rivers ranging from the mega rivers of the world to smaller streams cannot be explicitly described. Many cases demonstrated a "combined" channel planform of anabranching rivers and other channel patterns. For meandering channels, the formation of chute channel near meander bends often forms either short- or long-term local anabranching channel patterns (Kleinhans and van den Berg, 2011; Grenfell et al., 2012). For braided channels, some rivers draining in the Himalaya foothills, like the Brahmaputra River, develop many

anabranches with a high braided feature (Thorne et al., 1993; Latrubesse, 2008). The formation and the maintenance of anabranching channels are demonstrated to have a hydraulic efficiency that the total transport capacity of an anabranching channel system (with two or more anabranches) could exceed the transport capacity of a single-threaded channel system under the same hydrologic and geomorphologic setting (Nanson and Huang, 1999; Huang and Nanson, 2007; Nanson and Huang, 2008). The reduced width of each anabranch decreases the skin friction of the flow made by channel bed so that a greater hydraulic efficiency is obtained.

While research has been greatly focusing on why anabranching channels form, other studies have examined particular features or perspectives involved in anabranching channel and large rivers systems. The planform analysis of channel changes have been conducted for many large anabranching rivers in the world as it is an important indicator of the morphodynamic conditions of a river. From these analyses it is possible to gather that, large anabranching rivers present diverse morphodynamic conditions, both temporally and spatially, in terms of channel morphology and behavior, and interactions between flow regime, channel, floodplain, and the geologic setting (Sarker et al., 2014; Frias et al., 2015; Mendoza et al., 2016). The interaction between channel and floodplains is a critical issue for understanding the process of large anabranching rivers because floodplains provide space for the channel to erode and the channel conveys water and sediment. Large anabranching rivers tend to have larger floodplains, which initiates complex channel-floodplain interactions (Latrubesse and Franzinelli, 2002; Latrubesse,

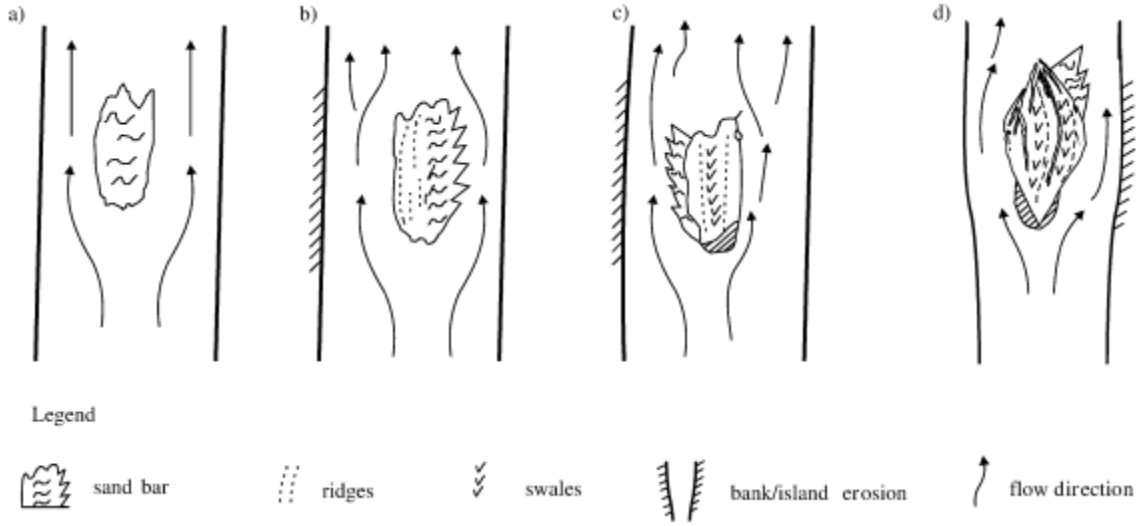


Figure 1.3
Conceptual model of the formation of anabranching islands forming from mid-channel bars, proposed by Latrubesse and Franzinelli (2002).

2015). Channel-floodplain interactions in the largest fluvial system of the world, the Amazon basin, are extremely active and complex in the ways of floodplain erosion, overbank and bar deposition, tributary input, and floodplain storage (Mertes et al., 1996; Dunne et al., 1998). As sediment supply plays a fundamental role in channel-floodplain interactions and channel behaviors (Milliman and Meade, 1983; Constantine et al., 2014), The spatiotemporal patterns of suspended sediment between channel and floodplain are also closely correlated in the Amazon basin, the largest fluvial system in the world developing anabranching channels (Park and Latrubesse, 2014). The formation of mid-channel island, as one of the two mechanism forming anabranching structures, has been studied substantially, but most has been conducted in smaller rivers (e.g. Bridge et al., 1986; Osterkamp, 1998). On the basis of large river system morphodynamics, Latrubesse and Franzinelli (2002) proposed a model, which describes the formation of typical

anabranching islands forming from mid-channel bars (Figure 1.3). In this model, a mid-channel bar gradually evolves into an island through lateral and vertical accretion and vegetation stabilization, with bank erosion, channel widening, and associated lateral accretion occurred. In addition, the formation and process of bifurcations and confluences, particularly bifurcations, have been extensively studied (e.g. Richardson and Thorne, 2001; Bolla Pittaluga et al., 2003; Zolezzi et al., 2009). Despite that mostly of them focus on bifurcations of braided channels, the approaches used to describe and quantify bifurcations are applicable for anabranching channels.

Due to the limited understanding of anabranching channels, especially for large and mega rivers, and barriers to conducting studies in large rivers, this thesis research aims to enhance our understanding of the form and process of anabranching channels of mega river systems. The research particularly focuses on the Madeira River, the largest tributary of the Amazon River which is ranked the fourth or fifth the largest rivers of the world by water discharge (Latrubesse, 2008) that develops unique patterns of mixed single-threaded and anabranching channels (see introduction of the field in Chapter 2). This thesis will study the morphodynamics of selected reaches of the Madeira River to understand its channel morphology and historic channel changes, channel-floodplain interactions, sediment transport regime, and the hydro-morphological features of anabranching structures. The research aims to expand our knowledge to a broader field that allows us to comprehend the nature of large and mega rivers thoroughly.

# Chapter 2: Study site

The Amazon River basin is the largest fluvial system of the world with the tremendous amount of water and sediment discharge and the greatest ecological diversity. The mainstem of the Amazon River and its numerous tributaries creates large areas of floodplains and many of them develop anabranching channels, including the Amazon River and its largest tributaries: Madeira, Negro, and Japura. (Latrubesse, 2008). The Madeira River, as the research target of the thesis, is the largest tributary of Amazon by water discharge and sediment load. It is also ranked the fourth or fifth largest rivers of the world by water discharge, with a mean annual discharge about 32,000 $m^3/s$ that is equivalent to the size of the Yangtze River. Nearly half of Amazon River's sediment load is contributed by the Madeira River, which is estimated to be 450 Mt/year and the specific sediment yield is 330 t/km year (Latrubesse et al., 2005). With most of the Madeira River developing anabranching channels, the river also presents a unique pattern of anabranching channels that is on a somewhat threshold between single-threaded straight channels and anabranching channels like what is developed in the mainstem of the Amazon River.

Given the geomorphic importance and uniqueness of the Madeira River, this thesis particularly focuses on a 150-km channel segment, downstream to the city of Porto Velho, Brazil (Figure 2.1). Among the studied channels, we divided them into three reaches with each developing a unique channel planform. The first reach is dominated by a complex of islands, forming patterns of anabranching channels, and the channel overall forms an odd box-shaped bend. The second reach starts with single-threaded channels


Figure 2.1
The smaller map shows the location of Porto Velho in the Amazon Basin, marked in green. The bigger satellite image shows the locations and channel planform of the three reaches, split by white lines. Reach 1 and 2 are split by a short river segment and reach 2 and 3 are connected. Channel pattern of the Madeira River is different from that of the Amazon River because single-threaded channels take a large portion of the river channel, whereas the anabranching portion is relatively small.

with some little islands, and followed by a U-shaped channel bend with an anabranching structure formed downstream. The third reach starts with a straight single-threaded channel, followed by another anabranching structure downstream. There are no other

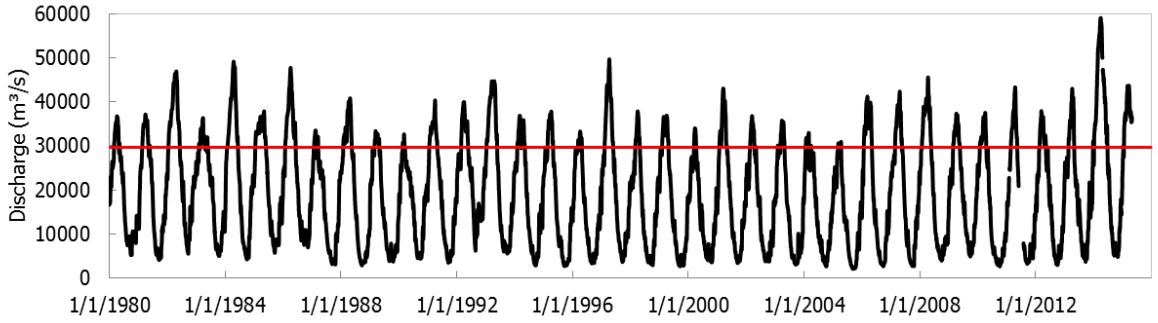


Figure 2.2
Historic discharge data of the Madeira River at Porto Velho. The red line indicates the position of bankfull discharge, which is 30,000 m³/s. Data credit: SO HYBAM.

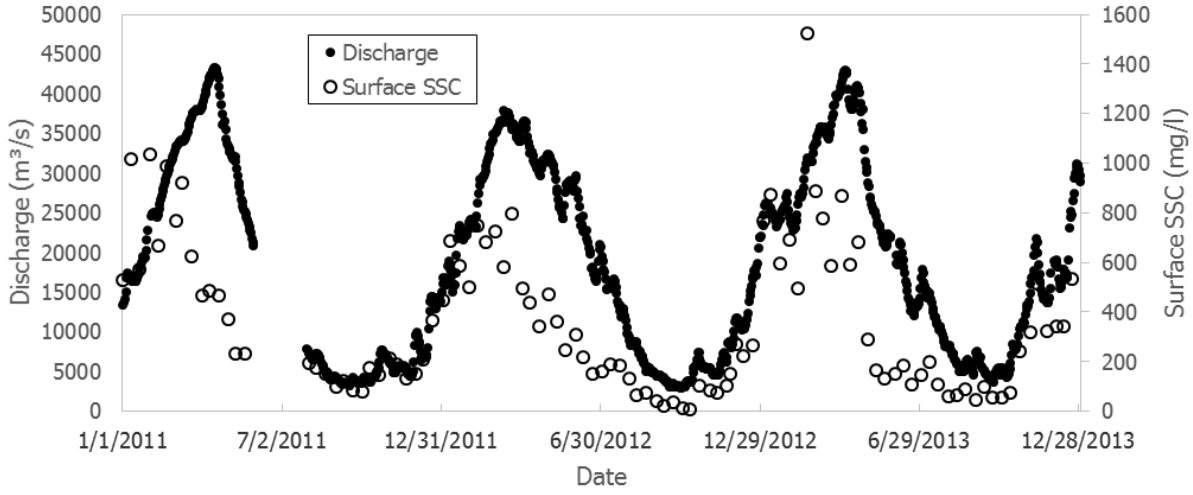


Figure 2.3
Historic discharge and surface suspended sediment concentration (SSC) data of the Madeira River at Porto Velho from 2011 to 2013. Data credit: SO HYBAM.

major tributaries joining the Madeira River along the studied reaches. Anabranching structures are developed in all three reaches, but the morphology and associated channel behavior and flow structure of those are different. Details of the geomorphology of the three reaches are introduced in Chapter 4.

Discharge regime of the river at Porto Velho shows large variability throughout a year, ranging from below 10,000 m³/s to above 30,000 m³/s. In some years, peak flow can

reach to above 45,000 $m^3/s$. Low-flow season is usually from October to December, and high-flow season is usually from March to May. The regime of suspended sediment concentration has a similar pattern of that of water discharge, but the peak-concentration occurs about two months earlier than the peak discharge. Measured surface suspended sediment concentration from 2011 to 2013 ranges from less than 50 mg/l to above 800 mg/l in a year, showing a greater variability than water discharge.

The Madeira River is currently under severe dam impact, making it the first major first-order tributary of the Amazon disrupted by humans. The first two dams in the Amazon basin: the Santo Antonio and the Jirau dams are both located on the Madeira River above Porto Velho. The San Antonio Dam was completed in 2012 and the Jirau Dam will soon finish construction and put in use. The water discharge at the San Antonio Dam is even greater than that at the Three Gorges Dam on the Yangtze River, China as the largest dam in the world. The operations of them are estimated to cause a variety of severe environmental and social impacts (Fearnside, 2014). Evidence have shown a remarkable reduction of suspended sediment load in the downstream channel (Latrubesse et al., 2017). The change of water and sediment regime in both upstream and downstream reaches of the dams may dramatically alternate the hydrologic and geomorphologic conditions, which may also lead to greater long-term environmental and social issues. In addition, not only the Madeira River, but almost the entire Amazon basin is proposed to develop hydroelectric projects on for the future few decades. Latrubesse et al. (2017) proposed a “Dam Environmental Vulnerability Index” to evaluate dam impacts of the Amazon River and the Madeira River is ranked the highest sub-basin which has the

Figure 2.4
The Madeira River downstream to Porto Velho. The photo was taken in December 2012 and the suspended sediment concentration was at a relatively low level of a year. However, the yellowish color of the water indicates high sediment load of the river. Photo credit: Dr. Latrubesse's Large River Group.

greatest vulnerability caused by dam impacts. Their evaluation further demonstrates the potential massive hydrophysical and biotic disturbances in the Amazon basin, under the impact of more than 400 complete and planned dams. Other challenges the Amazon basin, including the Madeira, facing include climate change, urbanization, agricultural and industrial exploitation will further cause environmental crisis such as severer erosion and bigger floods (Gentry and Lopez-Parodi, 1980; Forsberg et al., 1989).

# Chapter 3: Method

The research of this thesis employs both quantitative and qualitative approaches, with an emphasis on a quantitative approach. Results presented in Chapter four and five rely extensively on the analyses of data collected from the field, GIS and remote sensing, and a third party agency: SO HYBAM. In the following subsections, field measurements, GIS and remote sensing, and SO HYBAM will each be introduced in detail in the ways of data collection, organization, and usage involved in the research.

## 3.1 Field measurements

Most geomorphologic data in this thesis comes from what was collected in three fieldwork campaigns in July 2011, December 2012, and March 2013. All three fieldwork was conducted by members of Dr. Latrubesse's Large River Group. As shown in the 30-year hydrograph (Figure 2.2), July has relatively the smallest discharge, then December and March has the greatest discharge among the three. We focused on measuring parameters of channel and floodplain along the three reaches, which was described in Chapter 2. The field work of 2011 and 2012 conducted measurements for all three reaches, and the 2013 field work conducted measurements for reach 1 and reach 3. Field measurement data was collected by a variety of equipment or techniques, including Acoustic Doppler Current Profiler (ADCP), Bathymetry survey, water and sediment samples, GPS recording, and radiocarbon dating.

We used the Rio Grande ADCP in all three field work campaigns to measure parameters of channel flow. Those measurements are: cross-sectional discharge, flow

| | 2011 | | 2012 | | 2013 | |
|---|---|---|---|---|---|---|
| | Single | Anabranching | Single | Anabranching | Single | Anabranching |
| **Reach 1** | 13* | 12 | 4 | 13 | 5 | 6 |
| **Reach 2** | 3 | 3 | 3 | 3 | -- | -- |
| **Reach 3** | 7 | 5 | 7 | 5 | 3 | 4 |

Table 3.1
Number of ADCP transects measured in the field work campaigns of 2012, 2012, and 2013, separate by reach and channel type ("single" means crosssections of single-threaded channels and "anabranching" means cross-sections of anabranches). Reach 2 wasn't measured in 2013.
*including two cross-sections that are in single-threaded channels but was separate by a fluvial bar because of the low stage during 2011 field work

velocity profile, cross-sectional width and area, secondary flow direction and velocity, and backscatter. Channel mean depth is calculated from cross-sectional area and width. Width-depth ratio (*w/d*) is calculated from channel width and mean depth. Backscatter is used to quantify suspended sediment concentration of the channel flow. There are 42 cross-sections measured by ADCP in the 2011 field work, 35 cross-sections in the 2012 field work, and 18 cross-sections in the 2013 field work. Besides the 2013 field work that the ADCP only surveyed reach 1 and 3, 2011 and 2012 field work had ADCP data covered for all three reaches. Those ADCP cross-sections (transects) measured both single-threaded channels and branch channels within anabranching structures (anabranches). Particular positions of cross-sections measured with ADCP in downstream distance are presented in figures of Chapter 4.

Together with the ADCP measurements, Bathymetry surveys were conducted along the three reaches to measure channel depth and bed morphology at various locations. The Bathymetry data is point-based, so Bathymetry data availability depends fully on boat track. Bathymetry data availability varies year-by-year and reach-by-reach.

The 2011 Bathymetry data is a doublication of the ADCP transects, which had a very low density. Bathymetry data collected in 2012 extensively surveyed the channels in reach 1 in the upstream and downstream part of the large channel bend as well as most parts of reach 3 channels. The longitudinal density of the 2012 Bathymetry data for reach 3 is at least every 200 m. Bathymetry data of 2013 field work covered most parts of reach 1, except the first 5 km, and the bifurcation of the dominant anabranching structure in reach 3.

Water and sediment samples were collected at multiple places in the three reaches. Those samples include surface water samples and bed material samples to estimate surface suspended sediment concentration and grain sizes and bed grain sizes. There were 35 cross-sections measured with surface water samples in the field work of 2011 and 14 cross-sections in the field work of 2013. 11 sites were measured with bed material samples in 2011. Surface water samples are used to examine the distribution of suspended sediment along the studied reaches, and bed samples are used to examine spatial pattern of bedload transport in the channels.

During the field work of 2011, the research group also collected elevation data using GPS devices at water surfaces of 30 sites on both banks of the river. Using the coordinates recorded by GPS devices, we plotted the locations measured with surface water elevation on a map to calculate the channel distance between two sites with the elevation data. The channel gradient (slope), assuming uniform flow, is then calculated by the rise (elevation differences between two points) over run (channel distance between two points). We also dated (radiocarbon dating) 11 bank samples of single-threaded

channels and anabranches to know the age of bank materials. The depths of the sediment level where dating was conducted will be noted in the following chapters where the data is presented.

### 3.2 Remote sensing and GIS

The main use of remote sensing and GIS in this thesis is the analysis of channel changes in the context of channel morphodynamics. The analysis is also called multi-temporal analysis of the channel, which makes it able to examine the spatial pattern and distribution of erosion and deposition occurred in the channel over a given period. To do this, we downloaded satellite images from Earth Explorer, a USGS-run data source of satellite images, aerial photographs, and cartographic products. We used sequences of Landsat 5 and 8 images, which have a resolution of 30×30m, for the analysis of every five years since 1985. When selecting satellite images, there were three major criteria that are of my concern: data availability, data quality, and corresponding water stage of the date of the image. Among them, data quality was a big challenge because the Amazon basin is frequently covered by clouds which would significantly reduce the accuracy of analysis results or completely make the satellite images useless. Therefore, the images I chose in the multi-temporal analysis were not taken exactly for every five years (Table 3.2). The images were mostly taken around September, during a relatively low water stage to avoid too much difference. Although the corresponding water stage is important because a higher stage would potentially widen the river channel, which would affect the accuracy of results, it is not that critical because the Madeira River bank at the studied

| Year | 1985 | 1991 | 1995 | 2000 | 2004 | 2010 | 2015 |
|---|---|---|---|---|---|---|---|
| Sensor | Landsat 7 | Landsat 7 | Landsat 7 | Landsat 7 | Landsat 7 | Landsat 7 | Landsat 8 |
| Band | 4 | 4 | 4 | 4 | 4 | 4 | 5 |
| Image Date | 08/14 | 09/16 | 09/27 | 10/10 | 09/19 | 08/19 | 09/18 |
| Stage (m) | 7.12 | 3.05 | 3.05 | 3.45 | 2.89 | 3.49 | 5.14 |

Table 3.2
Information of satellite images used in the analysis and corresponding water stages.

sites are straight-up (see Figure 4.29, which demonstrates that increased discharge/stage doesn't change channel width obviously) so unless a huge difference (larger than 5 meters; the depth difference between low-stage and bankfull stage is about 10 m in Porto Velho), an increased water stage would not cause a dramatic width difference. In addition, the multi-temporal analysis only considers vegetated bank as the channel boundary—fluvial bars that usually appear inside the bank and remain above water surface during low water stages are still treated as part of the channel.

The multi-temporal analysis includes two parts, which are both presented in Chapter 4. First, using the "centerline" tool from the NCED Stream Restoration Toolbox and the georeferenced Landsat images, I drew the banklines where the boundary from waterbody/fluvial bars to vegetated banks is located and digitized the centerlines which marked the center of the channel for each of the year listed in Table 3.2. Having the georeferenced centerlines of different years, the trend of channel change (channel migration) is assessed. It is used to evaluate channel migration and calculate the migration rates at specific sites in the studied reaches. Second, using the same georeferenced images, I drew the banklines of each reach for each of the years, including

the shapes of islands (vegetated land area within a channel; not fluvial bars), and geoprocessed the polygons created to assess channel changes for all the six intervals and particularly, the interval of 1991-2010 because of its large time span.

### 3.3 Other hydrologic data

The French-Brazilian agency, SO HYBAM, collects a full set of hydrologic data for the Amazon rivers, including those of the Madeira River at Porto Velho station. The hydrologic data presented in Chapter 2 is downloaded from SO HYBAM. Daily water stage and water discharge data are used for the conversion and calibration of bankfull and bar-full conditions, and other corresponding water stages in the bifurcation morphodynamics in Chapter 5.

# Chapter 4: Geomorphology and channel evolution

This chapter introduces the overall geomorphology of the river channel and floodplain of the three reaches involved in the study and channel evolution of them. The geomorphologic introduction includes descriptions of the distribution of floodplains, Holocene and Pleistocene deposits, channel morphology (width, depth, and *w/d*), patterns of flow velocities, channel gradient, and unique geomorphological units. Channel evolution includes analysis of channel migration through centerline comparison and channel changes in two temporal scales: 19-year (1991-2010) and every five years (or 4 or 6 years) during 1985-2015. Channel changes are reflected in the analysis by areas of deposition and erosion of channel banks and islands. Vegetation is the main criterion to differentiate channel from banks and islands, whereas non-vegetated fluvial bars are considered part of the channel. In the first three sections of the chapter, Reach 1, 2, and 3, as introduced in Chapter 2, are described separately. The last section combines data of all three reaches for a synthesized description of the geomorphology and channel evolution. When introducing channel geomorphology, bankfull conditions of each reach are described in each of their own section, and conditions during low-discharge is presented as a whole in the last section. The purpose of this chapter is to discern the spatial characteristics of geomorphology of the three studied reaches and spatial and temporal patterns of channel changes, in order to better understand fluvial dynamics of the river presenting anabranching patterns.

### 4.1 Reach 1: Box-shaped channels with upstream and downstream anabranching structures

Starting at the location 30km downstream to Porto Velho, Brazil, the first reach is a 43 km-long segment. The dominant feature of reach 1 is the large box-shaped channel bend with anabranching structures upstream and downstream of the bend, and a single-thread channel at the bend apex. Among the three reaches defined, this reach has the most complex channel planform. More than 50% of the length of this reach is dominated by anabranching channels at all times in the past three decades. The river flows into the reach at the northeast direction, then forms several bifurcations with vegetated islands and front bars splitting the flow. Afterward, the channel makes a near 90º right turn, followed with a straight channel with branches extended from the bifurcations. The channel makes another near 90º turn to the left, with small areas of bars at the turning point, and shortly followed with another near 90º left turn in single-thread channel. After that, several bifurcations in different sizes form again with sand bars in the front. The channel splits into at least three branches after the bifurcations and makes the final 90º turn to the right. The branches then join together and form another single-thread channel at the end of this reach.

River channels at this reach are mostly surrounded by floodplains on both sides of the banks. The only exception is the outer bank at the apex of the big channel bend, which is about 20m higher than the inner bank—a value that is much higher than the levee height. Neither active floodplain or Quaternary floodplain are present at the outer bank. Floodplain is also developed on the islands as integral parts of anabranching

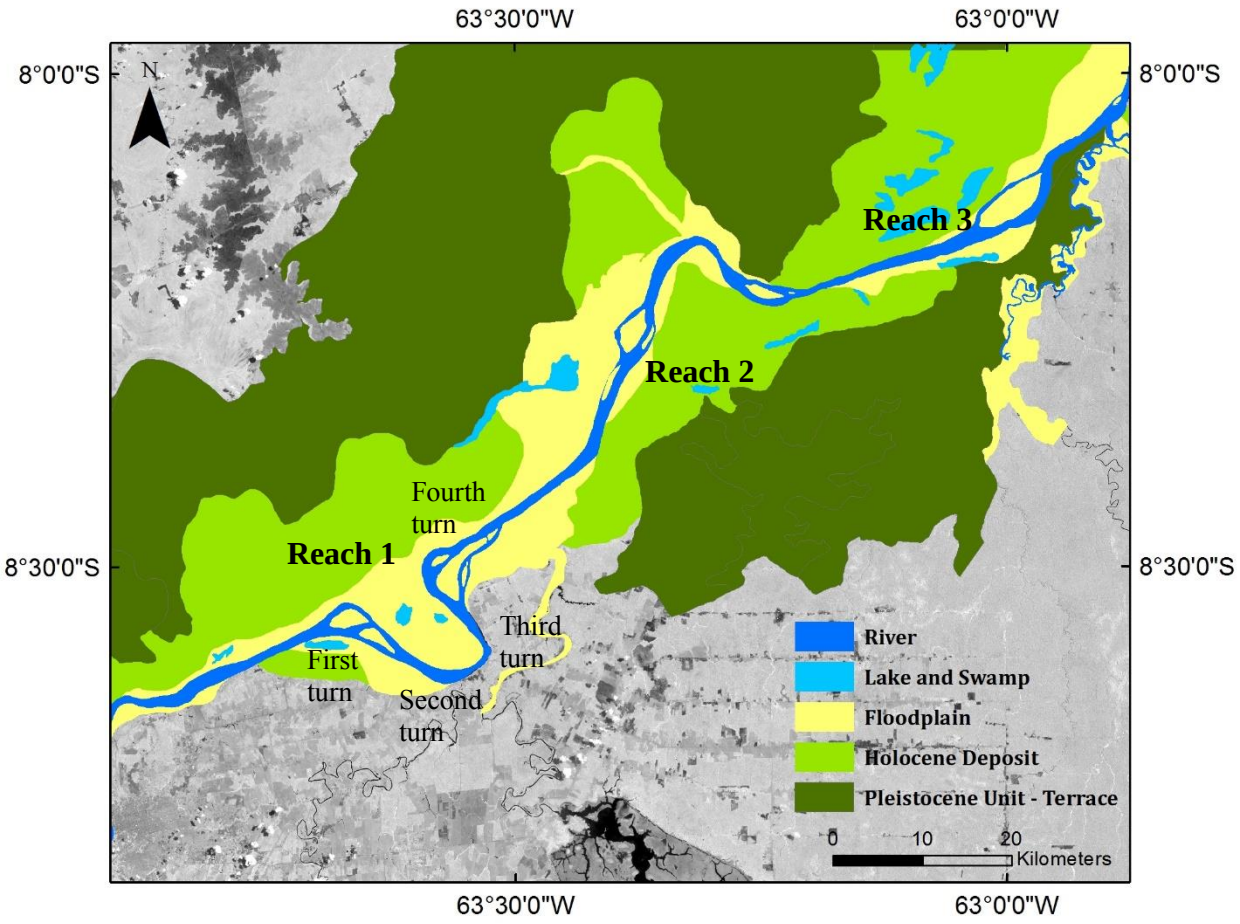


Figure 4.1
Geomorphologic units of the studied reaches of the Madeira River. The locations of Porto Velho is marked. Current active floodplain, Holocene floodplain, and Pleitoscene floodplain are shown in yellow, light green, and dark green, respectively. Geomorphologic units are analyzed by remote sensing and field measurements, by Latrubesse's Large River Group. The background image is by Landsat 8. The river flows to the right.

structures. The width of the floodplain varies in different channel segments. In the beginning of this reach, before the first 90º turn, the floodplain is the narrowest. Following with the first 90º turn and the associated anabranching structures, the floodplain becomes wider, which is in accordance with the amplitude of the channel

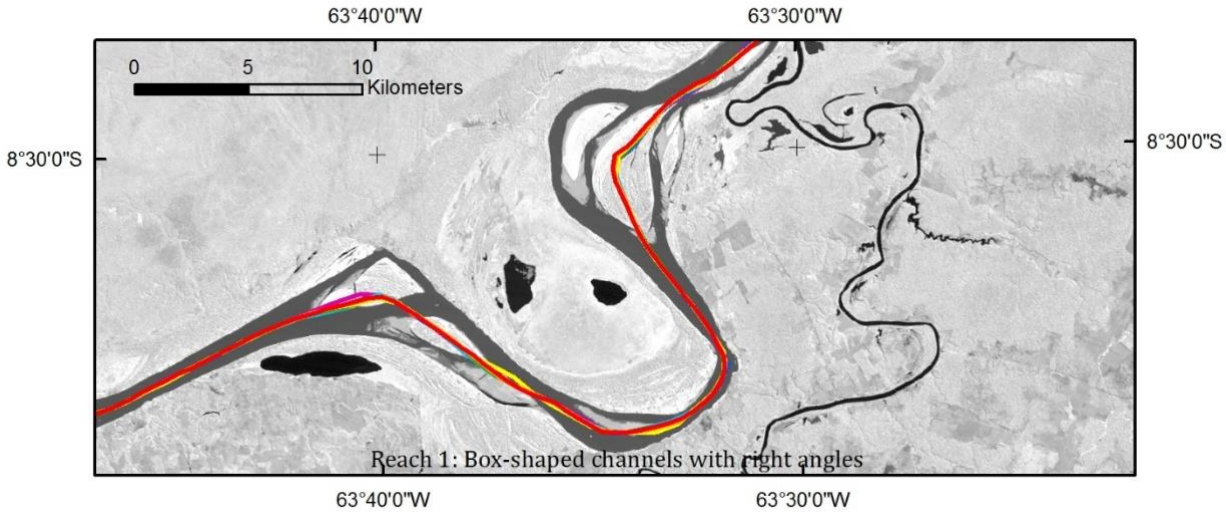


Figure 4.2
Reach 1 centerlines in 1985, 1991, 1995, 2000, 2004, 2010, 2015, represented in purple, blue, cyan, green, yellow, orange, and red, respectively. The overlapped lines indicate small lateral migration of the channel.

bend. After the last 90º turn, floodplain narrows down again but remains a good part on both sides of banks. Quaternary floodplains are asymmetric presented, with the left bank much wider and larger than the right bank. The lack of present and paleo floodplain formation suggests the presence of geologic control on the left bank side. This will be further discussed with channel evolution in the following passages.

The multi-temporal analysis of the channel shows that the lateral migration rate is very small. The centerlines for different years largely overlap on each other, indicating that the channel has almost no migration in the past three decades. Compared to channels with anabranching structures, single-thread channels, particularly the channel segment before it makes the first right turn, the channel segment at and near the box-shaped bend apex, and the segment after the bend apex, are more stable. Two places upstream to the bend apex of the channel are found with traceable lateral migration: the channel right

before it makes the first 90º turn, and the channel between its first and second 90º turn. For the first site, all other centerlines largely overlay but the 1985 one which is about 250 m towards the left bank from the other centerlines. Similarly, the second site has all years' centerlines overlaid together, besides the 2005 one which is about 280 m towards the left bank. Instead of progressive lateral migration throughout times, both sites present abrupt changes of the channels at a single time interval (around 5 years) and stable channels sustained at all other times. This indicates that those channel changes was caused by sudden changes of the hydro-geomorphology in the channel; after the hydro-geomorphologic conditions return to normal, the channel would remain stable. The channels at the anabranching structures at the last 90º turn has the most traceable progressive lateral migration, which has gradually shifted towards the right bank in the maximum of 200m from 1985 to 2015. Different from normal channel behaviors in meandering bends, the big channel bend was completely immobile in the previous 30 more years.

The cross section at the bend apex shows a pattern that is similar to that at a meander bend. The asymmetric channel has the thalweg close to the outer bank, and the deepest pool is 37m deep at the stage of 6 m (during 2011 field work). Because the channel here is highly stable which prohibits erosion to happen at the outer bank, the pool then has the potential to further deepen, unless the bed touches cohesive material or bedrocks. Besides the immobile channel at the channel bend, the lack of active point bars at the inner bank also help excludes the possibility of this channel being an active meander. Scroll-bar pattern can be found in satellite images at the inner bank, which

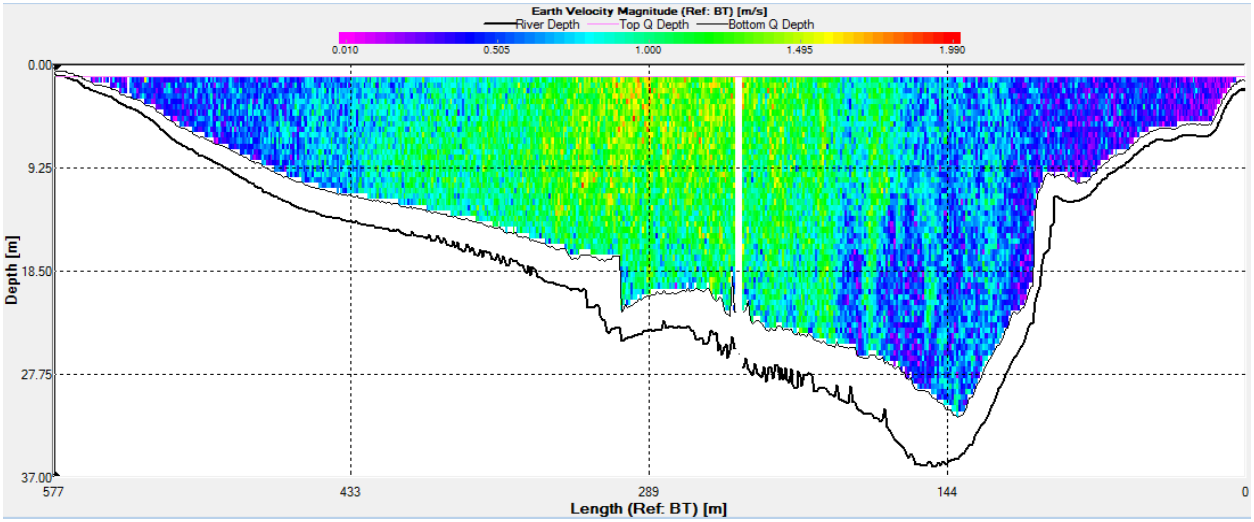


Figure 4.3
Cross section morphology and velocity profile at the apex of the channel bend in reach 1, measured by ADCP. Left side is the inner bank and right side is the outer bank of the channel bend. River flows into the page.

possibly indicates past lateral migration of the channel. The migration stopped at the latest in 1985, possibly farther before that, as the outer bank reaches to the cohesive material at today's outer bank and channel migration was forced to shut down.

The multi-temporal analysis of the studied reaches was conducted for around every five years from 1985 to 2015, depending on the availability and quality of data (see introductions in Chapter 3). The range of water stages associated with the satellite images used was kept as minimal as possible, and channel planform change will be presented in this chapter for every five-year (or close) interval and a 19-year interval, from 1991 to 2010.

There are lots of traceable channel changes from 1991 to 2010. Similar to the pattern of lateral migration, single-thread channels experience less channel change in terms of erosion and deposition, while river segments with anabranching structures,

particularly near the first and last 90º turn, had more dramatic channel evolution. The width of channels, including single-thread and branches, varied very little through times. This is given by the circumstances that erosion and deposition occurred equivalently at each site where channel changes occurred. The only significant channel change in single-thread channels occurred near the apex of the channel bend, where a 0.55 km² area was deposited at the inner bank, with no equivalent erosion at the outer bank. As shown in Figure 4.4, the width of newly deposited and eroded areas can reach up to 50% of the width of the branches in anabranching channels. Except for this site, other segments of single-thread channels: the segment before the first 90º turn, the segment between the first and second 90º turn, the segment downstream to the bend apex but before the next 90º turn, are all very stable in this 19-year interval.

The patterns of channel change at the two anabranching structures of this reach (the first and the last 90º turns) are different. Despite the fact that they may look similar and symmetric to the channel bend, the upstream anabranching structure had fewer islands and fewer island areas, which also had less channel change compared to the downstream anabranching structure. The upstream anabranching structure had two islands in 1991, one was located right at the turning point of the channel, and the other one located right downstream to the upstream island, divided by a 1.9 km wide branch channel. While the downstream island had almost no channel change except extremely little areas of erosion on the island head and tail and thin area of deposition along the side, the upstream island encountered 1.2 km² erosion on the side of the left branch, and split into another separate island right above it with 0.5 km² newly formed area at the

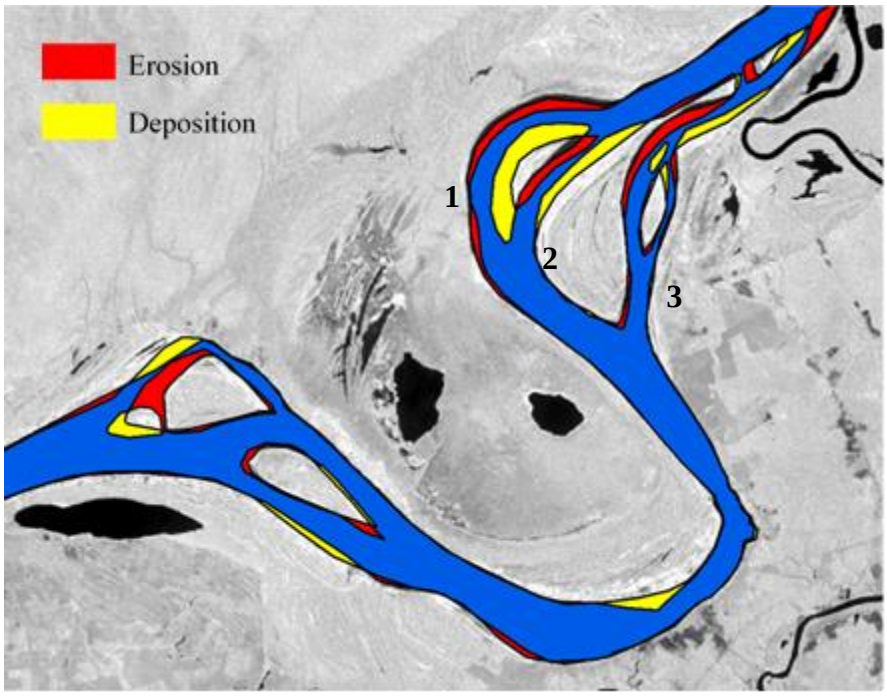


Figure 4.4
Channel evolution of reach 1, from 1991 to 2010. Areas shown in blue represent water surface areas unchanged, and areas shown in red and blue represent the sizes of erosion and deposition, respectively. The river flows from right to left on the page. Background Landsat image was taken in 2010.

upstream end. Accompanied by the erosion at the left branch, deposition also occurred on the other side of the bank. The areas of deposition and erosion in the upstream anabranching structure are close.

Channel change at the downstream anabranching structure (the last 90º turn of this reach) is more complex. First, the number of islands and their areas in 1991 were both greater than those at the upstream anabranching structure. There were in total 4 islands, which composed of 15.2 km² in 1991. As of 2010, there was at least a new small island formed in the branch in between two larger islands, and the total island area increased to 16.8 km². The growth of island area here was not mainly contributed by the

newly formed island; instead, the island located at the most left-bank-side had grown to 1.5 times of its original size in 1991. Second, the patterns of erosion and deposition in different branches in this anabranching structure differed. The most left-bank branch (marked #1 in Figure 4.4) had erosion along the left bank and deposition along the right bank (on the island), but the deposition belt was obviously wider than erosion belt, whereas erosion belt was longer because it was located at outer curvature. The branch next to branch 1 towards the right-bank direction (marked #2 in Figure 4.4) had similar erosion and deposition area, while the deposition belt along the right bank is slightly longer. The branch closest to the right bank (marked #3 in Figure 4.4) consisted of sub-branches due to the small mid-channel islands. Erosion in there occurred along the left bank of the branch, with no significant area of deposition on the other side of the bank until the branch switched its direction and became parallel to the wider branch on the left-bank side. The newly-formed island, shown in yellow in the middle of branch 3, was located right before the branch turned direction. Further downstream, erosion occurred on the right bank of the branch at the place when the river returns to a single-thread channel. Third, the shapes of the island in this downstream anabranching structure are generally long which yield to the flow direction of the channel. The island in between branch 2 and 3 is wide near its upstream end, but it forms an elongated shape downstream. The most downstream small island, by its location and shape, was seeming to be an extension of the long-and-thin island upstream. As erosion occurred on both sides near the downstream end of the island, it would possibly split in the near future to form another separate, small island downstream.

During the 1991-2010 time interval, the total area of deposition and the total area of erosion in reach 1 is largely equivalent, with 8.3 km² of deposition and 8.4 km² of erosion, which led to 0.1 km² of net erosion.

Channel change within each 5-year (or so) interval was more moderate than that occurred in the 19-year period (Figure 4.5). As the patterns of channel change from 1985 to 1991, single-thread channels were largely immobile in each of the 5-year interval, whereas the two anabranching structures at the first and last 90º turns experienced more channel change. Although deposition occurred on one side of a channel is uaually accompanied by erosion occurred on the other side of a channel in the analysis of 1991-2010 interval, the correspondence of erosion and deposition was not presently obviously in the analysis of each 5-year interval. Instead, in channels where deposition and erosion are each found on one side of the bank from the 1991-2010 analysis, deposition and erosion did not actually occur simultaneously. In particular, deposition generally occurred first, following with erosion in the next one or even two 5-year intervals. The erosion rate, compared to deposition rate, was also small, which occurred in very long and thin belts. Under a small scale as what is used in Figure 4.5, those long-and-thin erosion belts may not be represented clearly on the map. The total areas of deposition and erosion of the entire reach 1 varied in different time intervals, and net deposition and net erosion occurred intermittently in this reach (Figure 4.25 in the last section of this chapter). Although deposition and erosion were equivalent (only 0.1 km² difference) in the 1991-2010 interval, they fluctuated more in each 5-year interval. A net deposition occurred in the intervals of 1985-1991 and 2000-2004, and a net erosion occurred in the intervals of

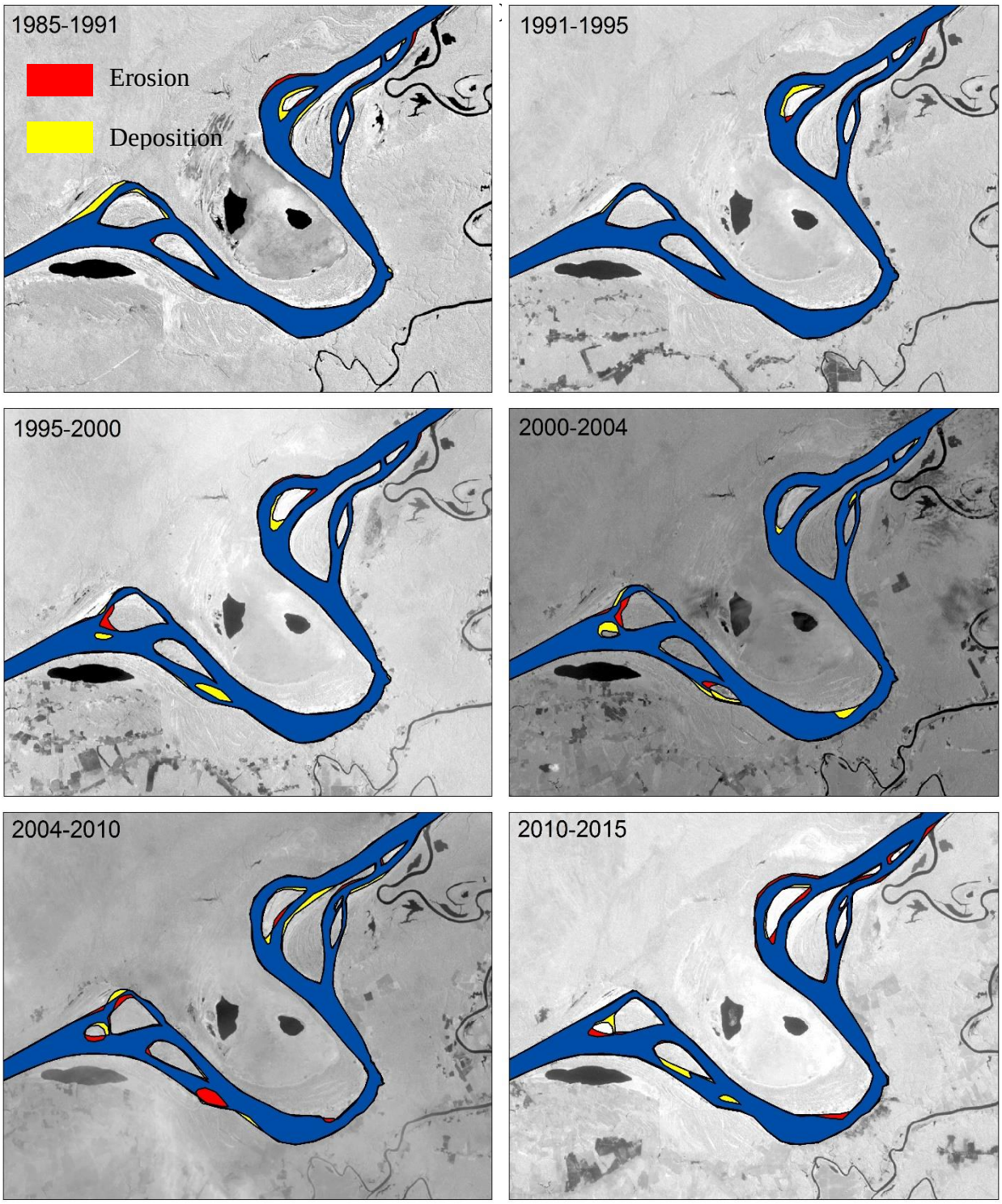


Figure 4.5
Channel evolution of reach 1, for every about 5-year interval, 1985-2015. Areas shown in blue represent water surface areas unchanged, and areas shown in red and blue represent the sizes of erosion and deposition, respectively. The river flows from right to left on the page. Background Landsat images were taken in each ending year of each 5-year (or so) interval.

1991-1995, 1995-2000, 2000-2004, and 2010-2015. The most intense erosion occurred during 2010-2015, and the most intense deposition occurred during 2000-2004.

In addition to the temporal variation described in the preceding passages, the spatial variation of channel morphology on the Madeira River is dramatic too. According to satellite images and field measurements, a number of spatial variations are illustrated, making the river dynamically active in both temporal and spatial scales. As water discharge of the studied reaches during 2013 field work campaign was very close (average discharge measured in single-thread channels in all three reaches is ~31,000 $m^3/s$) to the bankfull value at Porto Velho (30,000 $m^3/s$), data of 2013 is used to describe bankfull characteristics. The data collected in a lower discharge season in 2011 field work campaign, are presented at the end of this chapter.

Bankfull width, depth, and w/d vary dramatically in reach 1. The range of width in single-thread channels is between about 800 m and 1800 m, in which, the later value is more twice as large as the former. Widths of branch channels have more variation, ranging from 400 m to 1800 m in a stage near bankfull. Compared to many other anabranching rivers, the Madeira River has a smaller channel width, which is consistent with its relatively-thinner floodplain. The highest widths are located just upstream to places where channels start to split and form bifurcations. This trend can easily be traced in satellite images, where single-thread channels always widen and are followed with anabranching structures. The widths of branches vary greatly, as a larger branch is generally wider. The formation of a new mid-channel bar, like the one newly formed in the right branch of the downstream anabranching structure, can directly halve the width

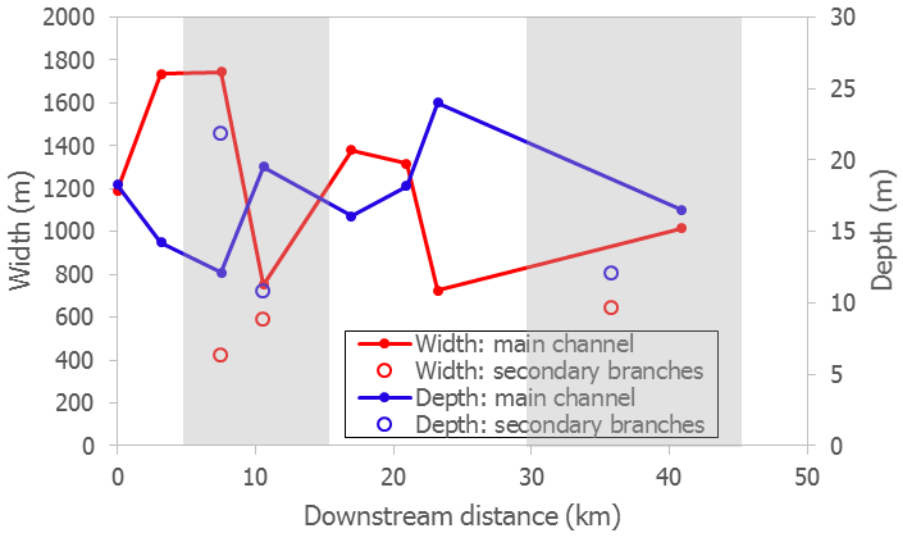


Figure 4.6
Channel bankfull width and depth of reach 1, measured by ADCP in bankfull stage (2013). Shaded sections indicate anabranching structures, and unshaded sections represent single-thread structures. Dots connected by line include cross sections of single-thread channels and the major branches in anabranching structures measured, and circles represent data for secondary branches.

of the channel. Channel depth (mean depth of each cross section) at this reach ranges from 13 m to 24 m for single-thread cross sections. In branches, it ranges from about 12 m to 23 m. Depths of branch channels can be either higher or lower than the depths in single-thread channels, depending on the form and processes conditions. For both width and depth in this reach, their spatial fluctuations do not have obvious difference among single-thread channel structures and anabranching structures, given that a branch can be as wide or deep as a single-thread channel. The values of *w/d* in reach 1 show a big variety as well as it ranges from below 30 to above 120 for single-thread channels, and the highest value in anabranching structures can reach above 140, indicating the channel is very wide comparing with its depth. It is also shown in reach 1 that channels with

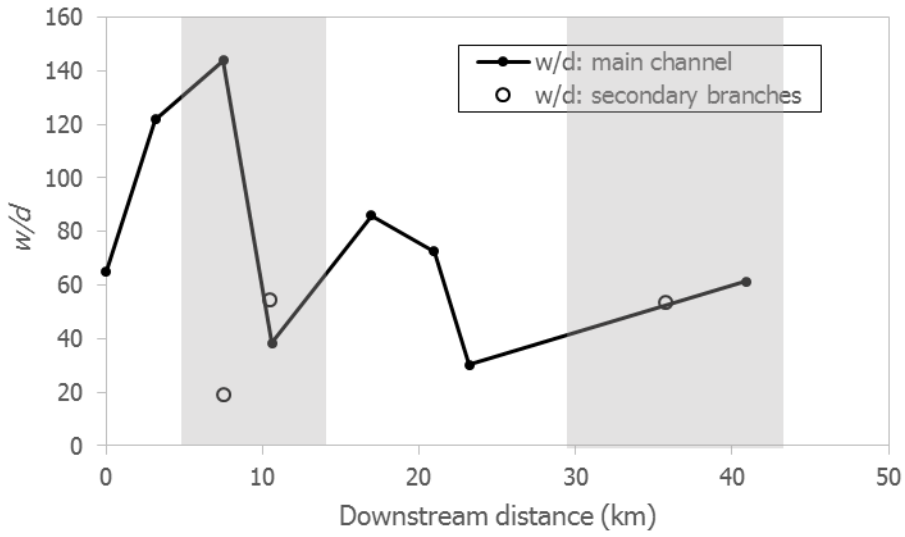


Figure 4.7
Channel bankfull *w/d* of reach 1, based on the data of width and depth in bankfull stage (2013). Shaded sections indicate anabranching structures, and unshaded sections represent single-thread structures.

bigger width normally have smaller width, vice versa. The spatial pattern of *w/d* is very similar to that of channel width. This trend can also be traced in 2011-low stage conditions, shown in figure 4.14. This demonstrates that spatial pattern of channel width alone in single-thread channels and major branches is able to indicate the spatial pattern of *w/d*, which is further an indicator of channel hydraulic radius. During low stage, channel depth dramatically decreases while channel width stays relatively constant, and *w/d* increases, with the largest value reaching up to 400 right before the channel bifurcates at the upstream anabranching structure.

Bankfull velocity in reach 1 stays relatively stable in single-thread channels and major branches in anabranching structures, ranging between 1.2 m/s to 1.7 m/s, whereas flow in secondary branches are slower. The two fastest flow measured, with their values

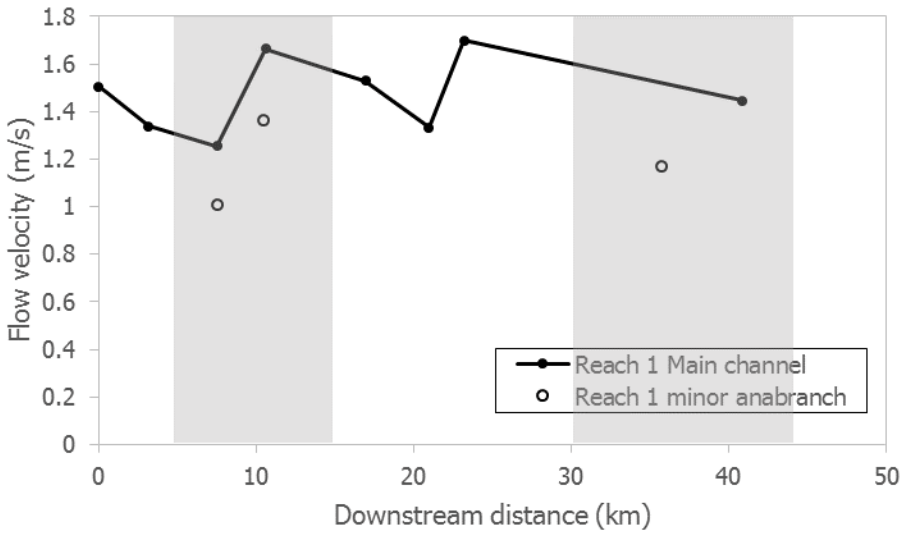


Figure 4.8
Average cross-sectional velocity in bankfull discharge of reach 1, based on ADCP data in bankfull stage (2013). Shaded sections indicate anabranching structures, and unshaded sections represent single-thread structures.

greater than 1.6 m/s, occurs one at the apex of the channel bend and the other one at the major branch in the upstream anabranching structure, after the first 90º turn. During low stage, as flow velocity generally decreases, a greater range is also presented, from 0.3 m/s to 1.5 m/s in single-thread channels and major branches. The velocity of flow at the apex of the channel bend, however, is significantly lower than many other cross sections measured in this reach in low-stage season, and the slowest flow of single-thread channels in reach 1 (also the slowest in all three reaches) is located 3 km downstream to the bend apex. From the data of low-stage season, flow velocities in major branches of anabranching structures are the local high values, compared to channels upstream and downstream to it. This trend is also reflected by the data of bankfull conditions in the upstream anabranching structure.

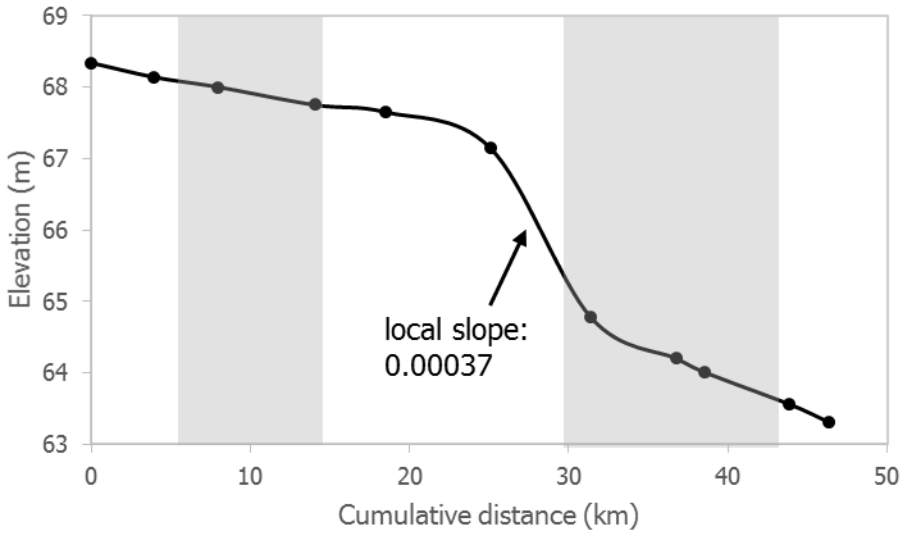


Figure 4.9
Elevation profile of reach 1. The dots represent locations where elevation is measured. Shaded sections indicate anabranching structures, and unshaded sections represent single-thread structures. The segment with the highest slope is labeled and pointed with an arrow.

The general slope of the entire reach 1 is 0.00012, calculated by knowing the elevation values of the reach's start and end points, as well as the course distance of the channel. The general slope of this reach is one to three times the slope values of most large anabranching rivers in the world, and is even three times as big as the slope recorded in Porto Velho (Latrubesse, 2008). The high slope in this reach is contributed by a unique segment of the river with a dramatically high value that reaches to more than 0.0003, meaning the channel elevation drops 0.3 m for every 1 km of downstream distance, shown in the elevation profile in Figure 4.9. This particular segment, starting from the 90º left turn downstream to the apex of the channel bend and ending at the bifurcation of the downstream anabranching structure, is significantly steeper than other segments upstream and downstream to it. It is a single-thread, straight channel which has

the narrowest section upstream, right downstream to the 90º left turn, and gradually widens until the channel bifurcates. The local slope of the channel upstream and downstream to this steep segment, is actually around 0.00005, with the downstream channel slightly steeper than the upstream channel. The two anabranching structures, marked in shaded zones in the figure, are mostly dominated by a gentle slope. The location of the bifurcation in the downstream anabranching structure (where the second shaded zone starts) occurs at the same location of when the steep channel returns to gentle, indicating that a gentles slope is more likely to produce an anabranching structure.

### 4.2 Reach 2: A pseudo-meander with a downstream anabranching structure

The second reach we identified starts 18 km downstream to the ending point of the first reach. It is a 36 km-long segment with multiple channel pattern developed. Anabranching channels account for about 20% of total length as of 2015 (see shaded areas in Figure 4.17). Although it doesn't present complex anabranching structure like what reach 1 has, changes on channel pattern is drastic in the past three decades. The dominant feature of this reach is a mobile single-thread channel followed by a stable anabranching structure. The river flows to the northeast direction at the upstream part of this reach with the channel pattern between single-threaded and anabranching (a large island only existed in the 1985-1991 interval, see the description of channel evolution), then gradually turns its direction to towards southeast, forming a meander-bend-like morphology (pseudo-meander). After that, the channel bifurcates and forms an anabranching structure, with a rhombus-shaped island that is 4 km long and 1.2 km wide

at its widest part. Downstream to the anabranching structure, the channel returns single-thread as the end of this reach. Looking at the whole reach, there is a considerable area of sand bars formed near islands and in secondary branches, as well as on the inner bank of the pseudo-meander.

Reach 2 floodplain shows a diverse pattern in terms of the size and distribution. As shown in Figure 4.1, the active floodplain is formed on both sides of channel banks at the entire reach except for the downstream anabranching structure. Upstream to the pseudo-meander, floodplain width on the left bank side is larger than that on the right bank side: the widest left-bank floodplain is more than 10 km at the beginning of this reach, and the width of the right-bank floodplain varies in 0-3 km. The floodplain then quickly narrows down towards the pseudo-meander, and stays relatively narrow at the after the pseudo-meander, at about 2 km wide on both sides, before it disappears at the anabranching structure. Mid-channel islands as part of the floodplain exist in this reach. Older Holocene and Pleistocene floodplain surround present-day floodplain. As very few or no active floodplain is formed at the anabranching structure, Holocene and Pleistocene floodplain remained next to the channel. The shape of present-day floodplain and Holocene and Pleistocene floodplain are similar to the channel shape. Older deposits and terraces are distributed semi-symmetrically. Holocene deposits at the outer bank of the pseudo-meander reaches far north into the Pleistocene deposits, which possibly indicates that today's pseudo-meander once had a greater sinuosity in the Holocene. There is also a narrow belt of active floodplain connected to the apex of the pseudo-meander, which indicates the deposits of a tiny tributary.

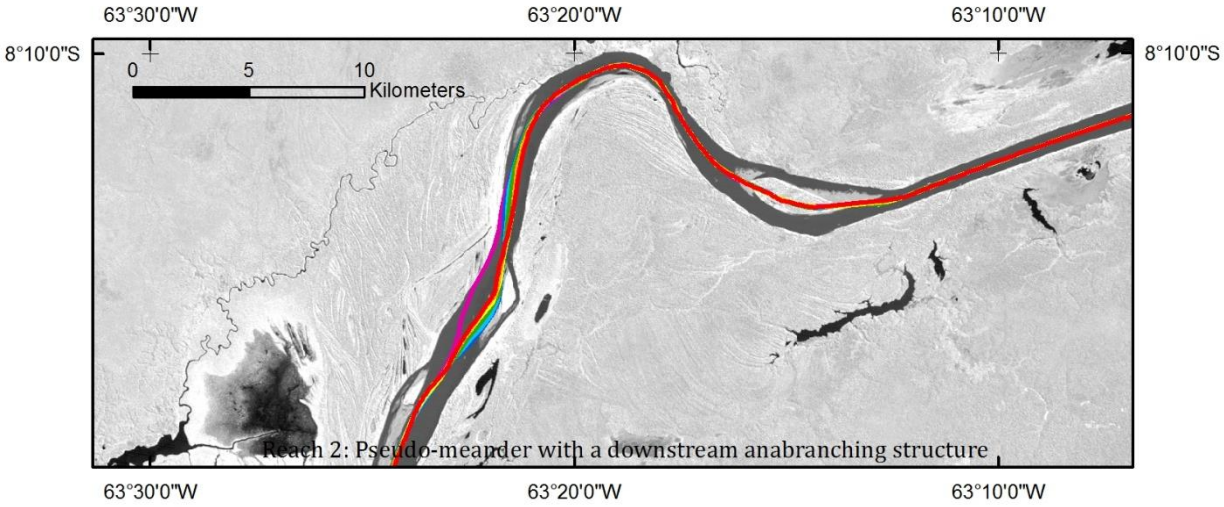


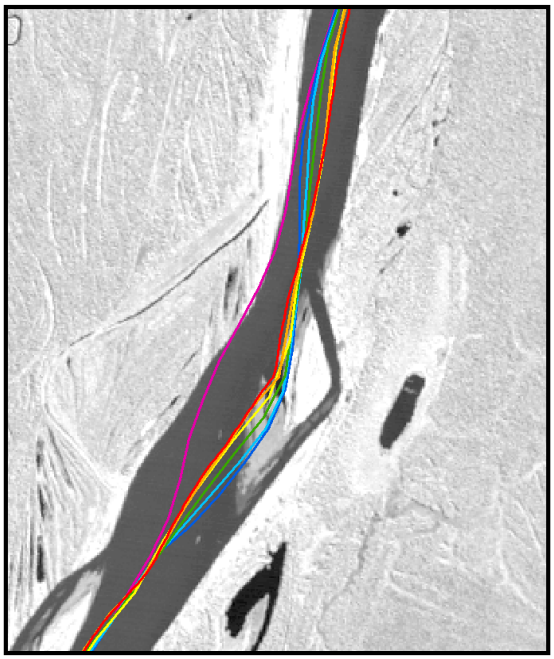

Figure 4.10 a (top) and b (bottom)
a) Reach 2 centerlines in 1985, 1991, 1995, 2000, 2004, 2010, 2015, represented in purple, blue, cyan, green, yellow, orange, and red, respectively. The overlapped lines indicate small lateral migration of the channel. b) Zoom-in view of the segments with lateral migration.

Channel migration in reach 2 is more prominent, compared to reach 1. The first half of this reach has obvious channel migration, whereas the second half of the reach has

almost no migration. At the beginning of this reach, the channel has no traceable migration. It then becomes more active downstream at the place where an anabranching structure was present only in the 1985-1991 interval but disappeared after 1991. In particular, the abandoned of a secondary branch of the left bank (see channel evolution section below) between 1985 and 1991 caused the channel centerline shift to the right-bank direction for 1.5 km. After 1991, this channel segment gradually shifted back, towards the left bank. From 1991 to 2015 it has shifted 420 m, at the migration of rate of about 17 m/year (Figure 4.10b). Channel migration also occurred in the channel segment right downstream (Figure 4.10b). This channel segment gradually shifted to the right-bank direction at relatively constant speed. Since 1985, the channel centerline has traveled 470 m, equivalent to the migration rate of about 16 m/year, a value very close to the migration rate at the upstream channel segment after 1991. Downstream to these two segments, the channel maintains highly immobile, including the pseudo-meander and the anabranching structure.

Channel changes from 1991 to 2010 in reach 2, with an identical pattern of channel migration, occurred in the first half of the reach upstream to the pseudo-meander. There were no significant channel changes at the beginning 2 km of this reach. As approaching the former anabranching structure, there was a small area of erosion on the left bank, together with a new-formed depositional island in the channel. This island is connected to a long sand bar upstream to it, of which the upstream end is even above the beginning point of reach 2. The right bank, on the other side of the channel, had a tiny area of erosion, which is possibly caused by the lateral aggradation of the sand bar and

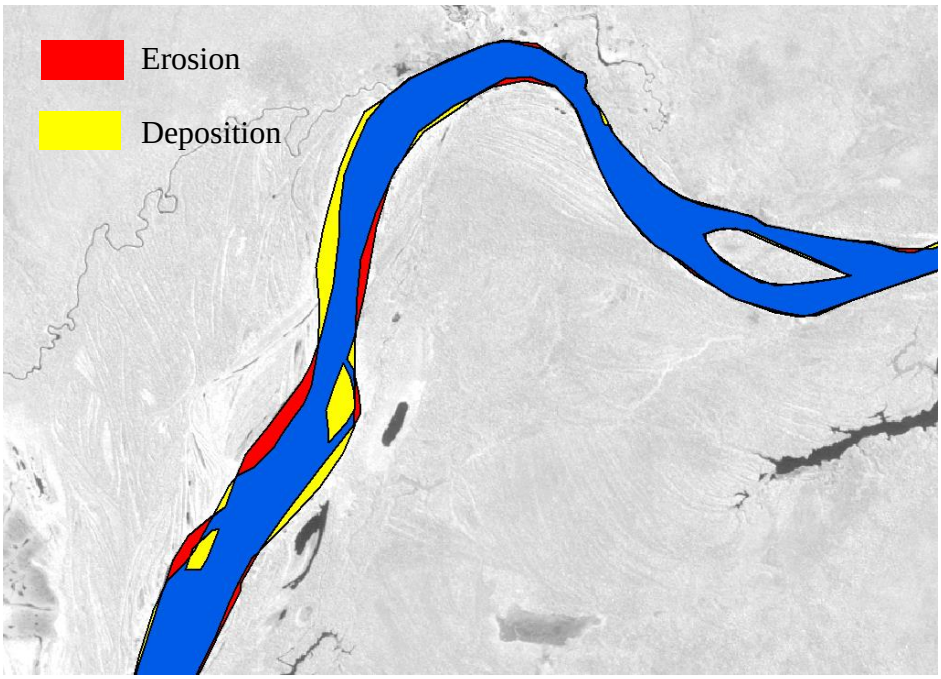


Figure 4.11
Channel evolution of reach 2, from 1991 to 2010. Areas shown in blue represent water surface areas unchanged, and areas shown in red and blue represent the sizes of erosion and deposition, respectively. The river flows from right to left on the page. Background Landsat image was taken in 2010.

the island. Downstream to them, erosion and deposition occurred along on the left and right bank, respectively. The erosion belt is slightly wider than the deposition belt, but another newly formed island was present on the right bank, separated by a narrow branch from the deposition belt. As the former anabranching structure returned single-threaded after 1990, the multi-temporal analysis for the 1991-2010 interval does not show changes of that. In the further downstream channel, the deposition and erosion belts switched positions: the left bank experienced deposition, and the right bank experienced erosion. In there, the depositional belt is slightly wider than the erosion belt on the other side. The semi-symmetric pattern of erosion and deposition along the two sides of bank led to

lateral migration of the channel, which is demonstrated by the centerline analysis: at the former anabranching structure area, the channel migrated towards the left bank at the rate of 17 m/year; the channel right downstream to it migrated towards the right bank at the rate of 16 m/year. Consequently, this channel segment has become straighter.

No significant channel changes occurred in the second half of reach 2. As normal river meanders constantly shift towards the outer-bank direction by eroding the outer bank and depositing a point bar on the inner bank, the meander-like bend in reach 2 does not have any migration in the past three decades. Neither does it have a well-developed point bar. Therefore, it is given the name "pseudo-meander". The only traceable channel changes occurred in the inner bank of the pseudo-meander, of which the inner bank had little areas of deposition (0.2 $km^2$) and erosion (0.15 $km^2$) occurred. In the downstream anabranching structure, the channel is highly stable until the ending point of this reach.

During 1991-2010, there was the total of 5.87 $km^2$ deposition and 4.01 $km^2$ erosion occurred in reach 2, which led to 1.86 $km^2$ net deposition (see Figure 4.26 at the end of this chapter). The net deposition is mostly caused by the newly formed island on the channel at the former anabranching structure in the first half of this reach.

The analysis of channel evolution in each 5-year (or so) interval since 1985 presents historical channel changes in shorter time intervals (Figure 4.12). The prominent channel change in 1985-1991, as mentioned above, is the abandonment of a secondary branch which made the channel return single-threaded. Within this 6-year period, the secondary branch was quickly filled with sediment and the raised bed largely prevents water from flowing in even at a low stage. Deposition also occurred along the left bank of

the main channel near the junction of the secondary branch. Erosion concurrently happened along the left bank of the main channel, upstream to the deposition area along the bank. On the right bank of the main channel, erosion occurred on the opposite side of both the erosion and the deposition area. In 1991-1995, the channel was changed mostly by depositing two new islands, one located at the beginning of reach 2, and the other located on the right bank at the former anabranching structure. Symmetric erosion and deposition were also presented: at the former anabranching structure, the channel shifted towards the left bank by eroding the left bank the depositing on the right bank; downstream to the former anabranching structure, the channel shifted towards the right bank by eroding the right bank and depositing on the left bank. In 1995-2000, the pattern of channel change largely remained the same and the two islands aggregated and became larger. In 2000-2004, the two islands did not expand, but a larger deposition area was formed on the right bank next to the island at the former anabranching structure. In 2004-2010, a large portion of the island at the beginning of this reach was eroded, whereas the other island had little lateral aggregation. During the last 5-year interval, 2010-2015, erosion became the dominant way of channel change. The island at the beginning of the reach expanded again at its upstream end, which was the only deposition occurred in 2010-2015.

The area analysis of erosion and deposition for each 5-year interval (Figure 4.25 at the last section of this chapter) shows that, the area of erosion was smaller than that of deposition in all the time intervals except the last one, 2010-2015. This means a net deposition occurred in this reach throughout 1985-2010. The largest net deposition area

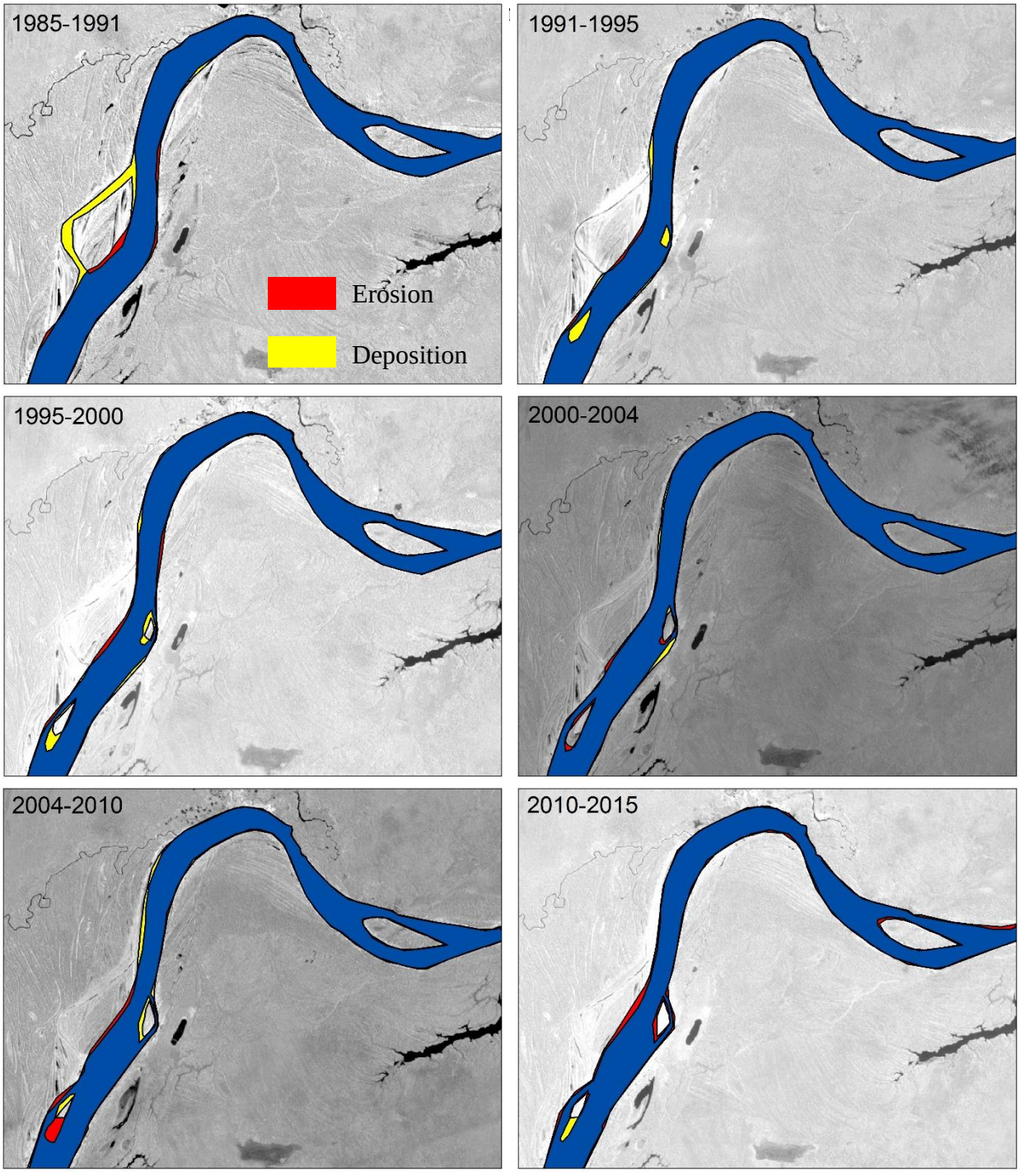


Figure 4.12
Channel evolution of reach 2, for every about 5-year interval, 1985-2015. Areas shown in blue represent water surface areas unchanged, and areas shown in red and blue represent the sizes of erosion and deposition, respectively. The river flows from right to left on the page. Background Landsat images were taken in each ending year of each 5-year (or so) interval.

occurred in 1985-1991 (2.36 km²), and the smallest occurred in 2010-2010 (0.09 km²) showing a general decreasing trend throughout the 30 years that the multi-temporal analysis was conducted on. In 2010-2015, the net erosion area (3.38 km²) offset more than half of the accumulated net deposition area in the past 25 years.

The evolution of the former anabranching structure in the first half of this reach well shows the mechanism of the abandonment of secondary branches and further, the final stage of an anabranching structure in large rivers. The secondary branch stayed active and filled with water in 1985, but in a few years, filled with sediment. From the images we selected that are taken in relatively low stages, the average width of it in 1985 is 250 m, and it reduced to 100 m in 1988. In 1991, the branch evolved to a ditch-sized channel that is only 30-40 m wide, partially blocked by sediment (Figure 4.13). The island surface had many scroll bars. Those scroll bars, as seen in 1985, looks more obvious than the scroll bars on the floodplain outside the banks. Some of them even had water in between. These are the indications of the island's younger age, as well as the evidence of lateral accretion of the island. Most parts of the island was vegetated in 1985 except the west corner covered by a bare-surfaced bar where it is located on the inner bank of a channel bend of the secondary branch. As the secondary branch was then abandoned, the west corner of the island gradually got vegetated and became part of the floodplain. Scroll bars on the island also became more polished and evolved into the surrounding floodplain.

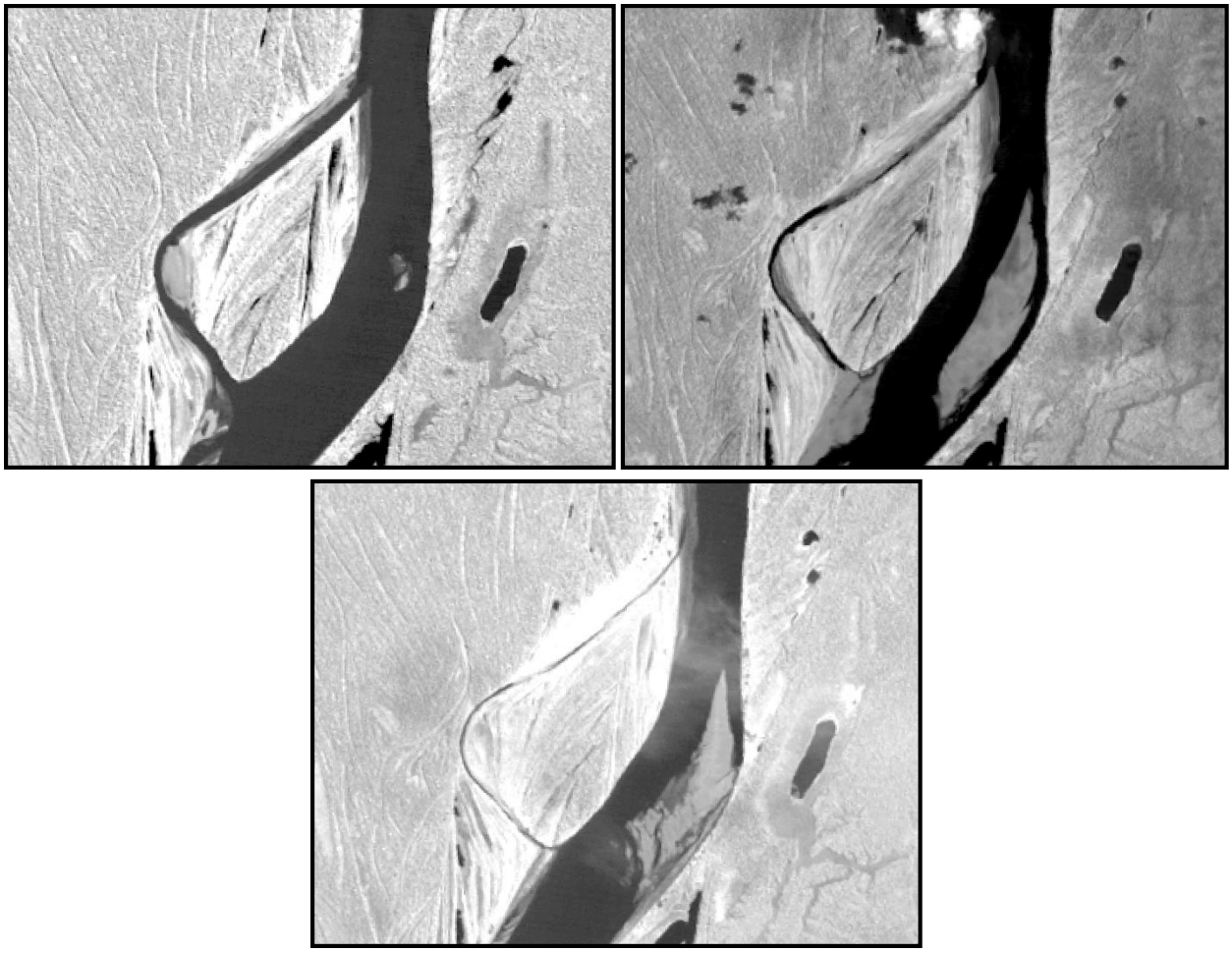

Figure 4.13
Evolution of an anabranching structure in reach 2, shown in 1985 (top left), 1988 (top right), 1991 (bottom). Rivers flows upwards.

The general slope of reach 2 is 0.000064, meaning the 6.4 cm drop per 1 km. This value, as elevations were not measured at any point within this reach, is computed by rise over run based on the most downstream available data in reach 1 and the most upstream available data in reach 3, and the distance of the channel course between these two points.

The width of single-threaded channels ranges from 500 m to 1800 m, and each segment within this reach did not have profound changes in terms of channel width. In anabranching structures, channel widths of major branches are within the range of single-threaded channels as well, whereas the secondary branches differed: the secondary branch of the disappeared anabranching structure was pretty narrow when it was active, and the one of the downstream anabranching structure had similar width with its corresponding major branch. Wider channels tend to form at right the bifurcations in front of anabranching structures, where sand bars are prominent during low-stage seasons. The narrowest channel, located right downstream to the pseudo-meander, is confined by unilateral geologic control on the left bank (Figure 4.14b). The 650 m-wide channel formed a deep pool near the left bank as an extension of the outer bank of the pseudo-meander right upstream. The deepest point is -40 m and the average depth of the cross section is 26 m at bankfull stage, a value that is significantly higher than others in this reach. The morphology of the cross section shows a similar pattern as a meander, where the thalweg is closer to the outer bank and that, the slope of the inner bank is smaller. Scroll bars can be traced from both satellite images and the right bank in the ADCP profile, which indicates past channel migration. Despite the fact that the pseudo-meander has not migrated over the past three decades, it was once active by eroding the

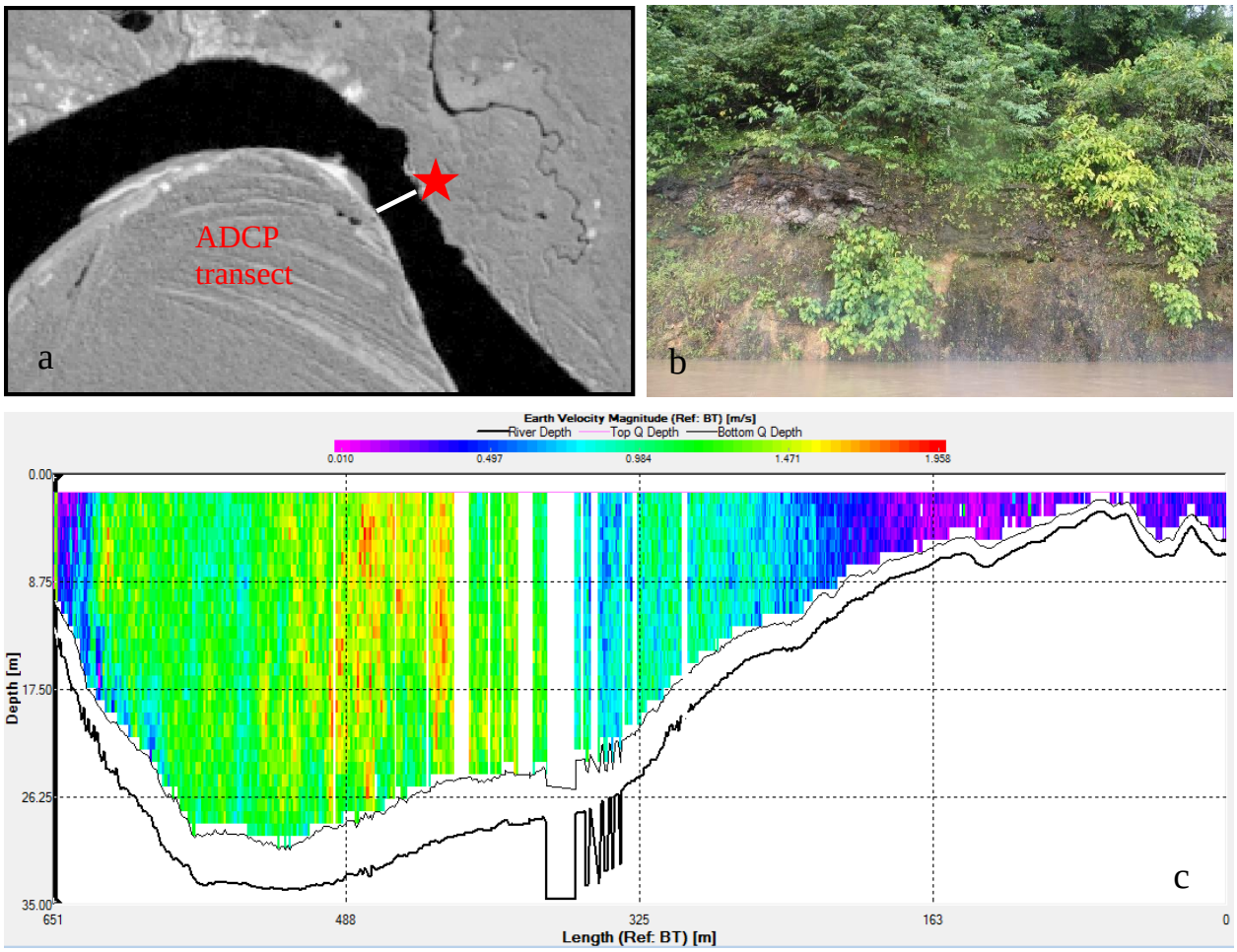


Figure 4.14

a) Locations of the picture in b), marked as a star, and ADCP profile in c), marked as a white line. River flows to the right; b) The left bank behaves as geologic control which shut down channel migration at this site; c) Cross section morphology and velocity profile of the narrowest channel, measured by ADCP. Left side is the left bank and right is the right bank. River flows into the page.

outer bank and forming point bars and scroll bars at the inner bank side. Once the channel reached cohesive materials as geologic control, it stopped migrating outwards and the extra energy was concentrated on incising the bed near the outer bank. The cross section morphology and the processes here are similar to the large channel bend in reach 1.

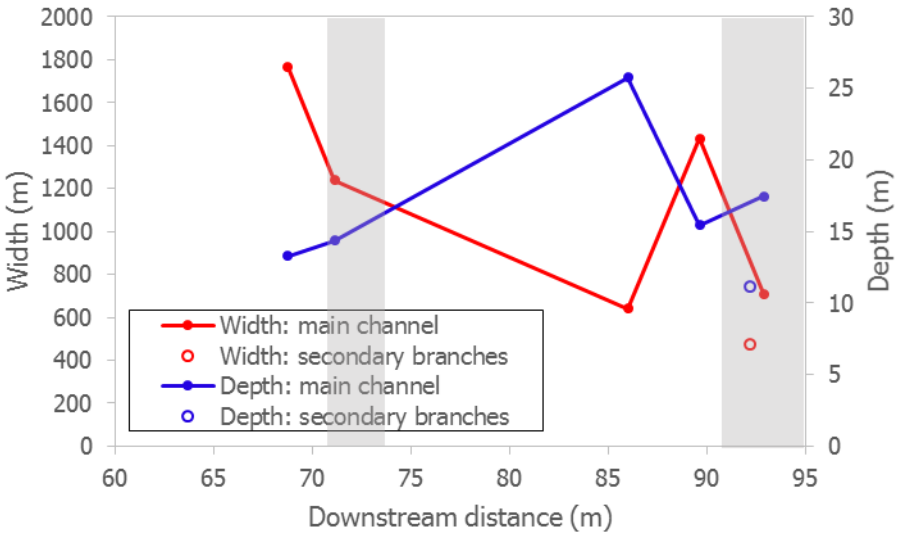


Figure 4.15
Channel bankfull width and depth of reach 2. Shaded sections indicate anabranching structures, and unshaded sections represent single-thread structures. Dots connected by line include cross sections of single-thread channels and the major branches in anabranching structures measured, and circles represent data for secondary branches.

Bankfull width, depth, and w/d in reach 2 are presented in Figure 4.15. As this reach was not surveyed during bankfull stage during the field work in March 2013, bankfull width is directly taken from non-bankfull data from 2012 field work because increased discharge within the channel hardly alters channel width. Bankfull depth is computed by adding the difference between the water stage in 2012 field work (7.78 m at Porto Velho) and bankfull stage (~13.83 m at Porto Velho) to the ADCP data collected in 2012 field work. The relations between width, depth, and *w/d* shows a similar pattern as the first reach: the downstream trend of channel width and depth are negatively related and that of *w/d* is highly similar to channel width. The range of *w/d* in bankfull condition is between 25 and 132. The narrowest point in this reach, described above, has the

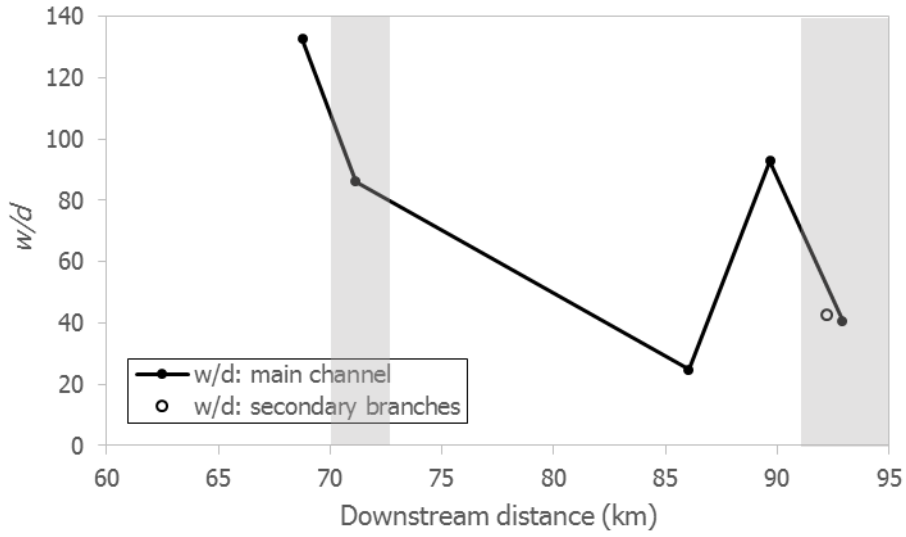


Figure 4.16
Channel bankfull *w/d* of reach 2. Shaded sections indicate anabranching structures, and unshaded sections represent single-thread structures.

smallest *w/d*. Channels with higher values of *w/d* are located closely above bifurcations as the starting point of anabranching structures. Compared to those, the major branches of anabranching structures have lower *w/d* values.

Flow velocity in reach 2 during a low water stage, measured in the field work in July 2011, ranges between 0.8 and 1.1 m/s in single-threaded segments (Figure 4.28 in the last section of this chapter). Velocity peaks are observed in the major branch of the two anabranching structures.

## 4.3 Reach 3: A single-threaded straight channel with a downstream anabranching structure

The third reach, as the most downstream reach we defined, is located right downstream to the second reach. The 35-km-long channel begins below the confluence of

the downstream anabranching structure in reach 2, where the second reach ends. Anabranching-structured channel accounts for about 31% of the total length of this reach, while the other channel segments are single-threaded. This reach is generally flowing in northeast direction, with some minor local changes and that the last 4 km of it flows to the north. The dominant feature of the first half of this reach, which is 17 km long, is a single-thread and straight channel with sinuosity close to one. Followed that is a large anabranching structure with a big sand bar formed in front at the middle of the channel. Its length is about 11 km. As of 2015, the anabranching structure is composed of three sub-islands in different sizes that are split by λ-shaped tiny branches. Sand bars are mostly exposed in the most upstream sub-island. Two branches are formed in the anabranching structure, and the right branch is visibly wider than the left one. The confluence, as the ending point of the anabranching structure, is 11 km downstream to the beginning of it where vegetation starts to grow. Downstream to the confluence, the channel gradually shifts its direction in a reversed "S" pattern with a lateral bar formed on the right bank. The rivers flow towards the north at the end of this reach.

Active floodplains, Holocene floodplain deposits, and Pleistocene units are all present in this reach, which formed along the channel (Figure 4.1). The active floodplain is relatively narrow compared to that of the previous reaches, particularly for the first 11 km. In this reach, the width of the active floodplain is proportional to the sinuosity of the channel. A straighter channel is formed with a narrower floodplain. The first 11 km of this reach forms a very straight channel with its sinuosity of nearly one, and the floodplains on each side of the banks are less than 1 km wide, whereas the channel width

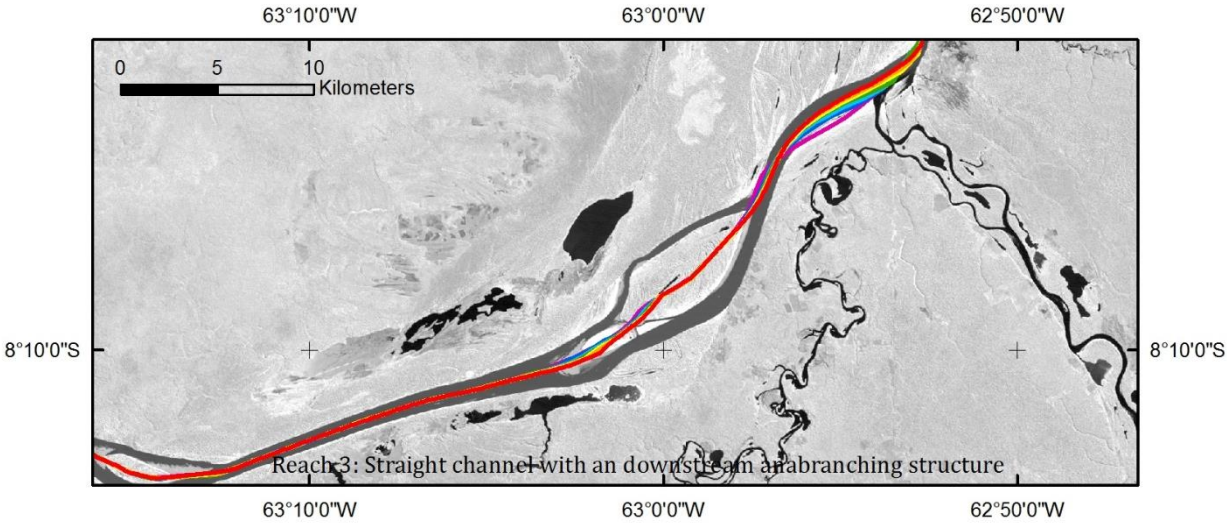


Figure 4.17
Reach 3 centerlines in 1985, 1991, 1995, 2000, 2004, 2010, 2015, represented in purple, blue, cyan, green, yellow, orange, and red, respectively. The overlapped lines indicate small lateral migration of the channel.

at this segment is 600-800 m at bankfull stage. The first 8 km doesn't even have active floodplains on the left bank. The floodplains get much wider where the straight channel bifurcates and divides into two branches. The channel itself is also wider there because of the central bar formation in front of the island. There is a small meandering tributary joining the Madeira River on its right bank, at the end of reach 3, forming active floodplains along its channel. Holocene floodplains are significantly wider along this reach. They are located in the outer regions of today's floodplains, and are larger on the side of the left bank than those on the right bank. Pleistocene units, as terrace deposits, covers a vast amount of area at the further outer regions. Several floodplain lakes are developed as well. Most of them are on the left-bank-side within the Holocene floodplain regions.

The patterns of channel migration of reach 3 are similar to the pattern of floodplain width that channels with narrower floodplains also experienced less lateral migration. The analysis of channel centerlines of the past three decades shows very little to no lateral migration for the first 11 km, single-threaded straight channel. The stability of the channel weakens at the bifurcation area and the anabranching structure below, where we see a gradual migration towards the right bank. It then returns immobile at the second half of the anabranching structure, by its longitudinal length. After the anabranching confluence where the channel returns single-threaded, lateral migration is present again. The first 2 km of the channel migrated towards the right bank, and the following 8 km, before the channel turns the direction to north, migrated at a dramatically faster rate towards the left bank. All three migration zones in this reach: the one at the bifurcation, the one after confluence, and the one followed downstream, show gradual migration with similar rates in between each interval. In the map (Figure 4.17), this pattern is shown by the sequential color change from purple to red and similar distance between the lines. The most downstream migration zone had the largest migration rate in this reach. From 1985 to 2015, the channel centerline has traveled about 920 m at the point with the largest migration, which is equivalent to about 30 m/year. There was another small island there at the left bank, where the channel turns direction to the north. The island became part of the left-bank floodplain during 2000-2004, making a local pattern of channel migration not sequential. The evolution of that island and the channel is presented in the following passage.

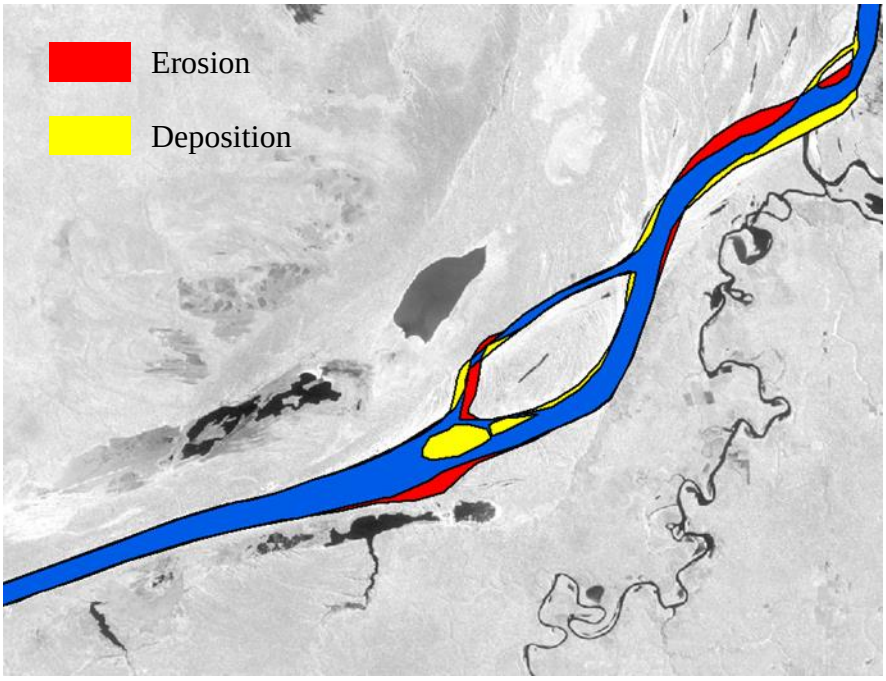


Figure 4.18
Channel evolution of reach 3, from 1991 to 2010. Areas shown in blue represent water surface areas unchanged, and areas shown in red and blue represent the sizes of erosion and deposition, respectively. The river flows from right to left on the page. Background Landsat image was taken in 2010.

As shown in Figure 4.18, channel changes during 1991-2010 are prominent in this reach, with most of the changes occurred at the bifurcation and its surrounding areas, and the channel segment between the anabranching confluence and the turning point of the channel to the north. The beginning 11 km, as illustrated by the centerline, was highly stable. No traceable erosion and deposition occurred in the channel until right above the bifurcation, where about 1.5 km² of the right bank was eroded longitudinally. Together with that, there was about 3 km² of newly formed area emerging at the channel center as the aggradation of the existed island. As of 2010, those newly-formed surface was divided from the main island, by λ-shaped small branches. In the first 2 km of the

secondary branch, erosion and deposition zones were symmetrically located along the two sides of the banks. Immediately downstream to that, the zones of erosion and deposition switched their sides. In the major branch, an elongated deposition zone was formed along the left bank and it extended to the left bank of the channel after the confluence. No significant erosion was present in response to the deposition zone on the right bank of the major branch. Another prominent channel change was located downstream to the anabranching confluence, where about 2.4 km² erosion occurred on the left bank, and an equivalent area of deposition occurred on the right bank. Before the channel turns to the north, there was a small island on the left bank. The branch of it was then abandoned, making the island connected to the floodplain. Subsequently, half of the island was eroded after the abandonment of the branch.

There was the total of 9.73 km² deposition and 7.74 km² erosion occurred in reach 3, leaving 1.99 km² net deposition. The net deposition was contributed by the aggradation of the island in the dominant anabranching structure of this reach.

Figure 4.21 presents channel changes for each 5-year (or so) interval. The temporal pattern of that shows dramatic differences from time to time. In 1985-1990, we see very little erosion occurred on the right bank above the bifurcation and little deposition and erosion symmetrically occurred in the secondary branch. Elongated deposition existed on the left bank of the major branch. The erosion and deposition downstream to the confluence were very dramatic, and the small island in the most downstream channel was yet becoming part of the left-bank floodplain. In 1990-1995 and 1995-2000, the entire reach 3 become relatively stable, with limited channel changes

ongoing in the places with former channel changes. The place with dramatic erosion and deposition in 1985-1991 had many small sizes of erosion and deposition as well. During 2000-2004, a large deposition area was formed in front of the island, leading to the bifurcation move upstream. Little erosion also occurred on the right bank of the bifurcation channel. The small island near the end of this reach was also connected to the left-bank floodplain. Besides those, the rest of the channel was highly immobile, including places with previous channel changes. During 2004-2010, the front island of the dominant anabranching structure continued to accrete with some other alternations in between that and the big island behind. Erosion continued on the right bank of the bifurcation. The zones of erosion and deposition downstream to the anabranching confluence became larger and traceable. After 2010, deposition was almost shut down in this reach, while significant erosion zones are presented in places with previous channel changes. The single-threaded straight channel was highly stable at all times throughout the 30 years. For the dominant anabranching structure of this reach, while new islands were developed in its upstream part, the downstream portion of the island neither aggregate nor shrink over the 30-year of analysis.

It is well illustrated in Figure 4.18 and 4.19 that channel change in the bifurcation and the surrounding area led to three consequences of the channel: widening, narrowing, and migration without channel width change. For the channel at and immediately above

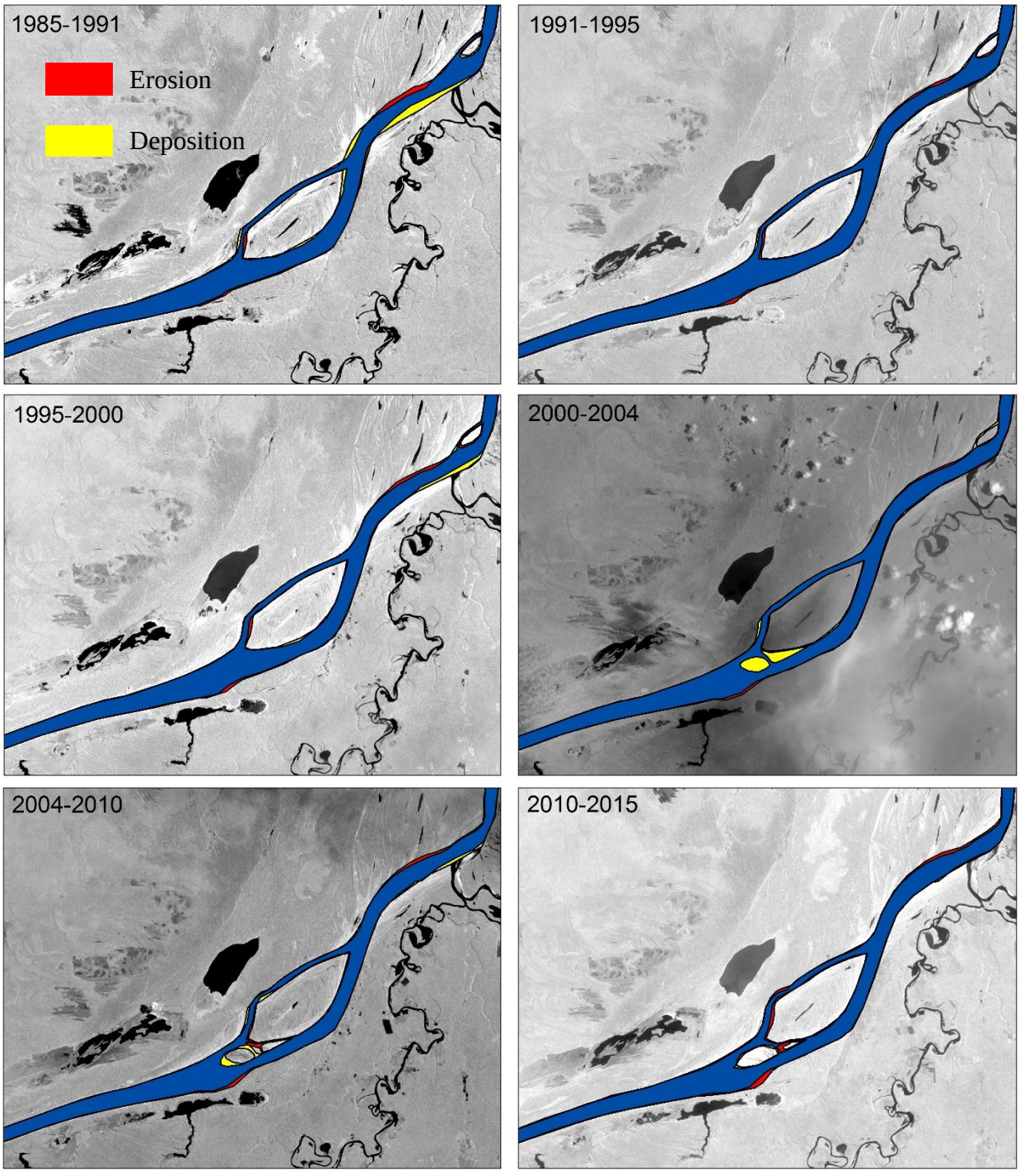


Figure 4.19
Channel evolution of reach 3, for every about 5-year interval, 1985-2015. Areas shown in blue represent water surface areas unchanged, and areas shown in red and blue represent the sizes of erosion and deposition, respectively. The river flows from right to left on the page. Background Landsat images were taken in each ending year of each 5-year (or so) interval.

the bifurcation, widening happened with continuous erosion on the right bank but offset by deposition on the other side. The major branch of the anabranching structure experienced slight narrowing by deposition on its left bank and no erosion on the other side of the bank. Channel migration, with no significant width adjustment, occurred in the first half of the secondary branch.

Although the big island of the dominant anabranching structure in this reach only aggradated at its upstream end by forming new alluvial land, while maintaining its downstream part largely the same size over the past 30 years, the presence of scroll bars indicates history of its lateral and vertical accretion. Those scroll bars were developed in different directions, with those near the left-bank side of the island parallel to the direction of the channel, and those near the right-bank side of the island perpendicular but slightly curved to the channel. Scroll bars with the later direction show well-organized downstream sequence, indicating that the island was expanding downstream while deposition was active there. The scroll bars parallel to the channel demonstrates the interactions between channel and floodplain on the island, that the flow in the channel scoured away pre-existed floodplains on the island and deposited new alluvial material to form new floodplains.

For the entire reach, a net deposition scenario was present in the intervals of 1985-1991, 2000-2004, and 2004-2010, and net erosion scenario was present in the intervals of 1991-1995, 1995-2000, and 2010-2015. 1985-1991 and 2000-2004 created the largest deposition area, and 2010-2015 created the largest erosion area.

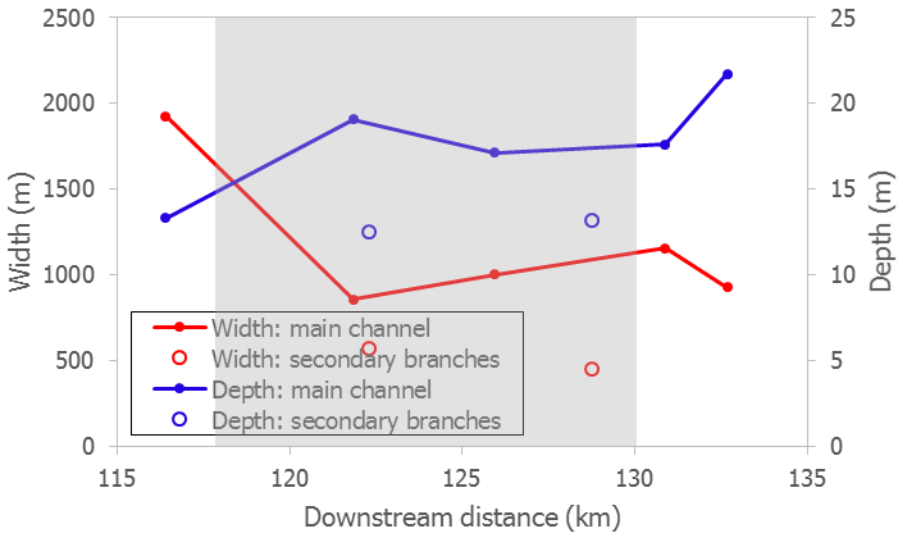


Figure 4.20
Channel bankfull width and depth of reach 3, measured by ADCP in bankfull stage (2013). Shaded sections indicate anabranching structures, and unshaded sections represent single-thread structures. Dots connected by line include cross sections of single-thread channels and the major branches in anabranching structures measured, and circles represent data for secondary branches.

Bankfull width in reach 3, among the cross-sections measured by ADCP, ranges between roughly 1000-2000 m for single-threaded channels and the major branch of anabranching structure. The width of the secondary branch is smaller, which is between 450-600 m. Width-averaged bankfull depth ranges between 14-22 m for single-threaded channels and the major branch, whereas the secondary branch is shallower as well, for about 13 m deep. Similar to the pattern reach 1 and 2 have, the downstream trend of channel width and depth show a quasi-negative correlation in single-threaded and the major branch channels, that a wider channel is shallower, and vice versa. The widest channel we recorded by ADCP, among cross-sections in single-threaded and the major branch channels, is almost 2000 m, and is located immediately above the bifurcation.

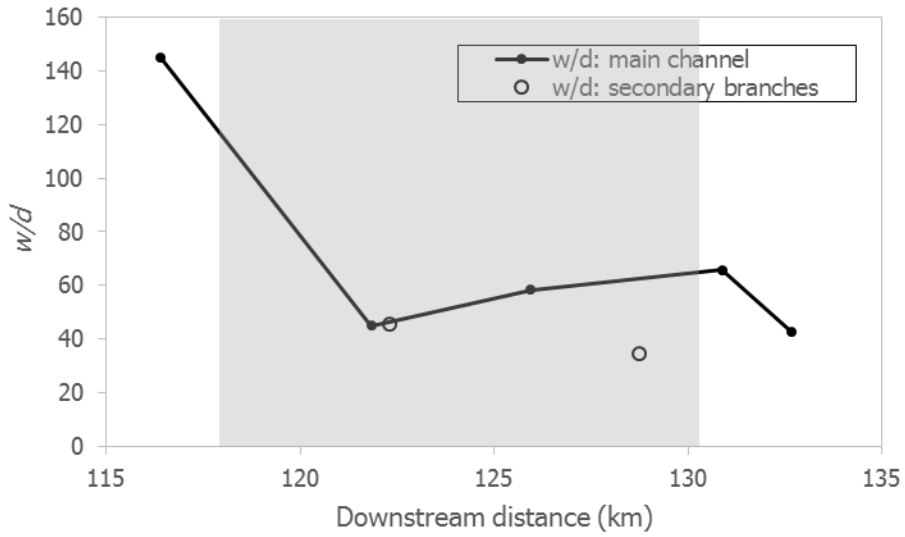


Figure 4.21
Channel bankfull *w/d* of reach 3. Shaded sections indicate anabranching structures, and unshaded sections represent single-thread structures.

This is also the shallowest cross-sections in the group. The deepest channel is located downstream to the anabranching confluence, with the average depth of about 22 m. The width of it is 925 m, which is the second smallest one recorded in this reach. Neither channel width nor depth has dramatic difference between single-threaded channels and the major branch of the anabranching structure. Although the width of the major branch is smaller than that immediately above the bifurcation, it in fact has similar width with other portion of single-threaded channels in this reach. The depth of the major branch is larger than that above the bifurcation but smaller than the channel downstream to the anabranching confluence. The value of *w/d* in reach 3 show a big range as the previous two reaches. The channel immediately above the bifurcation (the most upstream cross-section) has the largest *w/d*, of more than 140, and the most downstream cross-section we measured, downstream to the anabranching confluence, has *w/d* of about 40. Except the

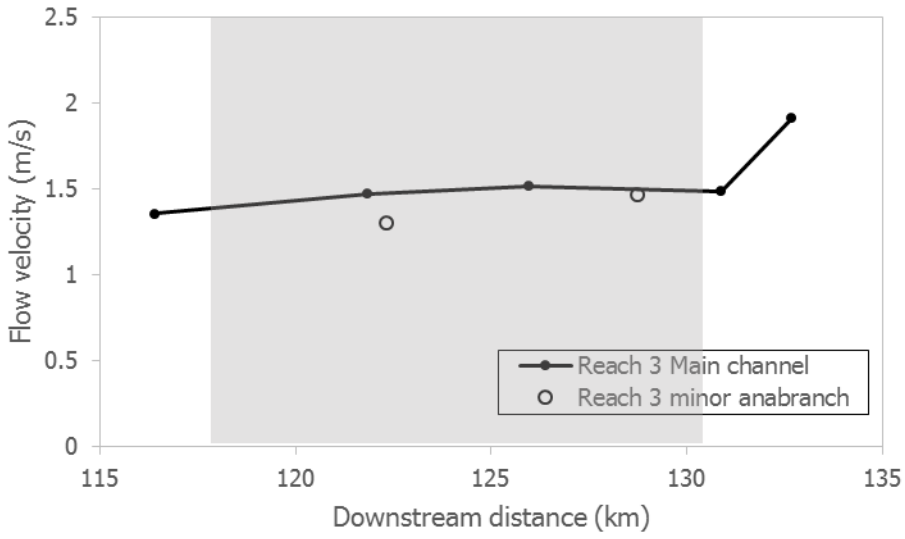


Figure 4.22
Average cross-sectional velocity in bankfull discharge of reach 3, based on ADCP data in bankfull stage (2013). Shaded sections indicate anabranching structures, and unshaded sections represent single-thread structures.

most upstream one, all other channels, including single-thread, major branch, and secondary branch, have the *w/d* within 34-66. Among the two cross-sections of the secondary branch, the upstream one has a very similar *w/d* value with that of the major branch. The downstream cross-section in the secondary branch has a smaller *w/d* value: 34.

Flow velocities among the 8 ADCP transects measured in reach 3 show an interesting similarity (Figure 4.22). Except the most downstream cross-section which had the average flow velocity of about 2 m/s, all other cross-section, including those located on single-threaded channels, major and secondary branches of anabranching structure, had flow velocities close to 1.5 m/s. Flow in the secondary branch had slightly smaller velocity, but the difference is less than 0.3 m/s. No significant velocity trend can be found

between the flow above and below the bifurcation. The cross-section at the confluence (second last point in the figure) had very similar flow velocity with those upstream ones. The most downstream cross-section, located 2 km below the anabranching confluence, had dramatic higher velocity than others.

The general slope of this reach is 0.000087, calculating by applying the elevation difference divided by longitudinal distance of the first and last points measured on the right bank (Figure 4.23). The elevation data was collected at multiple locations within and near the dominant anabranching structure of this reach, shown in Figure 4.23. Three points were measured on the left bank and four were measured on the right bank. In the anabranching structure, the left bank is actually the bank of the secondary branch, and the right bank is the bank of the major branch. The elevation profile were drawn separately in this case for the purpose of recognizing the slope difference between the two branches. It is found that, for the first 40% of the anabranching structure by its longitudinal downstream distance, the secondary branch had a greater slope than the major branch. For the rest 60% of its longitudinal downstream distance, the major branch had a greater slope than the secondary branch. The slope then increased abruptly immediately downstream to the anabranching confluence, which became four times bigger than that of the major branch (right bank). The turning point, as shown in Figure 4.23, is right at the confluence (right edge of shaded section). The difference of the elevation profiles between the two branches demonstrate different morphodynamic and hydrodynamic conditions within a typical anabranching structure. It is possibly due to the combination of two effects: bed slope difference (morphodynamics) and backwater (hydrodynamics).

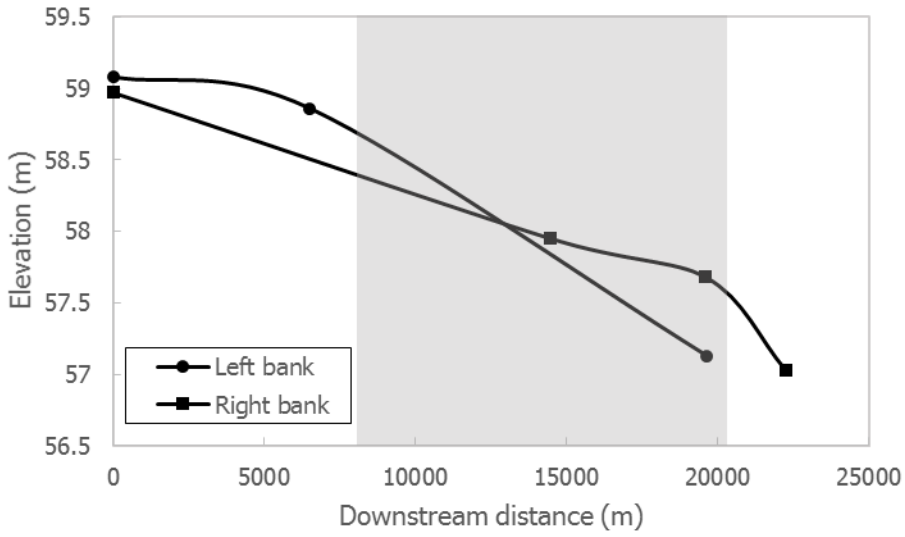


Figure 4.23
Elevation profile of partial reach 3. The dots represent locations where elevation were measured. Shaded sections indicate the dominant anabranching structure in this reach. Elevation was measured on both banks. The left bank corresponds to secondary branch in the anabranching structure, and the right bank corresponds to major branch in the anabranching structure. The most upstream point measured is located about 8 km (8000 m) upstream to the bifurcation (left edge of shaded section).

For bed slope difference, the secondary branch is shown to have a slope advantage; for backwater effect, the major branch is shown to "push" the water flowing out of the secondary branch and prevent it from flowing out. The most downstream channel segment, which had the largest slope, also had the fastest flow (Figure 4.22) and the largest lateral migration rate. This demonstrates the relations between slope, flow velocity, and migration rate, that, a larger slope tends to contribute to a faster flow and more active channel change, assuming the same cohesiveness of floodplain.

### 4.4 Data synthetization for all reaches

Previous three sections of this chapter have introduced the geomorphology and channel changes of the three reaches of the Madeira River downstream to Porto Velho, Brazil. In the meantime that all the three reaches we defined constitute an anabranching channel system, each reach has its uniqueness that reflects different morphodynamic conditions.

As presented in preceding sections, channel changes were analyzed in two temporal scales: 19-year interval (1991-2010) and each five-year interval (four to six years, depending on data quality and availability; 1985-2015). The area of deposition and erosion in each reach, for both the 19-year interval and each five-year interval, is

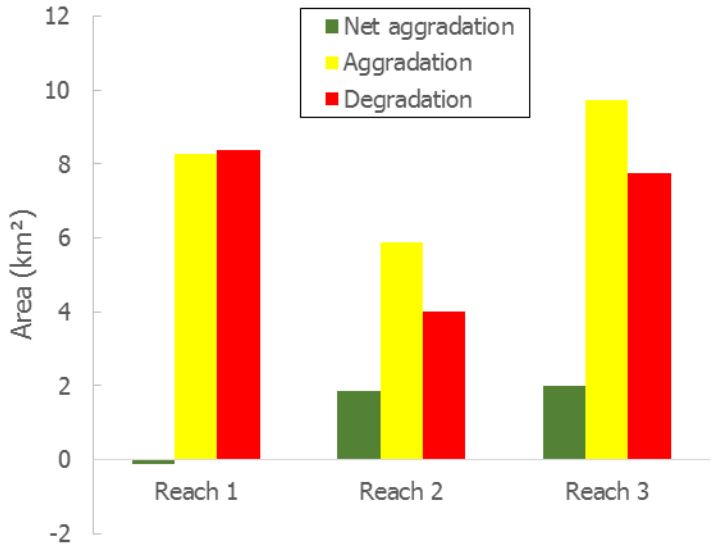


Figure 4.24
Area of erosion (degradation) and deposition (aggradation) between 1991 and 2010, for all three reaches.


Figure 4.25
Area of erosion (degradation) and deposition (aggradation) for each 5-year (or so) interval from 1985-2015, for all three reaches.

synthesized in Figure 4.24 and 4.25, respectively. From the 19-year interval analysis, reach 1 is shown to have the largest erosion area, and reach 3 had the largest deposition area. In addition, reach 1's deposition area was very close to its erosion area, which made

the net deposition area close to zero, while the other two reaches both had deposition areas greater than erosion areas, which results in tremendous net deposition (about 2 $km^2$ for each of reach 2 and 3). This shows a quasi-equilibrium morphodynamic condition of reach 1, and non-equilibrium morphodynamic condition of reach 2 and 3, during the 19 years. In the five-year interval analysis, larger temporal and inter-reach variation was present, as shown in in Figure 4.25. Among the six intervals, 1985-1991 and 2000-2004 had all three reaches with positive net deposition, and 2010-2015 had all three reaches with negative net deposition, whereas the other intervals had both positive and negative net deposition among the three reaches. Thus, 1985-1991 and 2000-2004 can be characterized as deposition-dominant, and 2010-2015 can be characterized as erosion-dominant, in terms of the morphodynamic conditions. The other three intervals: 1991-1995, 1995-2000, and 2004-2010, while the patterns of morphodynamics among the reaches were different, the areas of net deposition (either positive or negative) for any single reach, within any single time interval, was dramatically smaller than those in 1985-1991, 2000-2004, and 2010-2015, except reach 2 in 2000-2004. The values of the net deposition for those time intervals with alternative morphodynamic patterns among reaches were within ±1 $km^2$. Some of them were very close to 0. This indicates the general accordance of morphodynamic conditions of the three reaches that, although small inter-reach variation existed, the three reaches had largely the same morphodynamic response in reaction to large events that were able to produce drastic channel changes.

For all six intervals, channel changes were analyzed, reach 1 had the largest area of erosion than those of reach 2 and 3. The areas of deposition of reach 1 also exceeded those of reach 2 and 3, except the 1985-1991 interval that reaches 1 and reaches 3 had almost the same area of deposition. Reach 2 had the smallest area of deposition in the three reaches, for all six intervals, whereas its deposition areas varied, compared to the other two reaches. The net deposition of reach 2 remained positive in all intervals except 2010-2015, which was the only reach that had a continuous net deposition from 1985 to 2010. The last interval, 2010-2015, presented unique morphodynamic patterns among the six intervals because the three reaches consistently experienced the largest erosion and relatively weak deposition. The areas of deposition in 2010-2015 were the smallest for reach 2 and 3, compared to their respective previous areas of deposition. Therefore, the three reaches had the largest negative net deposition value, which means the most severe net erosion in the Madeira channel. The erosion event during this period was consistent with the closure and construction of two large dams: the Santo Antonio and the Jirau dams. While previous studies have illustrated the potential impact of the dams on the river geomorphology (e.g. Fearnside, 2013; Fearnside, 2014), the analysis results here best demonstrates the dramatic impact caused by the dams in terms of downstream channel scouring.

Previous sections of this chapter introduced bankfull characteristics of river channel for each reach in terms of a channel mean depth, width, *w/d*, and flow velocity at each ADCP transects measured during the three years' field work. In Figure 4.26, those variables at low-discharge season (about 7,600 $m^3/s$) are also presented in downstream

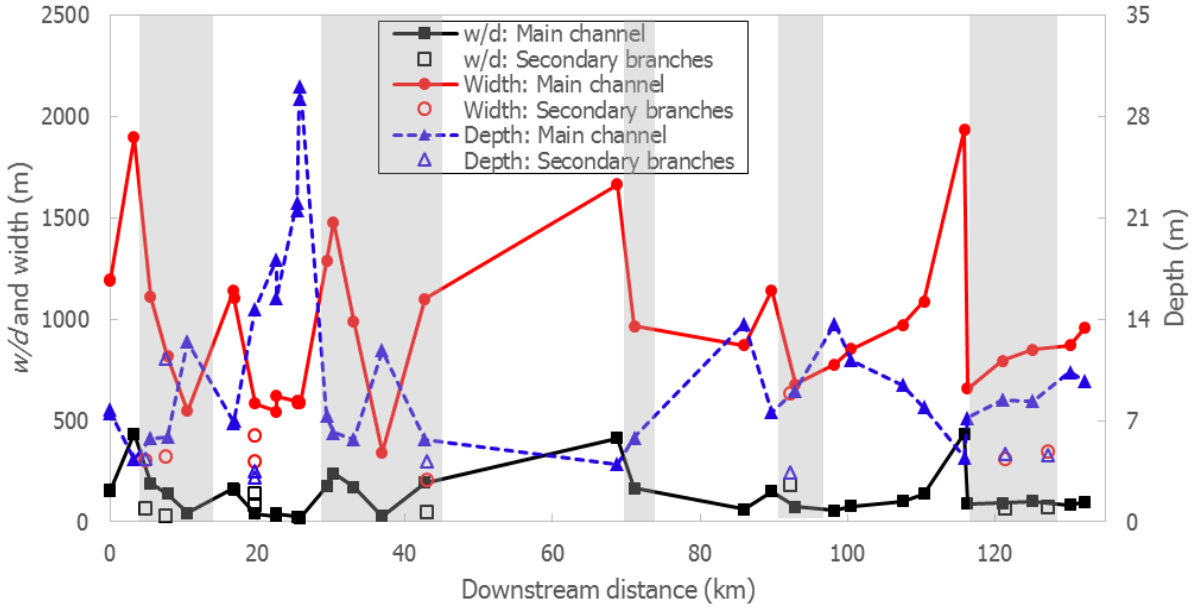


Figure 4.26
Channel width, depth, and *w/d* of all three reaches during low discharge (about 7,600 $m^3/s$; 2011 field work), in downstream distance, which starts at the beginning of reach 1 and ends at the ending of reach 3. Each dot represents an ADCP transect. Shaded sections indicate anabranching structures, and unshaded sections represent single-thread structures.

distance. All three reaches herein are combined together, and shaded and unshaded sections in the graph represent anabranching and single-threaded structures, respectively. Several observations can be derived. First, in the comparison of the bankfull width and low-discharge width, there's not a dramatic difference, which illustrates the weak dependence of channel width to the discharge variation. Second, although the deepest point presented in Figure 4.26, at low-discharge, is larger than that at bankfull discharge, most other ADCP transects show an obvious reduction of depth at low-discharge. The reason of that highest depth value at low-discharge is that the density of ADCP transects during the field work at low discharge (2011) was higher than that that during the field

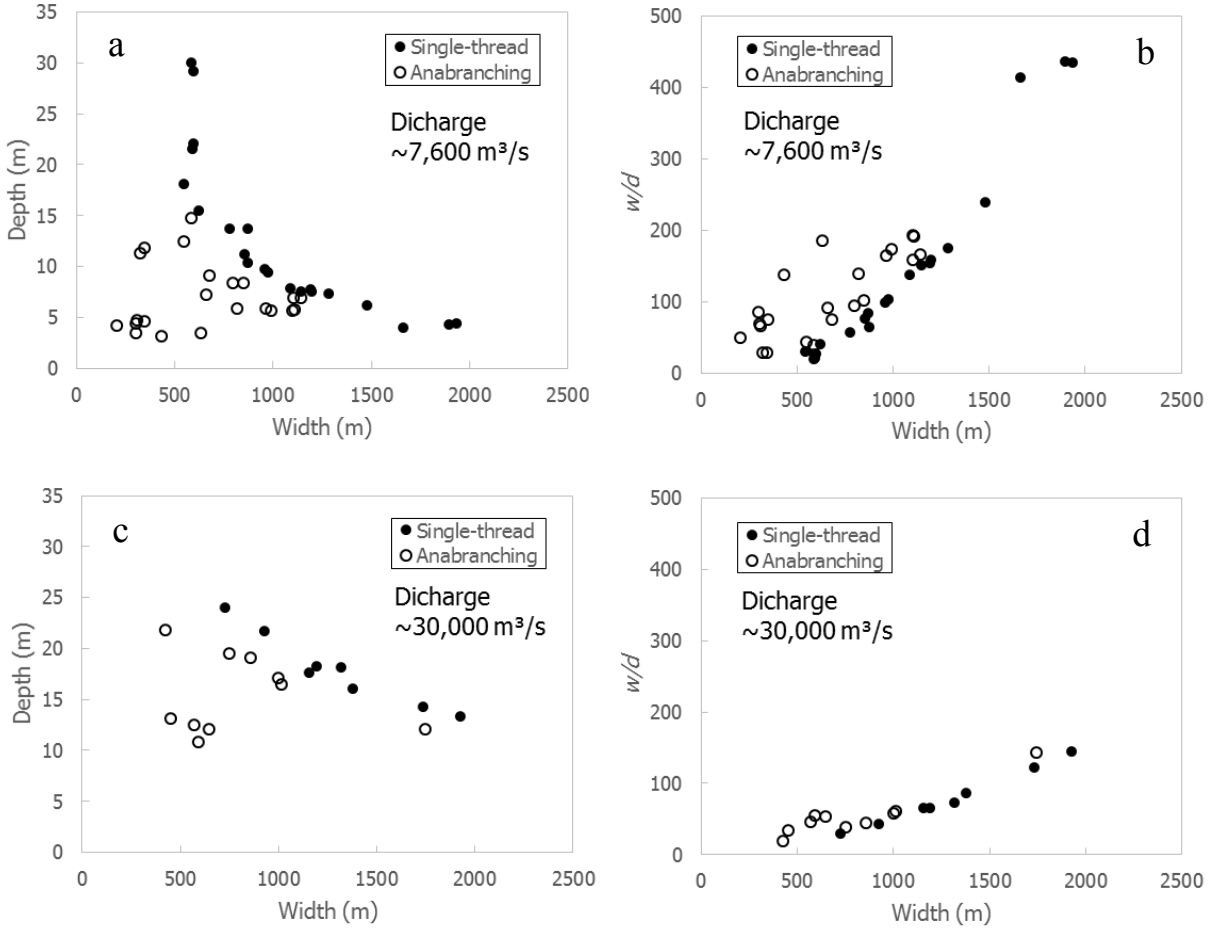


Figure 4.27
Relations between channel width and depth, and between channel width and *w/d*, combining ADCP data in all three reaches. Panel a) and b) illustrate the relations at low discharge, and c) and d) illustrate the relations at bankfull discharge. Single-threaded and anabranching structures are plotted separately. All panels have the same axis scale.

work at bankfull discharge (2013) so the deepest point measured with depth in 2011 was not measured in 2013. Third, with decreased channel depth and largely unchanged channel width, *w/d* increased significantly at low-discharge condition. For example, the initial point (downstream distance equals to 0) had *w/d* of 65 at bankfull discharge, but it increased to 154 when discharge reduced to 7,600 m³/s. Fourth, there's always a peak in

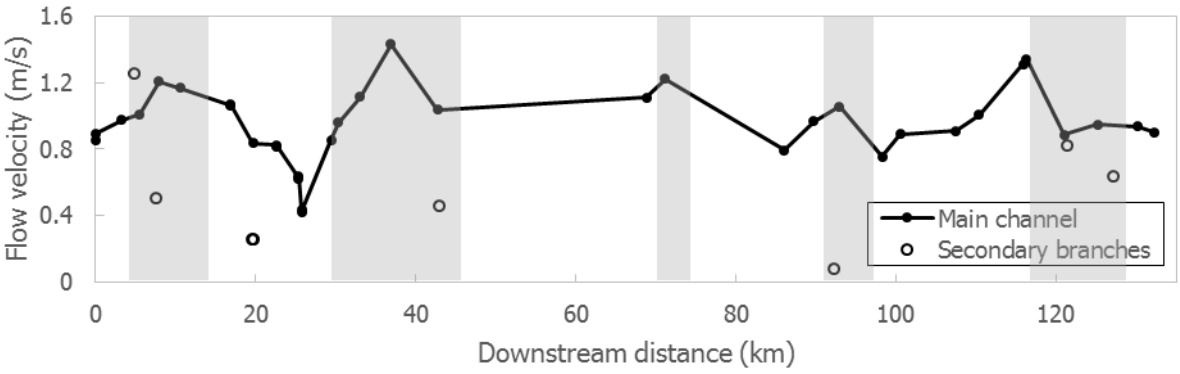


Figure 4.28
Flow velocities of all three reaches during low discharge (about 7,600 m³/s; 2011 field work), in downstream distance, which starts at the beginning of reach 1 and ends at the ending of reach 3. Each dot represents an ADCP transect. Shaded sections indicate anabranching structures, and unshaded sections represent single-thread structures.

the values of channel width and *w/d*, and a local-low value of channel depth as an anabranching structure starts, making them reliable indicators of the location of bifurcation. Fifth, as mentioned in previous sections, for single-threaded channels, the downstream trend of channel width, is inversely related to the downstream trend of channel depth, and the downstream trend of *w/d* is very similar, but not identical, to the downstream trend of channel width. The relations between channel width and depth and between channel width and w/d, for both single-threaded and anabranching structures, are plotted in Figure 4.29. Both the conditions of bankfull discharge (~30,000 m³/s) and low-discharge (~7,600 m³/s) are included. Although scattering exists, those relations are explicit, particularly for single-threaded structures: during both bankfull- and low-discharge seasons, channel depth decreased linearly with the increase of channel width, and channel *w/d* increased linearly with the increase of channel width. For channels at single-threaded structures, the rate of depth reduction with increased width was higher at

low discharge than that at bankfull discharge, and the rate of *w/d* increase with increased width was higher at low discharge than that at bankfull discharge. The conditions of channels in anabranching structures are more complex, with larger scattering, as the size differences between major and secondary branches vary greatly between one anabranching structure to another in terms of their width and depth. Among the relations presented in the four plots, the positions of anabranching channels are well-constrained in lower-left areas of the plots for the width-depth relations, and in upper-left areas of the plots for the width-*w/d* relations. At a certain width, the corresponding width and *w/d* of anabranching channels (major and secondary branches) could exceed those of single-threaded channels. The characteristics indicate single-threaded channels as the threshold of the nearby anabranching channels in terms of the width-depth and width-*w/d* relations.

Flow velocity in downstream distance, during low-discharge, is presented in Figure 4.30. Compared to that in bankfull discharge, which was shown in previous sections, there's an about 40% decrease (from the average of 1.5 m/s to 0.9 m/s). As also shown in bankfull condition, flow velocities in secondary branches are in general lower than the flow velocities of the major branch. In addition, velocity peaks always occur in places with anabranching structures, although the locations within an anabranching structures is not the same—for the first four anabranching structures by downstream distance, the local-high velocity occurs in or near the middle of the anabranching structures, whereas the most last one (most downstream) has the velocity peak in bifurcation area, immediately before the channel split. The lowest flow velocity among

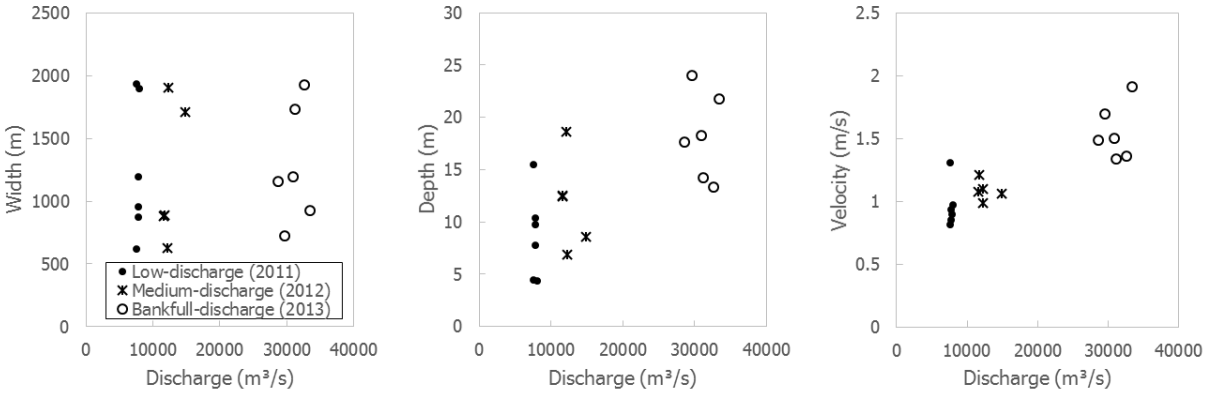


Figure 4.29
Relations between discharge and channel width, depth, and flow velocity in three series with low, medium, and bankfull discharge, at six cross-sections where ADCP data is available.

the entire three reaches is located in the first reach where the local slope is dramatically higher (Figure 4.9), and where the channel is the deepest in all three reaches (Figure 4.26).

In regards to changes of channel width, depth, and flow velocity in response to increased discharge, Figure 4.31 shows the relations between discharge and width, depth, and velocity, respectively, in selected single-threaded cross-sections where ADCP data is available at all three discharge levels. Each relation includes three series with different discharge level: low, medium, and bankfull. It is shown that, as discharge increases to bankfull, more than three times than the low-discharge level, the width largely remained unchanged, while depth and velocity became obviously larger. The finding here implies that the channel of the studied reaches has high banks that are nearly vertical, which is capable to not only hold a large amount of extra water but sustains the channel in similar width as that during low discharge. It also indicates why *w/d* decreases so drastically

from low-discharge to bankfull-discharge level. During high discharges, the excess volume of flowing water is demonstrated to get accommodated by increased depth and flow velocity.

It has also been introduced in the channel centerline analysis that the entire Madeira River channel we studied is very stable (Figure 4.2, 4.10, and 4.17), with most of the channels in the three reaches of extremely limited or no lateral migration. The multi-temporal analysis of channel evolution also reveals that most part (> 80%) of the channel in the three reaches didn't have drastic channel changes over the period of 1985-2015, although small-scaled and local channel changes occur occasionally. Three sites that had the largest channel migration in the three reaches, during 1985-2015, are selected and presented with their migration rate within the six time intervals of analysis. Of the three sites, one is located in reach 2 and the other two are located in reach 3 (their locations are shown on the map). Site 1 is located at the beginning of reach 2 and it is found with the biggest channel migration during 1985-1991. The abnormal large migration of that was due to the abandonment of a secondary branch, which led to the extinction of an anabranching structure. The process of that was shown in Figure 4.13. After 1991, lateral migration occurred with erosion and deposition occurred on opposite sides of the channel (see channel evolution section of reach 2). Site 2 is located near the bifurcation of the dominant anabranching structure of reach 3. The channel there has been constantly widening and affected by lateral accretion of the island towards upstream direction (see channel changes section of reach 3). Site 3 is located near the end of reach 3, where channel gradient is significantly higher than those of the two branch in the

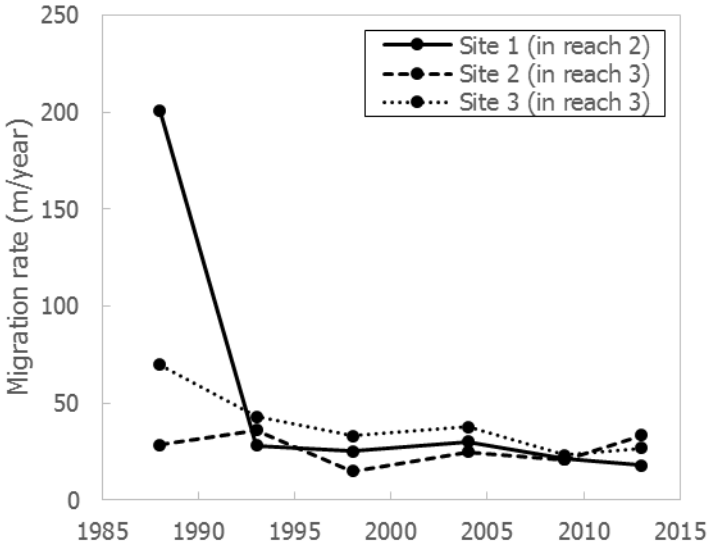


Figure 4.30
Migration rates at three sites of the studied reaches at the six five-year (or so) intervals. The locations of site 1, 2, and 3 are shown in Figure 4.12b, Figure 4.20b, and Figure 4.20c, respectively. Rates are measured at the points in each site with maximum migration distances.

anabranching structure upstream (Figure 4.23) and symmetric pattern of erosion and deposition occurred on the two sides of the channel (see channel changes section of reach 3). Except 1985-1991, migration rates on other time intervals of site 1 and all six intervals of site 2 and 3 had closer values, within 0-100 m/year. The average migration rate of the three sites, excluding site 1 during 1985-1991, is about 35 m/year. Besides the three sites, other segments of the channel in the three reaches had largely kept with untraceable channel migration. Although reach 1 had a lot of channel changes (Figure 4.4 and 4.5), they mostly occurred inside anabranching structures and did not have a big impact on the overall channel positions throughout times.

# Chapter 5: Analysis of channel morphodynamics

Based on the results of Chapter 4, this chapter includes the analysis of the morphodynamics of the studied reaches, including the spatial distribution of bed shear stress and stream power (the two indexes implying modes of sediment transport and the potential for channel erosion), mechanism of sediment transport at different water stage, an overview on barfull discharges, and the spatial distribution of suspended sediment concentration in branches. Bifurcation and confluence are fundamental geomorphological units to anabranching systems. In this chapter, hydrological and morphological features of bifurcations and confluences will be thoroughly discussed in both quantitative and qualitative approaches, in the context of existed models and theories. Further discussions on the form and process of anabranching structures will be made. The objective of this chapter is to better understand "why" the channels in the studied reaches develop the way they are on the basis of the results of "what", which is introduced in Chapter 4.

## 5.1 Bed shear stress

Bed shear stress is the exerted force of water flow acting on the bed surface that stimulates grain motion. It is extensively used to quantify modes of sediment transport in rivers (e.g. Dietrich et al., 1979). We calculated it here for the studied reaches by the depth-slope product ($\tau = \rho ghs$) to examine the potential of water flow on transporting sediment that, given the same bed grain size, bed sediment located in channels with a higher shear stress is more likely to be entrained. As what was expected from the spatial pattern of channel gradient and depth, the profile of reach 1's bed shear stress is relatively

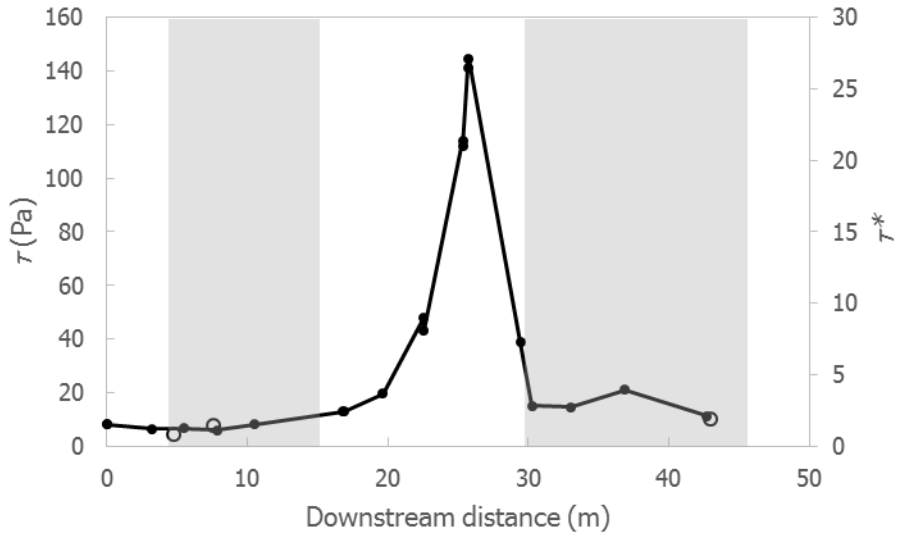


Figure 5.1
Bankfull bed shear stress of reach 1 in two scales: the left scale is dimensional shear stress (τ), and the right scale is dimensionless shear stress (τ*). Calculation is based on depth data collected in 2011 (low stage). Calculations of dimensionless shear stress uses 350 μm as the bed grain size. Bankfull stage is about 8 m higher than the stage of the day of data collection.

constant compared to the exception within the reach that the channel downstream to the large channel bend, where the channel gradient is significantly higher than other portions of channels of the reach (Figure 4.9), has a much larger shear stress. The highest bed shear stress is above 140 Pa, a value 5-10 times greater than the average bed shear stress upstream and downstream to it. Although averaged channel depths vary among different cross sections, such the variation has very limited effect on bed shear stress, compared to the role channel gradient plays. Among the two anabranching structures, the values of bed shear stress are close, but the downstream one is slightly larger than the upstream one. In addition, as what the slope pattern is, the downstream anabranching structure is formed at the location where bed shear stress returns to a lower level. The threshold value

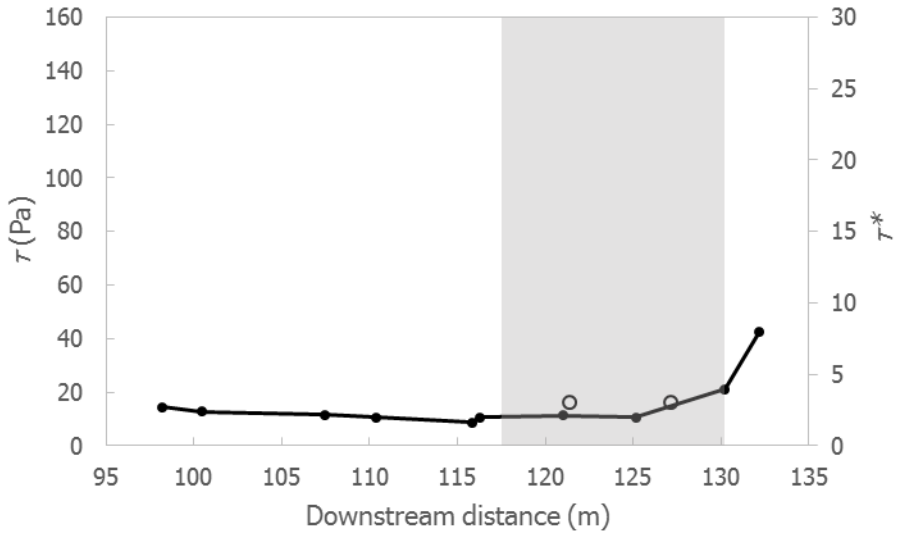


Figure 5.2
Bankfull bed shear stress of reach 3 in two scales: the left scale is dimensional shear stress (τ), and the right scale is dimensionless shear stress (τ*). Calculation is based on depth data collected in 2011 (low stage). Calculations of dimensionless shear stress uses 350 μm as the bed grain size. Bankfull stage is about 8 m higher than the stage of the day of data collection.

here of bifurcatation is about 20 Pa (equivalent to 3.5 for dimensionless shear stress, using the average bed grain size, 350 μm). Under the dimensionless scale, using 350 μm as the bed grain size, the value for upstream anabranching structure is about 1.5, for downstream anabranching structure is about 4, and the highest value in the steep channel segment is about 25.

Bed shear stress of reach 3 ranges from 10 Pa to above 40 Pa (2-9 for dimensionless shear stress) during bankfull condition, as shown in Figure 5.2. Spatial variation of it is limited compared to that of reach 1. The entire reach has a small span of bed shear stress except the very last portion, after the downstream distance of 125 km where the dominant anabranching structure of this reach ends. The increased bed shear stress here is at the same location of the increased channel gradient (Figure 4.25) and

increased activity of channel lateral migration (Figure 4.20 & 4.21; also shown as "Site 3" in Figure 4.32). Average channel migration here in the 1985-2015 interval is about 40 m/year with a symmetric pattern of erosion and deposition on the two sides of the bank. The greatest value of bed shear stress, as of what was measured, is about three times greater than that in other parts of the reach. Bed shear stress measured in anabranching structures (shaded section) does not vary too much with single-threaded channels, and the two secondary-branch cross-sections have slightly stronger calculated bed shear stress due to the slope.

**5.2 Stream power**

As another reliable index quantifying the potential of stream flow behaving on channel bank and bed and evaluating channel morphodynamics, stream power ($\Omega = \rho g Q s$) and particularly, specific stream power ($\omega = \Omega / w$; w is channel width) is often used as an indicator of sediment transport and channel erosion (e.g. Whipple and Tucker, 1999; Knighton, 1999). It is also widely used to build models on predicting channel behavior (e.g. Chang, 1979; Parker et al., 2015). For large rivers, the specific stream power is normally less than 25 W/m² (Latrubesee, 2008), a very small value primarily due to the gentle slope setting.

The pattern of stream power for reach 1 is similar to the pattern of channel slope because discharge along the reaches does not vary too much which makes slope the only significant variable controlling stream power. Similar to the patterns of slope and bed shear stress, specific stream power reaches above 70 W/m² as the peak value which

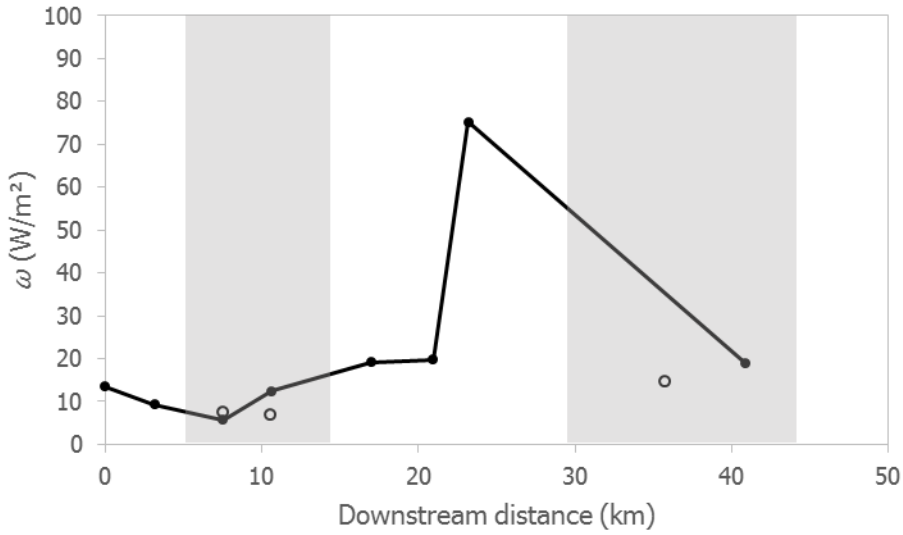


Figure 5.3
Bankfull specific stream power ($\omega$) of reach 1. Calculation is based on water discharge data collected in 2013 (bankfull stage).

occurred at downstream equals to about 25 km. This location is where the local high slope is, as shown in Figure 4.9. In other parts of this reach, the value ranges between about 5 to 20 W/m, regardless of either it is a single-thread channel or anabranching structures. The pattern of specific stream power indicates that flow at the steep channel segment generates the most energy against bank and bed. However, the channel there remains very stable over the past 30 years and the floodplain is absent on the right bank of the channel. What's more, the right bank is also at least 10 m higher than the left bank, which is connected to the geomorphologic unit at the outer bank at the apex of the channel bend. The lowest specific stream power recorded in single–thread channels is located right before the very first bifurcation of this entire reach, in where the channel is obviously wider which helps disperse the exerted energy by the flow. Among the anabranches, the lowest specific stream power is located at the major anabranch 3.5 km

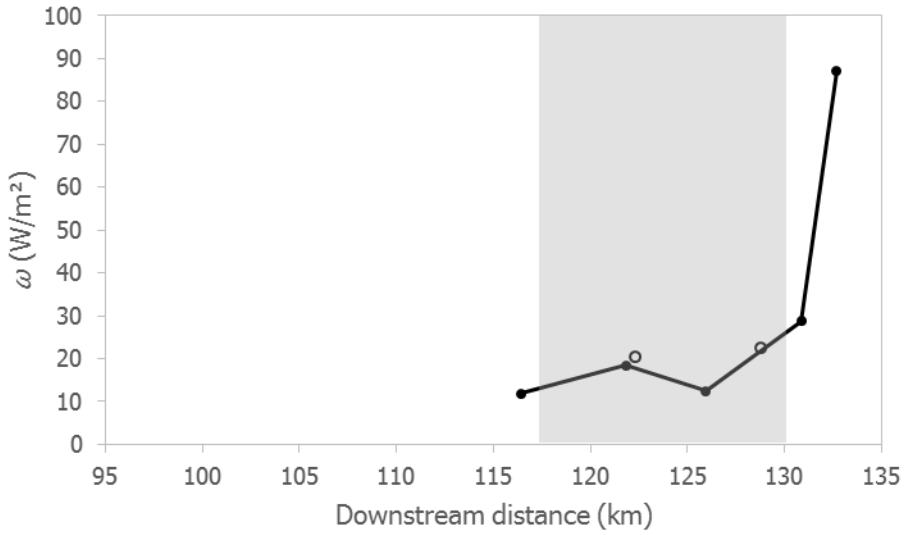


Figure 5.4
Bankfull specific stream power ($\omega$) of reach 3. Calculation is based on water discharge data collected in 2013 (bankfull stage).

downstream to the very first bifurcation of the upstream anabranching structure. The channel there carries less water because of the upstream water diversion at the bifurcation that reduces the flow energy. Additionally, there is another bifurcation formed only 800 m downstream to the upper-most bifurcation of the upstream anabranching structure, which makes the channel wider and shallower in the. Flow energy is thus further reduced.

Specific stream power of reach 3 is calculated and presented in Figure 5.4, based on available ADCP data of that reach of that year's measurement. Channels of the dominant anabranching structure has specific stream power between 10 and 25 W/m², and the secondary branch, although have smaller discharge, even gets larger values than the major branch due to the smaller channel width that leads to concentrated energy. The specific stream power increases drastically downstream to the anabranching structure to the peak value of almost 90 W/m² at the last point of measurement because of the

increase channel gradient there. Downstream channels could possibly reach to even higher values, depending on the channel gradient.

The pattern of specific power shows that anabranching structures tend to have a lower specific stream power than single-threaded channels, although a good part of single-threaded channels also has smaller specific powers. The range of specific stream power of the three anabranching structures (two in reach 1 and one in reach 3) is below 30 W/m², mostly below 25 W/m², which is consistent with the finding of Latrubesse (2008) defining 25 W/m² as the threshold value. Single-threaded channels within the studied reaches that have dramatically higher specific stream power values can be either active or inactive in terms of channel behavior. The channel with boosted specific stream power in reach 1 is constrained by local geologic units, especially on the right bank that prevents the channel to migrate. The other channel with high specific stream power in reach 3 is accompanied with the highest migration rate, of which the average value since 1985 is almost 50 m/year (Figure 4.30).

### 5.3 Bed sediment transport

The 11 bed sediment samples (10 are with available ADCP data) collected in the field work of 2011 shows a great diversity in their grain sizes, ranging from less than 200 μm to more than 550 μm. Locations and other characteristics of the samples are presented in Table 5.1. All the samples are sands, and the majority of them are medium sands. The channel types (anabranching or single-threaded) in which those sediment samples were

| Samples | Latitude | Longitude | Reach # | Channel type | Grain size (μm) |
|---|---|---|---|---|---|
| **1** | -8.560167 | -63.697033 | 1 | Single-threaded | 286.3 |
| **2** | -8.552083 | -63.686667 | 1 | Anabranching --secondary branch | 455.1 |
| **3** | -8.527833 | -63.579983 | 1 | Anabranching --main branch | 348.8 |
| **4** | -8.486533 | -63.594617 | 1 | Anabranching --secondary branch | 183 |
| **5** | -8.463183 | -63.512583 | 1 | Anabranching --secondary branch | 554.3 |
| **6** | -8.281317 | -63.375367 | 2 | Single-threaded with a mid-channel bar at low stage | 297.6 |
| **7** | -8.251667 | -63.368500 | 2 | Anabranching --main branch | 238.8 |
| **8** | -8.209467 | -63.277217 | 2 | Single-threaded | 487.8 |
| **9** | -8.198517 | -63.124983 | 3 | Single-threaded | 429.4 |
| **10** | -8.171933 | -63.054617 | 3 | Single-threaded | 356.4 |

Table 5.1
Samples of bed sediment collected from the 2011 field work. The two underlined and italicized grain size values are not sufficient to illustrate local bed sediment sizes. The sample numbers follow the downstream order that #1 is the most upstream sample.

collected are presented in Table 5.1 as well. Among them, five samples were collected in anabranching structures, and the other five were collected in single-threaded.

There is not a clear difference in bed grain sizes between anabranching and single-threaded structures. The Shields parameter is calculated for each of the samples using

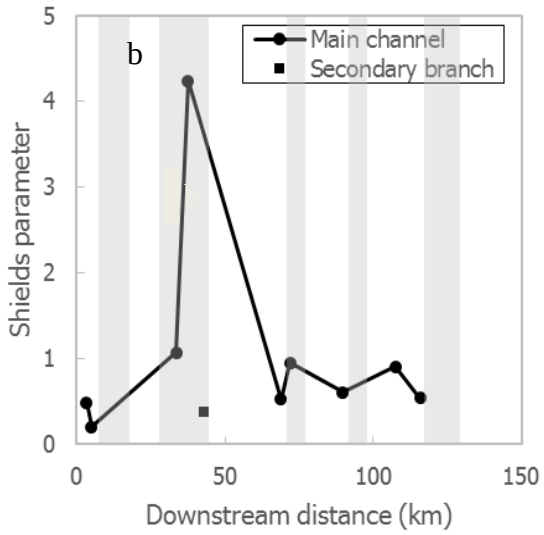


Figure 5.5
Shields parameter of the 10 bed sediment samples presented in downstream distance at the low-stage of 2011 field work. All of them are sands. Shaded sections indicate anabranching structures.

their corresponding bed shear stress during July 2011, a low-stage season. All of the bed sediment significantly exceeds the threshold Shields parameter for incipient motion, which is less than 0.1 (~0.06). Besides the extreme values located in reach 1, the Shields parameter of other sediment samples is relatively stable and the majority of them (9 out of 10) have the values around 0.8. The lowest value among the 10 samples is 0.2, and the highest can reach above 4. Since the samples were measured during a relatively low water stage, the potential of sediment motion in most part of a year could be much larger under the same sizes of bed material, indicating a great potential of the flow to transport sandy materials along the channel bed. There's no explicit trend of the distribution of bed grain sizes between single-threaded channels and anabranching channels from the samples we collected.

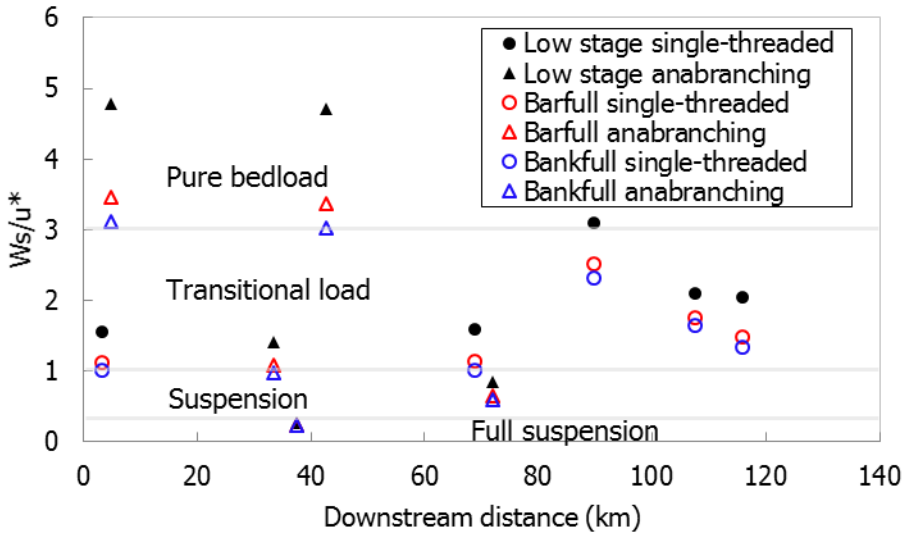


Figure 5.6
The modes of sediment transport along the studied reaches, based on the 10 bed sediment samples, introduced in Table 5.1, at three different water stages: low-stage (when the samples were collected), barfull stage, and bankfull stage.

Further determination on sediment transport shows that a transitional load (between pure bedload and suspended load) is the dominant load at all different water stages: low-stage, barfull, and bankfull stage. Using the approach of dividing the settling velocity ($w_s$) of the grain and the shear velocity ($u^*$) provided by the flow, pure bedload ($w_s/u^* > 3$), suspension ($w_s/u^* < 1$), and fully suspended load ($w_s/u^* \leq ⅓$) can be determined (Bagnold, 1966; Smith, 1977; Nino et al., 2003). The settling velocity for each grain size of bed sample is calculated by Stokes Law, assuming that the acceleration of gravity is 9.81 m/s$^2$, particle density is 2650 kg/m$^3$, water density is 1000 kg/m$^3$, and the viscosity is 0.001 kg/m-s. The results, as shown in Figure 5.6, indicate that the 12 bed material sample collected in the field work of 2011 have the $w_s/u^*$ values ranging from 0.004 to 5.4 in the condition of low-stage, which encompasses all types of sediment

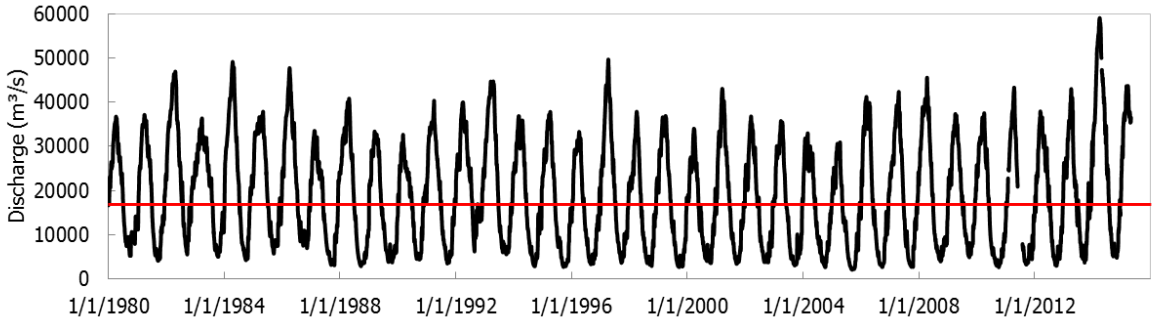


Figure 5.7
The black line shows seasonal variation of water discharge of the Madeira River at Porto Velho and the red line indicates the position of barfull discharge (~17500 m³/s). On average, 49% of days have discharge equal to or greater than the barfull discharge.

transport modes with the majority of the transitional load. Among them (black dots and triangles in Figure 5.6), three of them were pure bedload, five samples were transitional load, one sample were in suspension, and one in full suspension. Besides one case that is sitting on the boundary between full suspension and suspension, it makes sense that the bed sample collected have the transport modes mostly in pure bedload or transitional load. The barfull stage corresponds to the water stage when fluvial bars are just submerged by water. It is an important indicator of the morphodynamic condition of the Madeira River because it usually corresponds to the effective discharge of large rivers (Latrubesse, 2008). The position of barfull stage within the hydro-graph is presented in Figure 5.7, which implies that about 49% of days in a year have discharges equal to or greater than barfull discharge. The field work of 2012 has recorded that the stage difference between the top of a typical mid-channel bar near the end of reach 1 and the water surface (on Dec 15, 2012) is 2 m. By applying the stage difference between the field work of 2011 and 2012, the final stage difference between a barfull condition and

2011 field work condition is 4 m. This value is incorporated in the calculation of shear velocity at the barfull condition to get the new transport modes at that water stage. The results show that although all the samples have moved downwards in the figure, the transitional load was still the dominant transport mode: two samples were pure bedload, six samples were transitional load, one sample was in suspension, and one sample was in full suspension. At bankfull stage that is further 4 m higher than the barfull stage, two samples were pure bedload (both on the boundary to transitional load), five samples were transitional load, two samples were in suspension, and one sample was in full suspension.

### 5.4 Hydro-morphological characteristics of anabranching structures

The two essential geomorphologic units of an anabranching structure are bifurcation and confluence. This section focuses on the hydro-morphological features of two bifurcations in the studied reaches: the dominant anabranching structure in reach 2 (Structure A) and the dominant anabranching structure in reach 3 (Structure B). Maps with details showing channel changes of the two bifurcations are presented in Figure 5.8. The two anabranches in Structure A have equal widths, whereas the secondary branch is obviously narrower than the major branch in Structure B. Although the two anabranching structures are similar in terms of the number of branches and their shape of islands, the spatial and temporal pattern of channel changes is dramatically different that Structure A largely sustained the channels at the same locations and Structure B is unstable with lots

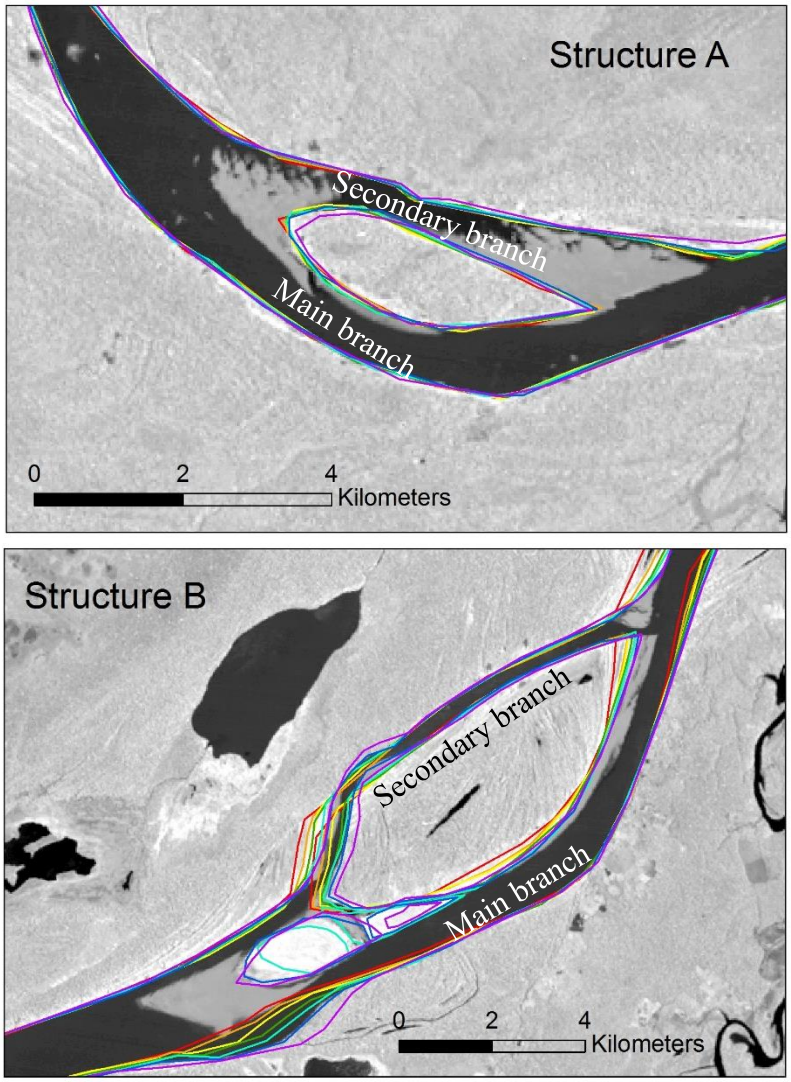


Figure 5.8
Channel changes of anabranching Structure A and B. In both maps, the river flows to the right so bifurcations are on the left and confluences are on the right. Lines with different colors indicate the banks (including islands' banks) of each year. Red, orange, yellow, green, cyan, blue, and purple corresponds to bank positions of 1985, 1991, 1995, 2000, 2004, 2010, 2015, respectively. The two maps have different scales due to the size of the two structures.

of channel changes. Particularly, while Structure A was highly stable over the 30 years, the bifurcation area of Structure B experiences channel widening at the right bank in front of the bifurcation, channel lateral migration at the immediate downstream channel of the

secondary branch, and tiny channel narrowing in the major branch. The island was meanwhile had continuous aggradation at its upstream end and splitting into three parts divided by interconnected channels. Both bifurcations have fluvial bars in the front, which can be seen from the satellite image in Figure 5.8, taken during a low water stage. Large pieces of fluvial bars can also be seen in the secondary branch of anabranching Structure A.

The surface morphology of the two structures also shows the difference that the island of Structure A has a similar height of the surrounding floodplain on the left bank, of which the forests are evenly developed and no dramatic surface texture can be traced from the satellite images. Structure B, however, has many obvious scroll bars developed on the island surface in multiple orientations. The majority of the traceable scrolls are south-north orientated that were developed orderly towards the downstream end of the island, which explicitly indicates the lateral accretion of the island. Some other scrolls near the island's north edge are longitudinal and are perpendicular and intersect to the south-north orientated scrolls, which are not only evidence of lateral accretion, but also of lateral erosion on the northern edge of the island. Although scroll bars are extensively developed on the island of Structure B, the surrounding floodplains don't have many of those developed except the upstream areas near the bifurcation. The spatial distribution of scroll bars indicates the aggradation history of the island.

Sedimentary and stratigraphic records are extensively used for reconstruction of river (e.g. Yang et al., 2000; Latrubesse et al., 2010). The sedimentary features at three locations in Structure B, as shown in Figure 5.9, demonstrate the evolutionary process of

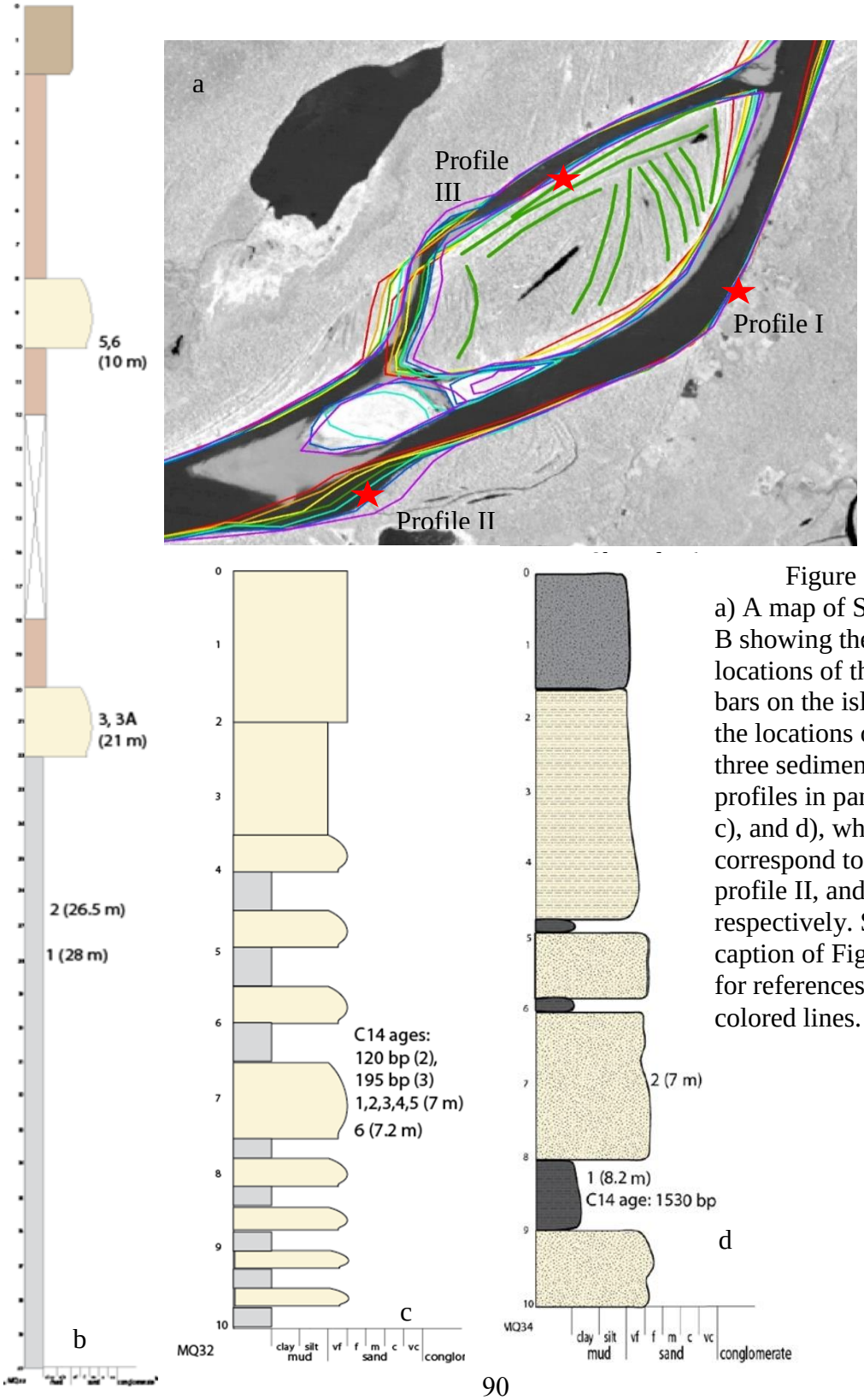


Figure 5.9
a) A map of Structure B showing the locations of the scroll bars on the island and the locations of the three sedimentary profiles in panels b), c), and d), which correspond to profile I, profile II, and III, respectively. See the caption of Figure 5.8 for references of the colored lines.

this anabranching structure. Profile I and II (Figure 5.9b and 5.9c) are located on the right bank of the main branch and Profile I is upstream to Profile II. Profile III is located on the northern edge of the island, which is on the right bank of the secondary branch. Among the three profile locations, the bank where profile I is remained very stable with no channel changes since 1985, whereas the bank of profile II was continuously eroded which led to channel widening and profile III had smaller channel changes but is close to one of the scroll bars identified. The bank of profile I is 40 m high, a significantly larger value than the height of the banks at profile II and III which are both 10 m. A good part of profile I is cohesive fine material and two sandy layers exist in between the fine material layers indicating fluvial deposits in history. The dominant fine material layers of profile I support the finding of inactive channel changes. On the other hand, profile II and III demonstrate an active channel morphodynamics that both profiles have interspersed fine material layers and/or sandy layers. The alternating layers in the middle and lower part of profile II indicate frequent flooding at earlier times (about 100 years ago according to the dating results), which brought sandy deposits in between the finer back-swamp deposits during non-flood times. The continuous sandy deposits at the upper part of profile II indicate erosion of the channel bank that led to the missing of back-swamp which used to be behind the bank. The bank erosion is demonstrated in the analysis of channel changes and can be seen from the rapid position change of the bank in Figure 5.9a. Profile III has the back-and-forth pattern of sandy and finer material layers as well,

Figure 5.10
The bank of profile III is highly vertical and is about 10 m higher than the water surface when the discharge of the Madeira River is about 12,000 m³/s. Photo taken during 2012 field work.

but sandy layers dominant the most part, implying an active deposition activity, which explains the vast distribution of scroll bars on the island as well as its aggradation history.

To quantify the hydrological differences between the two bifurcations, the asymmetry index $r_Q$, proposed by Zolezzi et al., (2009) in describing braided channel systems, is used. The index $r_Q = Q_{br}/ Q_m$, where $Q_{br}$ is the discharge in secondary branch and $Q_m$ is the discharge in main branch (major channel). The range of $r_Q$ is between 0 and 1, and the larger of the value, the more symmetric the two branches are. The results show that $r_Q$, for both structures, increases with increasing total water discharge. In a low-stage season (2011 field work), the asymmetry index is 0.07 for Structure A and 0.14 for Structure B, meaning the discharge in major branches is about

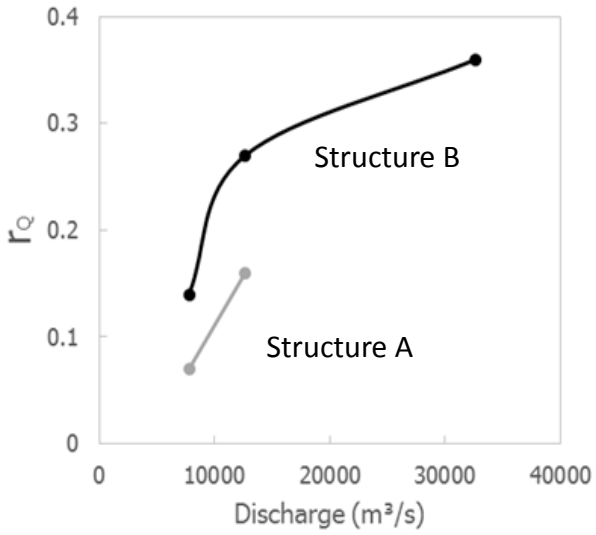


Figure 5.11
Asymmetry index of the bifurcations of Structure A and B at different discharge level, based on the ADCP data collected. Structure A doesn't have relevant data for high discharge. The horizontal axis: discharge, represents the total discharge in the channel.

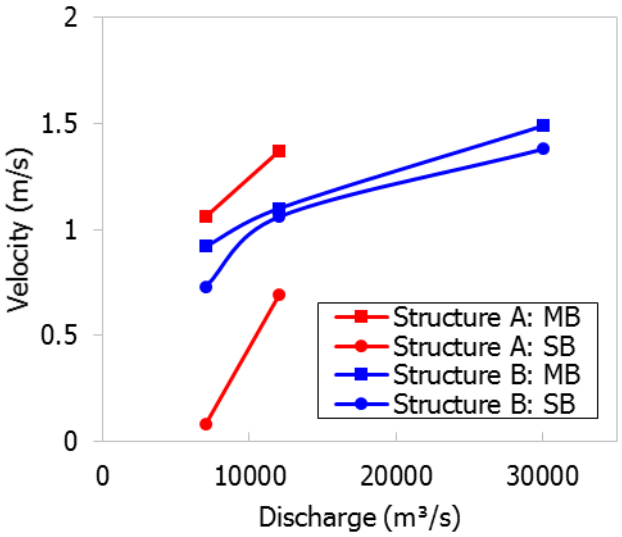


Figure 5.12
Comparison of the flow velocities in the main anabranch (MB) and secondary anabranch (SB) at the two anabranching structures. The horizontal axis, discharge, represents the total discharge of the river. Discharge under 10,000 m³/s was measured in 2011 field work. Discharge right above 10,000 m³/s was measured in 2012 field work. Discharge above 30,000 m³/s was measured in 2013 field work.

10 times bigger than that in secondary branch. In a high-stage season close to bankfull

discharge, the index for Structure B increases to 0.36. According to the data of Structure B, the asymmetry index increases more abruptly from a relative low discharge to a medium discharge than from a relatively medium discharge to a higher discharge. In addition to discharge, Figure 5.12 presents the comparison of flow velocity measured by ADCP in the main and secondary branches of the two anabranching structures. The flow in all cases became faster as water discharge increased. The two anabranches of Structure A are very uneven that the flow in the main anabranch of Structure A was the fastest and the flow in the secondary anabranch is the slowest at least during low and medium discharge seasons. The secondary anabranch of Structure A had its flow velocity close to zero at low-discharge and increased abruptly as water stage raised, which reactivate the channel. Flow in Structure B, however, had similar velocities at all three discharge levels recorded, and the secondary anabranch had slightly slower flow than that of the main anabranch.

The comparison of the asymmetry of anabranching structures and flow velocity at the anabranches of the two anabranching structures show a significant difference that demonstrates diverse hydrologic conditions of anabranching channel systems. A further comparison of channel morphology is made and is presented in Table 5.2. Mean channel

| **Width (m)** | **Structure A** | **Structure B** | **Depth (m)** | **Structure A** | **Structure B** |
|---|---|---|---|---|---|
| **Main anabranch** | 678 | 822 | Main anabranch | 9.1 | 8.4 |
| **Secondary anabranch** | 633 | 328 | Secondary anabranch | 3.4 | 4.7 |

Table 5.2
Mean channel width and depth of the anabranches of the two anabranching structure.

width and depth are used here to represent the general channel morphologic conditions at the four anabranches in the two anabranching structures. As mentioned in previous sections, the channel widths of the main and secondary anabranches of Structure A are about equal, and Structure B's secondary anabranch is dramatically narrower than the main anabranch. However, the mean channel depth of the secondary anabranch of Structure B is 1.3 m bigger than that of the secondary anabranch of Structure A. Because of the depth difference, the secondary anabranch of Structure A could not maintain fully active with flowing water throughout a year. A large amount of deposited sand near the entrance and exit of the secondary branch of Structure A further prevents water flowing in, which obstruct the channel at lower water stages.

Regarding the formation mechanism of anabranching channel systems, Nanson and Knighton (1996) and Nanson (2013) categorized them as either floodplain avulsion (erosion-triggered) or in-channel accretion (deposition-triggered). The erosion-triggered anabranch is caused by overbank flow or bank failure which a new interconnected channel is formed in the floodplain, and deposition-triggered anabranch is the product of channel split due to in-channel accretion. For the two anabranching structures introduced in this section, channel changes in Structure A were demonstrated to be very little, whereas it is very active in Structure B in terms of accretion of the fluvial bar and some other changes as described above. This illustrates the activeness of in-channel accretion of Structure B. The presence of scroll bars on the island, the interspersed layers of sandy and muddy deposits in the sedimentary profile of the island, and height difference between the bank on the island (Profile I) and the bank on surrounding floodplains

(Profile III) further demonstrate the deposition-triggered formation of anabranching Structure B. On the other hand, the relation between the main anabranch and the secondary anabranch of Structure A makes the secondary anabranch a chute channel, a type of channel often seen in meandering rivers that could be the product of multiple processes: floodplain avulsion, in-channel accretion, and scroll-slough development (Grenfell et al., 2012). Although we only have limited data on Structure A, the stable channel and the similarity of surface texture and elevation between the island and surrounding floodplains demonstrates that it is possibly an erosion-triggered anabranching structure caused by floodplain avulsion. Further investigations on the development of bifurcations and the partitioning of streamflow in anabranches suggested that the effect of upstream channel bend (or meander) could lead to greater bed incision at the anabranch near the side of the outer bank of the channel bend (Kleinhans et al, 2008; Kleinhans et al., 2013). In this study, both anabranching structures, with slight channel bend before or at the anabranching section, confirm the finding that a deeper channel tends to form on the side of the outer bank of the channel bend. Those deeper anabranches are meanwhile the main anabranches.

Given the importance of the mid-channel bar at the bifurcation of anabranching Structure B to the development of the anabranching structure as the aggregation of the front bar leads to an upstream extension of the anabranching structure, this study particularly analyzes the hydro-morphological relations between the mid-channel bar and its surrounding channel at the bifurcation of Structure B. Using the bathymetry data, we focus on the channel depth at two geomorphologic units: the mid-channel bar and the

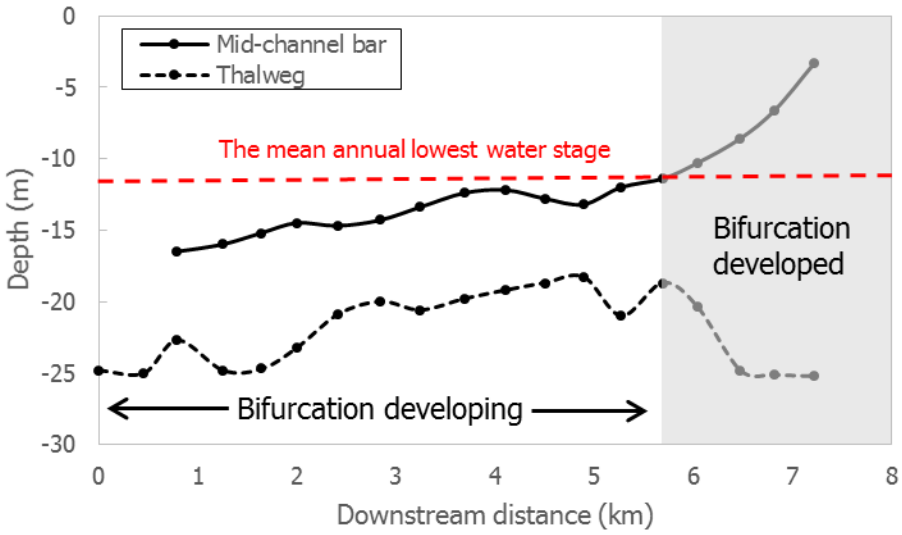


Table 5.13

Channel depth at thalweg and at the mid-channel bar at the bifurcation of anabranching Structure B. The data was collected from the bathymetry survey in the field work of 2013 under the bankfull stage (~30,000 $m^3/s$). The red dashed line indicate the mean lowest annual stage, which is -11.5 m. This line intersects with the depth line of mid-channel bar (black line) at the downstream distance where the thalweg starts to get significantly deeper. Based on this finding, the sections of "bifurcation developing" and "bifurcation developed" are divided.

thalweg (the deepest point of the channel at each cross-section), of which the former represents bar development and the later represents channel bed incision. The depths are measured at each cross-section for about every 500 m at the bifurcation. The bathymetry data used here were collected at the water discharge near bankfull, thus the fluvial bar was fully under water surface and the channel remains single-threaded until it reaches to the downstream distance of 8 km (right end of the figure). Results are presented in Figure 5.13, with the black line indicating the height of the mid-channel bar and the black bashed line indicating the depth of the deepest point of the channel. The mid-channel bar begins at the downstream distance of ~900 m in the figure, where the middle of the

single-threaded channel starts to form a “ridge” which connects to the island downstream. Those two lines present different trends as they approach downstream towards the island: the mid-channel bar, in general, increases in height, and the depth at the thalweg fluctuate at the beginning of the bifurcation (downstream distance 0-2 km), slightly raises in the middle (downstream distance 2-5 km), and abruptly drops (at downstream distance 5.8 km). The depth difference, before the the downstream distance of 5.8 km, remains at about 7-8 m, where thalweg depth decreases slowly with the rise of the bar. After downstream distance of 5.8 km, the thalweg gets much deeper, to about 25 m, a value similar to the thalweg depth at downstream distance of zero, and the mid-channel bar also gets significantly higher. The red dashed line in the figure indicates the annual lowest water stage: 2.7 m, which is the mean value of the lowest recorded daily stage data from 2000 to 2010. The intersection between the red dashed line and the depth line at mid-channel bar is at downstream distance of about 5.8 km, which coincidentally is where the thalweg gets rid of the impact of mid-channel bar and becomes deeper. Based the observations that thalweg gets significantly deeper and mid-channel bar gets higher at 5.8 km and that the annual lowest stage intersects with the depth at mid-channel bar at 5.8 km, the sections “bifurcation developing” and “bifurcation developed” are determined. In “bifurcation developing” section, the mid-channel bar is below the lowest water level of a year and the elevation of it increases slowly. The thalweg also increases slightly with the mid-channel bar, although it also fluctuates at a few places. The downstream end of this section is the most upstream place of flow separation in a year. In the “bifurcation developed” section, the mid-channel bar is above the lowest water level and the elevation

of it increases at a higher rate towards the downstream direction than that in the upstream part. The thalweg there also gets significantly deeper to about 25 m deep, which is as deep as the thalweg at downstream distance of 0.

# Chapter 6: Conclusion

Anabranching channels are the dominant channel pattern of large rivers. As the largest tributary of the Amazon River and one of the largest rivers in the world by water discharge, the Madeira River develops anabranching channels with alternate single-threaded channels, which presents diverse combinations of channel planform. By conducting studies on three representative reaches of the river, this research has particularly answered two questions: First, how the Madeira River channel changes on temporal and spatial basses? Second, how channel morphology differs spatially, particularly between single-threaded channels and anabranching channels? In addition, the research provides information to understand the formation mechanism and processes of anabranching channels in terms of channel behaviors, channel morphology, and sediment transport. The results reveal a great complexity of channel morphodynamics of the Madeira River. Those are also implications of the form and process of other large anabranching rivers in the world.

Studies were conducted in three selected reaches of the river downstream to Porto Velho. Reach 1 is dominated by a box-shaped channel bend with anabranching structures formed at the upstream and downstream ends of the bend. Reach 2 contains a pseudo-meander with a downstream structure. Reach 3 contains a sing-threaded and straight channel with a downstream anabranching structure. The spatial-temporal analysis of channel changes for the period of 1985-2015 in the three studied reaches demonstrates that the Madeira River channel is relatively stable. Besides three sites that had obvious channel migration with the average rate of 35 m/year and a case of secondary-anabranch

abandonment, 130 km of the channel out of the total channel length of the three reaches, 150 km (87%), did not migrate. For anabranching structures, channel changes largely occurred internally within the channel, meaning the size and amount of islands and anabranches were adjusted without alternating the size and position of the whole channel. The only big external change in anabranching structures occurred because of the abandonment of a secondary anabranch in reach 2 that led to a big move of the channel centerline (Figure 4.10 and 4.12; in 1985-1991). For single-threaded channels, they remained very stable everywhere except for one site at the end of reach 3 that has significantly larger channel gradient and erodible floodplains. The activeness of channel changes in terms of the areas of erosion and deposition varied among different reaches and different times. Channel erosion became extremely severe after 2010 in comparison with deposition by a factor of at least three, suggesting the impact of the Santo Antônio Dam and the Jirau Dam upstream, as what was evaluated by Latrubesse et al., (2017). Geologic setting, in a number of places, has large impacts on channel behaviors, which triggers bed incision to form asymmetric cross-sections and deep pools. The channel width is highly insensitive to an increased water level, indicating the presence of nearly upright banks that prevent the exchange of water and sediment between the channel and the floodplains. Besides two sites with very large slope, the unit stream power at bankfull stage of the single-threaded and anabranching structures that were surveyed is below 25 $W/m^2$, the threshold value for mega rivers proposed by Latrubesse (2008). The actual bed shear stress significantly exceeds the shear stress required for incipient sediment motion, and sediment collected from the channel bed at low-stage level can be suspended or

partially suspended during higher water stages. The two formation mechanism of anabranching structures: floodplain avulsion (erosion-triggered) and in-channel accretion (deposition-triggered), are demonstrated by two anabranching structures in the studied reaches. Channels were obviously more active in deposition-triggered anabranching structures than in erosion-triggered anabranching structures. The annual-low water stage is suggested to relate to bed morphology in bifurcations for at least the deposition-triggered anabranching structure.

# References


Ashmore, P. E. (1982). Laboratory modelling of gravel braided stream morphology. *Earth Surface Processes and Landforms*, 7(3), 201-225.

Bagnold, R.A., 1966, *An approach to the sediment transport problem from general physics*: U. S. Geological Survey Professional Paper, 422-I, 37.

Bledsoe, B. P., & Watson, C. C. (2001). Logistic analysis of channel pattern thresholds: meandering, braiding, and incising. *Geomorphology*, 38(3), 281-300.

Bolla Pittaluga, M., Repetto, R., & Tubino, M. (2003). Channel bifurcation in braided rivers: equilibrium configurations and stability. *Water Resources Research*, 39(3).

Bridge, J. S. (1993). The interaction between channel geometry, water flow, sediment transport and deposition in braided rivers. *Geological Society*, London, Special Publications, 75(1), 13-71.

Bridge, J. S., Smith, N. D., Trent, F., Gabel, S. L., & Bernstein, P. (1986). Sedimentology and morphology of a low‐sinuosity river: Calamus River, Nebraska Sand Hills. *Sedimentology*, 33(6), 851-870.

Carling, P., Jansen, J., & Meshkova, L. (2014). Multichannel rivers: their definition and classification. *Earth Surface Processes and Landforms*, 39(1), 26-37.

Chang, H. H. (1979). Minimum stream power and river channel patterns. *Journal of Hydrology*, 41(3-4), 303-327.

Charlton, R. (2007). *Fundamentals of fluvial geomorphology*. Routledge.

Chitale, S. V. (1973). Theories and relationships of river channel patterns. *Journal of Hydrology*, 19(4), 285-308.David

Church, M., & Ferguson, R. I. (2015). Morphodynamics: Rivers beyond steady state. *Water Resources Research*, 51(4), 1883-1897.

Constantine, J. A., Dunne, T., Ahmed, J., Legleiter, C., & Lazarus, E. D. (2014). Sediment supply as a driver of river meandering and floodplain evolution in the Amazon Basin. *Nature Geoscience*, 7(12), 899.

Dietrich, W. E., Smith, J. D., & Dunne, T. (1979). Flow and sediment transport in a sand bedded meander. *The Journal of Geology*, 87(3), 305-315.

Dunne, T., Mertes, L. A., Meade, R. H., Richey, J. E., & Forsberg, B. R. (1998). Exchanges of sediment between the flood plain and channel of the Amazon River in Brazil. *Geological Society of America Bulletin*, 110(4), 450-467.

Eaton, B. C., Millar, R. G., & Davidson, S. (2010). Channel patterns: braided, anabranching, and single-thread. *Geomorphology*, 120(3), 353-364.

Fearnside, P. (2013). Decision-making on Amazon dams: Politics trumps uncertainty in the Madeira River sediments controversy. *Water Alternatives*, 6(2), 313.

Fearnside, P. M. (2014). Impacts of Brazil's Madeira River dams: Unlearned lessons for hydroelectric development in Amazonia. Environmental Science & Policy, 38, 164-172.

Formann, E., & Habersack, H. M. (2007). Morphodynamic river processes and techniques for assessment of channel evolution in Alpine gravel bed rivers. *Geomorphology*, 90(3), 340-355.

Forsberg, B., Godoy, J. M., Victoria, R., & Martinelli, L. A. (1989). Development and erosion in the Brazilian Amazon: A geochronological case study. *GeoJournal*, 19(4), 399-405.

Frias, C. E., Abad, J. D., Mendoza, A., Paredes, J., Ortals, C., & Montoro, H. (2015). Planform evolution of two anabranching structures in the Upper Peruvian Amazon River. *Water Resources Research*, 51(4), 2742-2759.

Gentry, A. H., & Lopez-Parodi, J. (1980). Deforestation and increased flooding of the upper Amazon. *Science*, 210(4476), 1354-1356.

Geodynamical, hydrological and biogeochemical control of erosion/alteration and material transport in the Amazon, Orinoco and Congo basins (SO HYBAM). Retrieved from http://www.ore-hybam.org/.

Grenfell, M., Aalto, R., & Nicholas, A. (2012). Chute channel dynamics in large, sand‐bed meandering rivers. *Earth Surface Processes and Landforms*, 37(3), 315-331.

Huang, H. Q., & Nanson, G. C. (2007). Why some alluvial rivers develop an anabranching pattern. *Water Resources Research*, 43(7).

Kleinhans, M. G. (2010). Sorting out river channel patterns. *Progress in Physical Geography*, 34(3), 287-326.

Kleinhans, M. G., & van den Berg, J. H. (2011). River channel and bar patterns explained and predicted by an empirical and a physics‐based method. *Earth Surface Processes and Landforms*, 36(6), 721-738.

Kleinhans, M. G., Ferguson, R. I., Lane, S. N., & Hardy, R. J. (2013). Splitting rivers at their seams: bifurcations and avulsion. *Earth Surface Processes and Landforms*, 38(1), 47-61.

Kleinhans, M. G., Jagers, H. R. A., Mosselman, E., & Sloff, C. J. (2008). Bifurcation dynamics and avulsion duration in meandering rivers by one‐dimensional and three‐dimensional models. *Water resources research*, 44(8).

Knighton, A. D. (1999). Downstream variation in stream power. *Geomorphology*, 29(3), 293-306.

Knighton, A., & Nanson, G. C. (1993). Anastomosis and the continuum of channel pattern. *Earth Surface Processes and Landforms*, 18(7), 613-625.

Knighton, D. (1998). *Fluvial forms and processes*: London. Edward Arnold.

Lane, E. W. (1955). Importance of fluvial morphology in hydraulic engineering. *Proceedings (American Society of Civil Engineers)*; v. 81, paper no. 745.

Langbein, W. B., & Leopold, L. B. (1970). *River meanders and the theory of minimum variance. In Rivers and river terraces* (pp. 238-263). Palgrave Macmillan UK.

Latrubesse, E. M. (2008). Patterns of anabranching channels: The ultimate end-member adjustment of mega rivers. *Geomorphology*, 101(1), 130-145.

Latrubesse, E. M. (2015). Large rivers, megafans and other Quaternary avulsive fluvial systems: A potential "who's who" in the geological record. *Earth-Science Reviews*, 146, 1-30.

Latrubesse, E. M., & Franzinelli, E. (2002). The Holocene alluvial plain of the middle Amazon River, Brazil. *Geomorphology*, 44(3), 241-257.

Latrubesse, E. M., & Park, E. (2017). Rivers and Streams. *The International Encyclopedia of Geography*.

Latrubesse, E. M., Arima, E. Y., Dunne, T., Park, E., Baker, V. R., d'Horta, F. M., ... & Ribas, C. C. (2017). Damming the rivers of the Amazon basin. *Nature*, 546(7658), 363-369.

Latrubesse, E. M., Cozzuol, M., da Silva-Caminha, S. A., Rigsby, C. A., Absy, M. L., & Jaramillo, C. (2010). The Late Miocene paleogeography of the Amazon Basin and the evolution of the Amazon River system. *Earth-Science Reviews*, 99(3), 99-124.

Latrubesse, E. M., Stevaux, J. C., & Sinha, R. (2005). Tropical rivers. *Geomorphology*, 70(3), 187-206.

Leopold, L.B., Wolman, M.G., 1957. River channel patterns-braided, meandering and straight. *US Geological Survey Professional Paper*, vol. 282B, pp. 39–85.

Lewin, J., & Ashworth, P. J. (2014). Defining large river channel patterns: alluvial exchange and plurality. *Geomorphology*, 215, 83-98.

Makaske, B. (2001). Anastomosing rivers: a review of their classification, origin and sedimentary products. *Earth-Science Reviews*, 53(3), 149-196.

Makaske, B., Smith, D. G., & Berendsen, H. J. (2002). Avulsions, channel evolution and floodplain sedimentation rates of the anastomosing upper Columbia River, British Columbia, Canada. *Sedimentology*, 49(5), 1049-1071.

Mendoza, A., Abad, J. D., Frias, C. E., Ortals, C., Paredes, J., Montoro, H., ... & Soto‐Cortés, G. (2016). Planform dynamics of the Iquitos anabranching structure in the Peruvian upper Amazon river. *Earth Surface Processes and Landforms*, 41(7), 961-970.

Mertes, L. A., Dunne, T., & Martinelli, L. A. (1996). Channel-floodplain geomorphology along the Solimões-Amazon river, Brazil. *Geological Society of America Bulletin*, 108(9), 1089-1107.

Miall, A. D. (2006). How do we identify big rivers? And how big is big?. *Sedimentary Geology*, 186(1), 39-50.

Millar, R. G. (2000). Influence of bank vegetation on alluvial channel patterns. *Water Resources Research*, 36(4), 1109-1118.

Miller, J. R. (1991). Development of anastomosing channels in south-central Indiana. *Geomorphology*, 4(3-4), 221-229.

Milliman, J. D., & Meade, R. H. (1983). World-wide delivery of river sediment to the oceans. *The Journal of Geology*, 91(1), 1-21.

Nanson G.C. (2013). Anabranching and Anastomosing Rivers. In *Treatise on Geomorphology*, vol. 9, Fluvial Geomorphology, edited by E.Wohl, 330–345. San Diego: Academic Press.

Nanson, G. C., & Huang, H. Q. (1999). Anabranching rivers: divided efficiency leading to fluvial diversity. *Varieties of Fluvial Form*, 7, 477-494.

Nanson, G. C., & Huang, H. Q. (2008). Least action principle, equilibrium states, iterative adjustment and the stability of alluvial channels. *Earth Surface Processes and Landforms*, 33(6), 923-942.

Nanson, G. C., & Knighton, A. D. (1996). Anabranching rivers: their cause, character and classification. *Earth surface processes and landforms*, 21(3), 217-239.

Nicholas, A. (2013). Morphodynamic diversity of the world's largest rivers. *Geology*, 41(4), 475-478.

Nino, Y., Lopez, F., Garcia, M., (2003), Threshold for particle entrainment into suspension. *Sedimentology*, 50(2), 247–263.

Osterkamp, W. R. (1998). Processes of fluvial island formation, with examples from Plum Creek, Colorado and Snake River, Idaho. *Wetlands*, 18(4), 530-545.

Park, E., & Latrubesse, E. M. (2014). Modeling suspended sediment distribution patterns of the Amazon River using MODIS data. *Remote Sensing of Environment*, 147, 232-242.

Parker, C., Thorne, C. R., & Clifford, N. J. (2015). Development of ST: REAM: a reach‐based stream power balance approach for predicting alluvial river channel adjustment. *Earth Surface Processes and Landforms*, 40(3), 403-413.

Parker, G. (1976). On the cause and characteristic scales of meandering and braiding in rivers. *Journal of fluid mechanics*, 76(03), 457-480.

Potter, P. E. (1978). Significance and origin of big rivers. *The Journal of Geology*, 86(1), 13-33.

Richardson, W. R., & Thorne, C. R. (2001). Multiple thread flow and channel bifurcation in a braided river: Brahmaputra–Jamuna River, Bangladesh. *Geomorphology*, 38(3), 185-196.

Rosgen, D. L. (1994). A classification of natural rivers. *Catena*, 22(3), 169-199.

Sarker, M. H., Thorne, C. R., Aktar, M. N., & Ferdous, M. R. (2014). Morpho-dynamics of the Brahmaputra–Jamuna River, Bangladesh. *Geomorphology*, 215, 45-59.

Schumm, S. A. (1977). *The fluvial system*. Wiley, New York.

Schumm, S. A. (1985). Patterns of alluvial rivers. *Annual Review of Earth and Planetary Sciences*, 13(1), 5-27.

Smith, J.D., 1977, Modeling of sediment transport on continental shelves, in *The Sea; Ideas and Observations on Progress in the Study of the Seas*, Volume 6, John Wiley & Sons, New York, N.Y., 539-577.

Tal, M., & Paola, C. (2010). Effects of vegetation on channel morphodynamics: results and insights from laboratory experiments. *Earth Surface Processes and Landforms*, 35(9), 1014-1028.

Thorne, C. R., Russell, A. P., & Alam, M. K. (1993). Planform pattern and channel evolution of the Brahmaputra River, Bangladesh. *Geological Society*, London, Special Publications, 75(1), 257-276.

Van den Berg, J. H. (1995). Prediction of alluvial channel pattern of perennial rivers. *Geomorphology*, 12(4), 259-279.

Whipple, K. X., & Tucker, G. E. (1999). Dynamics of the stream-power river incision model: Implications for height limits of mountain ranges, landscape response timescales, and research needs. *Journal of Geophysical Research: Solid Earth*, 104(B8), 17661-17674.

Yang, D., Yu, G., Xie, Y., Zhan, D., & Li, Z. (2000). Sedimentary records of large Holocene floods from the middle reaches of the Yellow River, China. *Geomorphology*, 33(1), 73-88.

Zolezzi, G., Bertoldi, W., & Tubino, M. (2009). Morphological analysis and prediction of river bifurcations. In *Braided rivers: Processes, Deposits, Ecology and Management* (pp. 233-256). Blackwell Publishing Ltd Oxford, UK.